



universität
wien

MASTERARBEIT

Titel der Masterarbeit

**"Tectonic evolution of the Northern Mount Lebanon
region with particular reference to the Lower
Cretaceous Chouf Formation (Lebanon)"**

Verfasser

Harald Bauer, B.Sc.

angestrebter akademischer Grad

Master of Science (M.Sc.)

Wien, 2014

Studienkennzahl lt. Studienblatt: A 066 815

Studienrichtung lt. Studienblatt: Masterstudium Erdwissenschaften

Betreut von: Univ. Prof. Mag. Dr. Bernhard Grasemann

Contents

Acknowledgments	5
Abstract	7
1 Introduction	9
1.1 Stratigraphy of Lebanon	11
1.1.1 Jurassic	13
1.1.2 Cretaceous to Eocene	16
1.1.3 Cretaceous - a revised stratigraphy	21
1.1.4 Miocene to Quarternary	23
1.2 Main tectonic features	23
1.2.1 The Northern Mount Lebanon area	27
1.3 Tectonic evolution of the Lebanon area	27
1.3.1 The opening of the Neotethys	30
1.3.2 Early Cretaceous extension	30
1.3.3 Eocene extension	31
1.3.4 The closing of the Neotethys	31
1.3.5 Neotectonic rifting along the Dead Sea Transform Fault	32
1.4 Lebanon's tectonic structures in a regional context	33
1.4.1 Mount Lebanon and the Palmyride Ranges of Syria	33
1.4.2 The Levantine margin	34
1.5 Field campaign 2012	34
2 The Qartaba Structure	37
2.1 Location and layout of the Qartaba structrue	37
2.2 Overview stops during the 2012 field campaign	38
2.2.1 Stop 6 - Bhassis	38
2.2.2 Stop 8 - Bhassis	38
2.2.3 Stops 12 & 13 - Qartaba	39
3 Thin section analysis	41
3.1 Stop 14 - Abeih (?) Fm.	42
3.1.1 Sample 14/01	42
3.1.2 Sample 14/02	43
3.2 Stop 18 - Bikfaya Fm.	44
3.2.1 Sample 18/01	45
3.3 Stop 21 - Kesrouane Fm.	46

3.3.1	Sample 21/01	46
3.4	Stop 22 - Bhannes Fm.	47
3.4.1	Sample 22/01	48
3.4.2	Sample 22/02	51
3.4.3	Deposition and seismic indicators	54
4	The evolution of the Lower Cretaceous Chouf Formation	55
4.1	Stratigraphy and syn-depositional tectonics	55
4.1.1	Stratigraphic contacts	55
4.1.2	Syntectonic deposition	56
4.2	Field observations	58
4.2.1	Stop 2 - Jeita Grotto	58
4.2.2	Stop 4 - Mairouba	59
4.2.3	Stop 5 - Ain Ed Delbe	60
4.2.4	Stop 7 - Bhassis	61
4.2.5	Stop 14 - Hrazmin	62
4.2.6	Stop 18 - Moukhada	63
4.2.7	Stop 23 - Hourata	63
4.3	Heavy mineral analysis	64
4.3.1	Methodology	65
4.3.2	Results	65
4.4	Isopach model	67
4.4.1	Previous work	67
4.4.2	Data background and methodology	71
4.4.3	Results	75
4.5	Isochore model	78
4.6	Discussion	81
4.6.1	Heavy mineral analysis	81
4.6.2	Isopach model	81
4.6.3	Isochore model	81
5	Conclusions	85
5.1	The Qartaba structure and thin section analysis	85
5.2	The evolution of the Lower Cretaceous Chouf Formation	85
	Bibliography	87
	List of Figures	93
	List of Tables	95
	Appendix	97
	I. Zusammenfassung	97
	II. Lists and field report	98
	III. Curriculum Vitae	152

Acknowledgments

This project was funded by OMV in a cooperation with the University of Vienna. Many thanks to my supervisor Bernhard Grasemann who has been very supportive and from whom I could learn a lot. Also many thanks to Gábor Tari from OMV for offering this opportunity. Thanks to my fellow students Georg Hatzenbichler and Chloé Asmar who have worked with me on the same project. Further assistance from Christian Baal, Mathias Bichler, Susanne Gier, Ben Huet, Sabine Hruby-Nichtenberger, Jörn Peckmann, Michael Wagreich and András Zámolyi was very appreciated.

Acknowledgments

Abstract

The inner study area of this work comprises the Northern Mount Lebanon area, roughly between North of Beirut and South of Tripoli, where the field work was carried out and the samples have been taken. The extended study area for remote-sensing and isopach studies reaches further to the South.

Thin section analysis from samples of different stratigraphic sequences concentrated on the (bio-)stratigraphic classification and structural interpretation of the rock units in question. Investigations led to the development of a deformation model for the Qartaba structure describing two phases of deformation: an initial phase of folding and flexural slip accompanied by the opening of veins was followed by a second phase characterized by pressure solution processes (stylolite formation). Observations of possibly coseismic formed, dynamic recrystallized quartz in thin sections of volcanoclastic rocks of the Bhannes Fm. suggest deformation due to seismic events.

However, the main focus of this work is on the evolution of the sandstones of the Lower Cretaceous Chouf Formation. Due to the obvious thickness variations its syn-depositional tectonic environment has been highly debated in the past. Heavy mineral analysis has been carried out and the preservation of only the most stable heavy minerals points to a pre-existing sandstone as a source and thus agrees with provenance hypotheses found in the literature. Using field and remote sensing data an isopach model has been developed, which shows N-S trending wave-like internal thickness variations of the Chouf Fm. and with regard to the E-W-striking normal faults leads to the suggestion of a syn-rift deposition of these sandstones as proposed by [Collin et al. \(2010\)](#). The constructed isochore map does not much differ from the isopach map due to the low bedding dip angles of the Chouf Fm.

Abstract

1 Introduction

Lebanon is located at the Eastern edge of the Mediterranean Sea bordering Syria in the North and East, whereas Israel to the South. Geographically the country can be divided in four parts, from West to East: the narrow coastal strip, the Mount Lebanon (highest peak al-Qurnat as-Sauda at 3,088 m), the Bekaa valley and the Anti-Lebanon Mountains (highest peak Mount Hermon at 2,814 m). Between Mount Lebanon and the Bekaa valley the country is intersected by the local continuation of the Dead Sea Transform Fault, the NNE-SSW striking Yammouneh fault. Several minor faults branch off this fault towards the NE and NW. Lebanon's main geographic and geologic structures all follow that NNE-SSW trend (Figure 1.12). A simplified geologic map is shown in Figure 1.1.

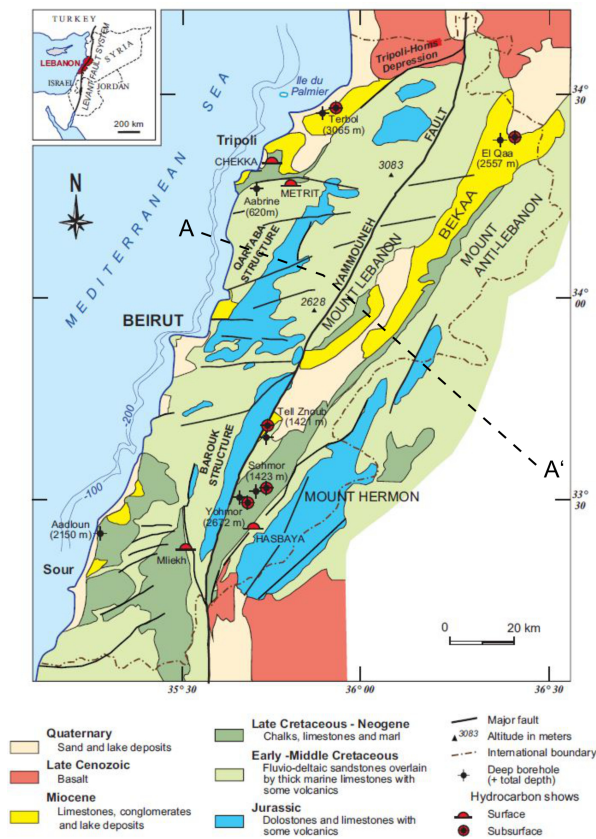


Figure 1.1: Simplified geologic map of Lebanon with the main tectonic structures, based on Dubertret (1955), Ukla (1970), Beydoun and Habib (1995). Location of Qartaba structure and wells is shown here. Cross section A - A' is shown in Figure 1.2. Modified from Nader (2011).

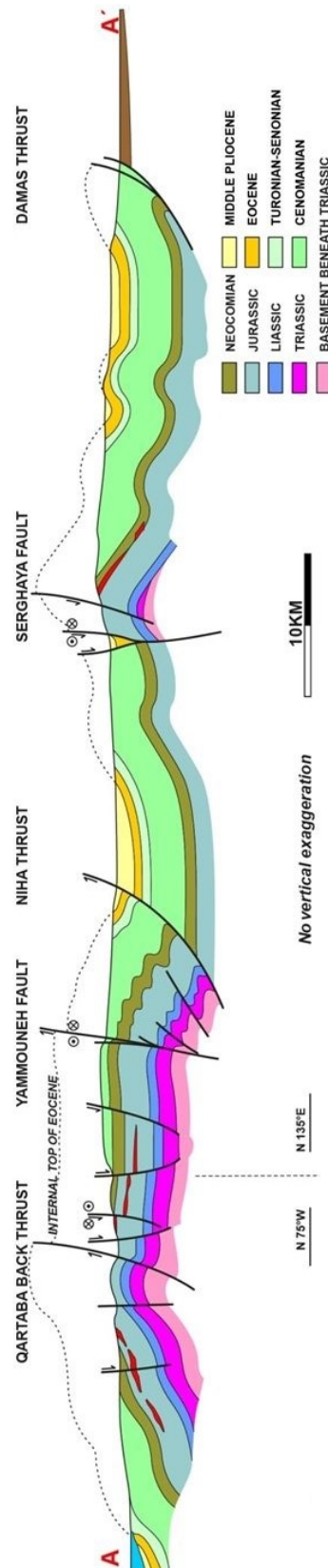


Figure 1.2: Cross section through Northern Lebanon. Location shown in Figure 1.1. From Daeron (2005).

1.1 Stratigraphy of Lebanon

The oldest rocks to be found onshore Lebanon are top Triassic / basal Jurassic. Walley (1997) distinguishes three sedimentary packages: the Jurassic, the Cretaceous to Eocene and the Miocene to Quaternary. The layer-cake geology and rare vegetation makes it easy to identify the distinct formations in the field (Figure 1.3). Many stratigraphic units are not yet examined in detail and several unit boundaries are not yet exactly defined. The following summary is mostly based on the stratigraphic summary from Walley (1997). A stratigraphic chart of Lebanon is found in Figure 1.4

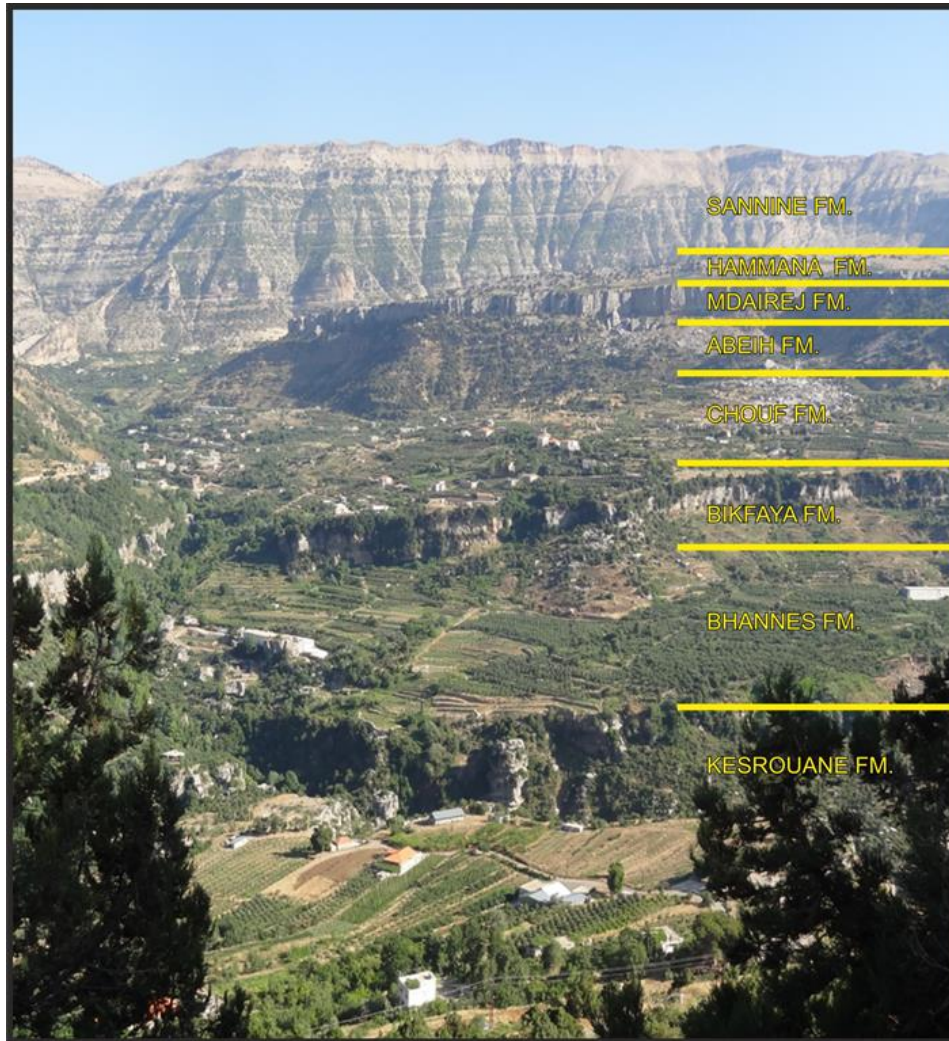


Figure 1.3: The layer-cake stratigraphy of Lebanon, Qartaba region. Picture taken looking towards the South at stop 11 of the 2012 field campaign (N 34°05'44", E 35°52'24").

1 Introduction

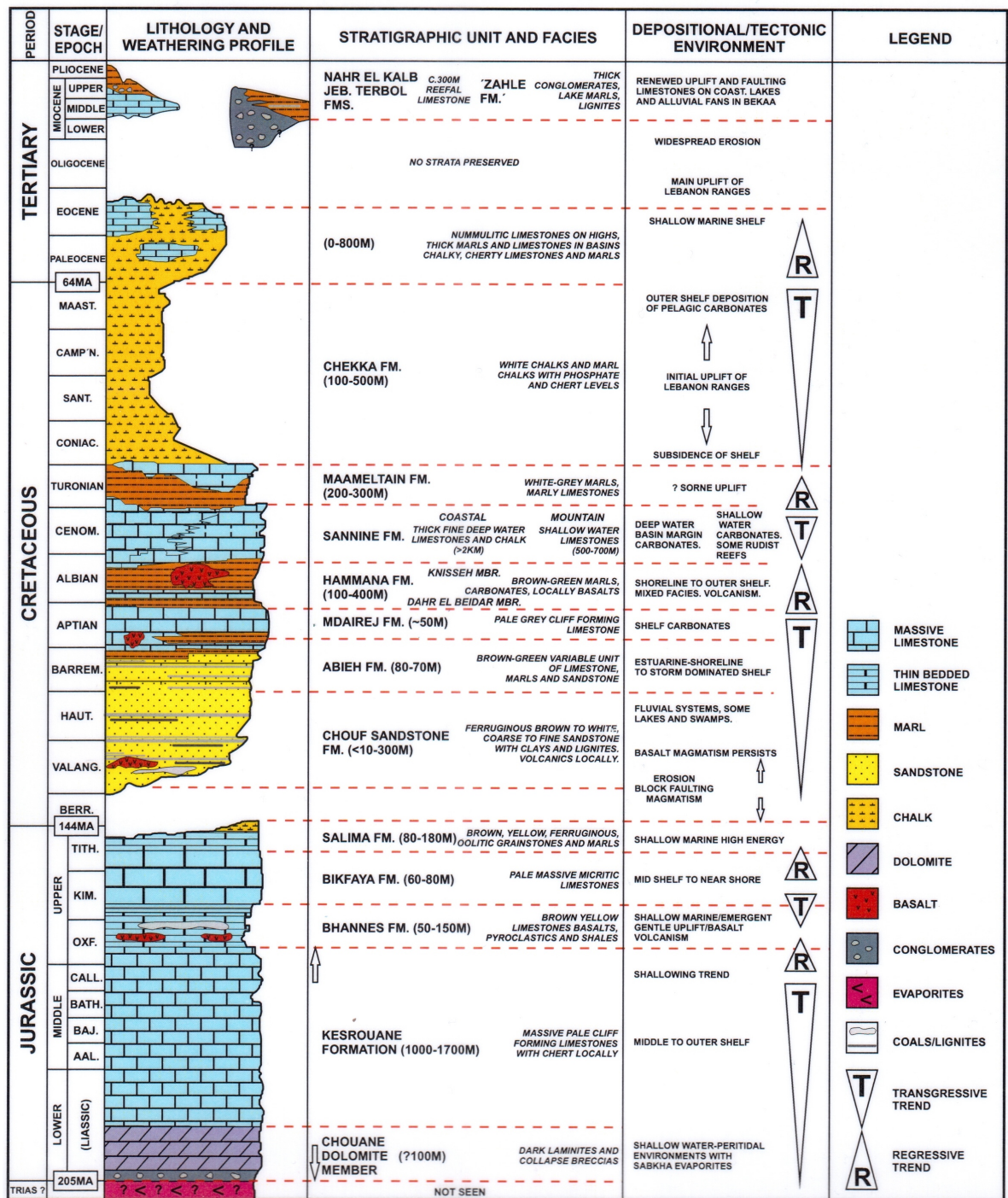


Figure 1.4: A stratigraphic chart of Lebanon, modified from Walley (1997).

1.1.1 Jurassic

The exact thickness of the Jurassic sequence in Lebanon is not known. Estimates vary between 1,500 and more than 2,000 m in the Mount Lebanon region, and 2,700 m and up to 3,000 m in the southern Anti-Lebanon region, respectively. It forms a coherent lithostratigraphic succession almost solely built up of mostly massive, cliff forming carbonates and terminates with a well-marked unconformity, which is marked by erosional surfaces and incised valleys at the top delimiting it from the overlying Lower Cretaceous Chouf Fm.

Kesrouane Fm.

The transgressive, mostly Lower to Middle Jurassic Kesrouane Fm., about 1 to 1.7 or even 2 km thick, represents a shallow water carbonate shelf deposition. The lower and thinner Chouane member, named after the Chouane dam in the Nahr Ibrahim valley, is made up by several hundred meters of dark dolomites containing well developed microbial laminites, collapse breccias and tepees. [Walley \(2011\)](#) referring to Germaine Noujaim Clark assumes that the basal parts of this unit, outcropping near the mentioned dam at the very base of the Nahr Ibrahim gorge, are possibly in part Late Triassic. The upper, much thicker Nahr Ibrahim member comprises massive pale cliff forming limestones, locally with chert, and terminates during a regressive trend in the Oxfordian or possibly Early Kimmeridgian ([Collin et al., 2010](#)). Karstification is abundant in this formation ([Figure 1.5](#)), which serves as one of the most important water reserves of Lebanon ([Nader and Swennen, 2004a](#)). A thin section from the Kesrouane Fm. is described in [section 3.3](#).



Figure 1.5: The Bataara sinkhole at stop 20 of the 2012 field campaign in the top sequence of the Jurassic Kesrouane Fm. This carbonates are one of the most important water reserves of Lebanon. The cave is also known as the "Cave of the Three Bridges". During the spring melt, a 90-100 m cascade falls behind the three bridges and then down into the 250 m chasm (Courbon, 1989).

Bhannes Fm.

The Bhannes Fm., formerly thought to be mainly Oxfordian, has recently be dated to be clearly Kimmeridgian (Collin et al., 2010). It is a variation of different lithologies including carbonates, marls, lavas and pyroclastics. Its thickness varies between 50 and 150 m. However, it can be locally much thicker near volcanic vents. In spite of its diversity it can be easily recognized in the field. Its recessive, flats forming topography due to its much weaker resistance to weathering is in sharp contrast to the cliff forming carbonates of the Kesrouane Fm. below and the Bikfaya Fm. above. Walley (1997) discriminates three facies. A) Fine to medium bedded, grainy carbonates, yellowish colored when weathered. B) Chocolate brown, brown-yellow and some lignite bearing marls. C) Basalt lavas and associated ashes, tuffs and agglomerates containing fragments of the underlying Kesrouane limestones (Stop 22, samples and thin sections 22/01 and 22/02, see Figure 1.6 and section 3.4). The absence of pillow lavas and the occurrence of laterites, paleosoil and lignite horizons indicate a continental, subaerial depositional environment. According to Walley (1997) the cause of that volcanism might rather be

related to mantle plume activity than rifting, whereas [Collin et al. \(2010\)](#) suggest the latter.



Figure 1.6: Volcanoclastic rocks and dark limestones of the Bhannes Fm. at stop 22. NW-SE striking dextral strike slip fault cuts through the cataclastic rocks.

Bikfaya Fm.

Similar to the Kesrouane Fm. the Late Kimmeridgian to Tithonian ([Collin et al., 2010](#)) Bikfaya Fm. is made up by massive pale micritic limestones (see [Figure 1.7](#) and thin section analysis in [section 3.2](#)). Deposition started due to a transgressive trend and ended during a regressive regime. It is varying in thickness, but about 60 to 80 m thick at the type locality. Fossils (corals, bivalves and stromatoporoids) and chert occur. The Bikfaya Fm. seems to lie conformably on the Bhannes Fm., however, soil horizons indicate depositionary time gaps.



Figure 1.7: The massive limestone cliff of the Bikfaya Fm. above the volcanoclastic rocks of the Bhannes Fm. at stop 24.

Salima Fm.

The shallow water carbonates of the Salima Fm. consist of mainly thin bedded brown-yellow ferruginous oolitic limestones alternating with brown marls. Due to its weak resistance towards weathering it developed a recessive topography. As a result of pre-Chouf Fm. erosion today's thickness of the Salima Fm. varies significantly between a few meters and 180 m. The base of the Salima Fm. is Tithonian and recent data show that it extends until the Valangianian ([Clark and Boudagher-Fadel, 2001](#)).

1.1.2 Cretaceous to Eocene

The Cretaceous units start with a clear lithostratigraphic break and evidence of erosion is found in most places. However, in the Metn and Kesrouane areas a transition zone within the uppermost meters of the end Jurassic Salima Fm. with quartz rich ferruginous grainstone can be observed. [Walley \(2011\)](#) identifies another lithostratigraphic break at the base of the Cenomanian Sannine Fm. The Cretaceous to Eocene sequence terminates with a major erosive gap due to a period of tectonic uplift. There are no strata preserved from the Upper Eocene and Oligocene. The Cretaceous stratigraphic nomenclature used here is commonly used by researchers working in Lebanon. However, a revised division

of the Cretaceous units into three main periods has been created recently to put them in a regional (levantine) context (Ferry et al., 2007). A stratigraphic chart for comparison with the stratigraphic chart of Walley (1997) (Figure 1.4) is shown in Figure 1.11 and discussed in subsection 1.1.3.

Chouf Fm.

The formation of the Lower Cretaceous (\sim Valanginian to Hauterivian) Chouf Fm. or Chouf Sandstone Fm. (also Grès de Base) is a major topic of this work and will therefore be described in more detail in chapter 4. It comprises an often ferruginous brown to white sandstone associated with clays, shales and lignites. Some darker layers contain woody or coaly fragments, mostly also pyrite, marcasite and amber. Its mainly clastic components distinguish it from the dominantly carbonate sequences of the Jurassic and rest of the Cretaceous. Basaltic volcanics and volcanic tuffs weathered to reddish clay occur. Substantial thickness variations and syn-sedimentary tectonics are also discussed below. Field observations and pictures are found in section 4.2.

Abeih Fm.

The Barremian to earliest Aptian, more diverse Abeih Fm. is an upward transition from terrigenous clastic sandstones into marls and fossil rich limestones on top (Figure 1.8). The fossils are gastropods, bivalves and foraminifers. Also some amber can be found and locally basalts and pyroclastics occur. Thickness varies from several tens of meters up to 170 m in the Chouf area. The base is defined by the first bivalves bearing clays following the Chouf sandstone. To the top the Abeih Fm. is delimited by the massive cliff forming limestones of the Mdairej Fm.



Figure 1.8: The Abeih Fm. at stop 19 near the village of Boaatara consists of tens of decimeter thick bedded, brownish limestones alternating with centimeters thick marl layers. The layers are bend into synform as part of the monoclinial structure of the Eastern limb of the Qartaba structure.

Mdairej Fm.

The Aptian Mdairej Fm. is built up of one single sheer-sided, pale grey, massive limestone cliff, what makes it easy to be identified in the field. The shallow marine, transgressive limestones are short of macrofossils. Thickness varies in a range of a few tens of meters. The transition zone between the Mdairej Fm. and the overlying Hammana Fm. is shown in [Figure 1.9](#).

Hammana Fm.

The Albian Hammana Fm. consists of regressive, generally brown coloured, marine bivalves bearing thin bedded carbonates, marls and terrigenous sands. The carbonates are replacing the clastic sediments upwards, indicating an end of the regressive trend towards the end of the deposition of the Hammana Fm. Three lithostratigraphic subunits are distinguished: the Couches à Orbitolina: soft sands, clays and thin limestones; the Banc de Zumoffen: ferruginous brown, cliff forming carbonates; and the Couches à Kne-miceras (an ammonite): grey green glauconitic marls passing upwards into alternating

marls and frequently bioclastic carbonates. The first two Walley (1983) merges into a Dahr el Beidar Member and the latter one he names Knisseh Member. Locally at least two different levels of volcanics and pyroclastics occur, sometimes over 100 m thick. The transition zone between the Hammana Fm. and the underlying Mdairej Fm. is shown in Figure 1.9.



Figure 1.9: The transition between the Aptian Mdairej Fm. and the Albian Hammana Fm. is marked by an alternating layering of limestone and red paleosols (gravels and clay).

Sannine Fm.

The Sannine Fm. (Figure 1.10) is about 600 m thick and therefore the second big carbonate sequence after the Kesrouane Fm. It's reaching from the Upper Albian to the Turonian, and is divided into a 'coastal' and a 'mountain' facies zone corresponding to their geographic position today (Walley, 2011). The upper boundary is defined by the occurrence of Turonian fossils (ammonites or the rudist bivalve hippurites). This biostratigraphic definition makes it more difficult to identify the formation's upper boundary in the field. However, in fact this is not a problem for the mountain area since

1 Introduction

the Sannine Fm. is the highest to be seen there. The ‘coastal’ facies consists of more marly limestones, whereas the ‘mountain’ facies comprises mostly medium to thick bedded shallow water both limestones and marly limestones with limited biota including echinoids, gastropods and bivalves. Some rudist-rich units occur. Furthermore, within the ‘mountain’ facies reef, back-reef and lagoonal units can be identified. Several famous fossil fish deposits are to be found within this formation.



Figure 1.10: Massive limestones of the Sannine Fm. at stop 36.

Maameltain Fm.

This 200-300 m thick ([Dubertret, 1975](#)) carbonate unit is limited to the Turonian and only crops out along the coast. It comprises thin bedded alternations of chalky marls and limestones as well as massive to thin bedded Hippurites (rudist bivalves) bearing limestones. The lower beds also include levels with ammonites. [Walley \(1997\)](#) points out that new data show the possibility that the carbonates of the Maameltain Fm. are not always younger than those of the Sannine Fm. but could locally be a lateral facies equivalent.

Chekka Fm.

The Chekka Fm. starts in the Coniacian and extends locally into the Paleocene and Early Eocene. It represents the drowning of the former Turonian rudist platform and consists of various white to dark grey carbonates including chalk, marly chalk and chalky to marly limestones. The chalky beds include chert bands and phosphate nodules. Thickness varies from a few tens of meters up to 500 m and more (Renouard, 1955). These well-bedded pelagic chalk strata, deposited on the outer part of a continental platform, show some sort of depositional cyclicity. This pelagic paleo-environmental condition and the variation in thickness of the sediments preserved may indicate uplift events during the first phase of Syrian Arc deformation in the Senonian (Walley, 1997, 1998). Based on recent facies and microfacies analysis Hawie et al. (2014) divided the Senonian sequence into four sub-units: Upper Santonian, Lower Campanian, Upper Campanian and Lower Maastrichtian.

Paleogene Fm.

The Paleogene strata are restricted to the Paleocene and Eocene. Due to major uplift as part of the second phase of Syrian Arc deformation no Upper Eocene and Oligocene strata are preserved Walley (1998). As mentioned above it is not clear to what extent the Chekka Fm. extends into the Paleocene and Eocene. However, two Eocene facies reaching at least 900 m of thickness are distinguished (Dubertret, 1975; Walley, 1997). Early Eocene strata consist of chalky-marly limestones containing chert nodules. Middle Eocene sediments comprise nummulitic limestones.

1.1.3 Cretaceous - a revised stratigraphy

Ferry et al. (2007) have proposed a revised division of the Cretaceous sequences in Lebanon putting them into a Levantine context. The Cretaceous strata are divided into three parts, all of them starting with a transgression sequence.

The first, Valangian to Upper Aptian part is divided into five depositional units separated by emersion surfaces: Salima Fm., Chouf Fm. sst., Jeita Fm., Jezzine Fm. and Dar El Beidar Fm. However, the Jezzine Fm. at the end of the Lower Aptian shows an emersion surface only in northern Lebanon but a simple transgression surface in the South. The lithology comprises carbonates and clastics.

The second part reaching from the Upper Albian to the end of the Turonian comprises the deposits of large carbonate platforms covering a big part of the Arabian craton. The corresponding formations are the Upper Albian Niha Fm. and Nahr Ibrahim marls, the Cenomanian Aitou Fm, the end-Cenomanian to Lower Turonian Ghazir Fm. and the Upper Turonian Abou Ali Fm.

The third, Senonian part of the Cretaceous strata involves the El Jaouz Fm. comprising micritic limestones and chalks. It continues into the Eocene.

Figure 1.11 shows the revised stratigraphic chart of the Cretaceous including sequence stratigraphic data (transgressions/regressions), volcanic events and valley incisions.

1 Introduction

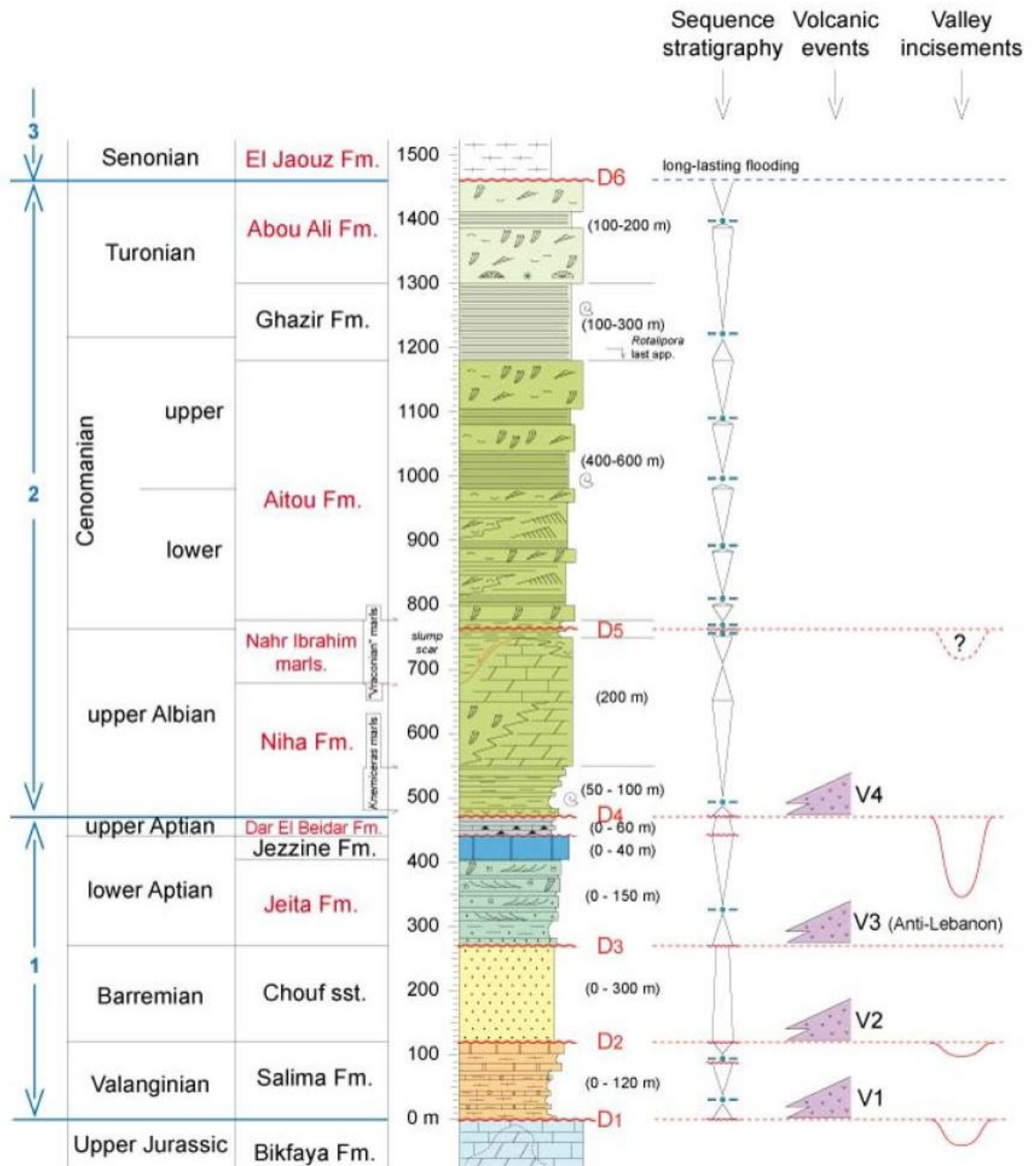


Figure 1.11: A revised stratigraphic chart of the Cretaceous of Lebanon from [Ferry et al. \(2007\)](#). Numbers 1 to 3 refer to the three proposed stratigraphic periods of the Cretaceous, formation names in red are new. D1 to D6 represent unconformities, V1 to V4 refer to volcanic events.

1.1.4 Miocene to Quarternary

A Middle to Upper Miocene carbonate sequence crops out at different isolated locations along the coast and not all of them are classified (Walley, 1997). However, a 285 m thick late Middle Miocene limestone sequence called Jebel Terbol Fm. is identified in the North of Lebanon, along the coast near Tripoli and further South at Ras Chekka. It's lying unconformably on the Upper Cretaceous Sannine Fm. Around Nahr el Kalb a 200-300 m thick massive littoral limestone sequence is named Nahr el Kalb Fm. Near the coast it contains corals, algae and bivalves but going landward passes into sands and conglomerates. In the interior of the country around Zahle Dubertret (1975) describes a sequence of clastics, calcareous breccias, conglomerates, sandy silty marls, lignites, limestones and lacustrine marls. This probably 1.5 km thick Zahle Fm. of continental sediments can be found at both sides of the Bekaa valley associated with alluvial fan conglomerates on the uplift flanks (Walley, 1997). Pliocene to Pleistocene strata are not yet classified. They include coastal sediments at different locations and marine Lower Pliocene rocks around Tripoli which unconformably overlie the late Miocene continental sediments. In the Bekaa and Akkar area fluvial and lacustrine sediments reach into the Holocene. Besides, alluvial fans associated with fault scarps and glacial and periglacial deposits associated with high altitudes occur.

1.2 Main tectonic features

From a structural point of view three NNE-SSW striking main features can be distinguished in Lebanon: from West to East the Mount Lebanon anticline, the Bekaa syncline and the Anti-Lebanon anticline (Figure 1.12). The two anticlines are major uplifts with Jurassic rocks in their core, whereas Late Cretaceous rocks form the highest point of Mount Lebanon, Qornet es Saouda at 3,088 m and Middle Jurassic rocks form the highest point of the Anti-Lebanon range, Mount Hermon at 2,814 m. The Bekaa valley, a synclinorium lying in between, is an elevated upland basin ranging between 700-1000 m asl and filled with Neogene sediments. The coastline and narrow continental shelf as well as the Lebanese section of the Dead Sea Transform Fault (DSTF), the Yammouneh Fault, all follow the same NNE-SSW directed trend. The Yammouneh fault is a transpressional segment of the DSTF along the Lebanese restraining bend responsible for the further uplift of the Mount Lebanon and Anti-Lebanon ranges and showing recent strike-slip activity (Gomez et al., 2006). However, GPS measurements and the lack of present-day seismicity indicate that this fault is currently in a state of tectonic quiescence accumulating interseismic strain (Gomez et al., 2007).

Other important faults are the Râchâïya Fault, Roûm Fault and Serghaya Fault, all equally sinistral branches of the Yammouneh Fault. The Beit ed Dine-Qabb Elias Fault is an E-W-striking dextral strike-slip fault separating the Northern Mount Lebanon from the Southern Mount Lebanon and turning northwards at its eastern end to join the Yammouneh Fault. The Akkar Fault delimits the Northern Mount Lebanon uplift towards the lower lying rocks to the North (Figure 1.12, Figure 1.14).

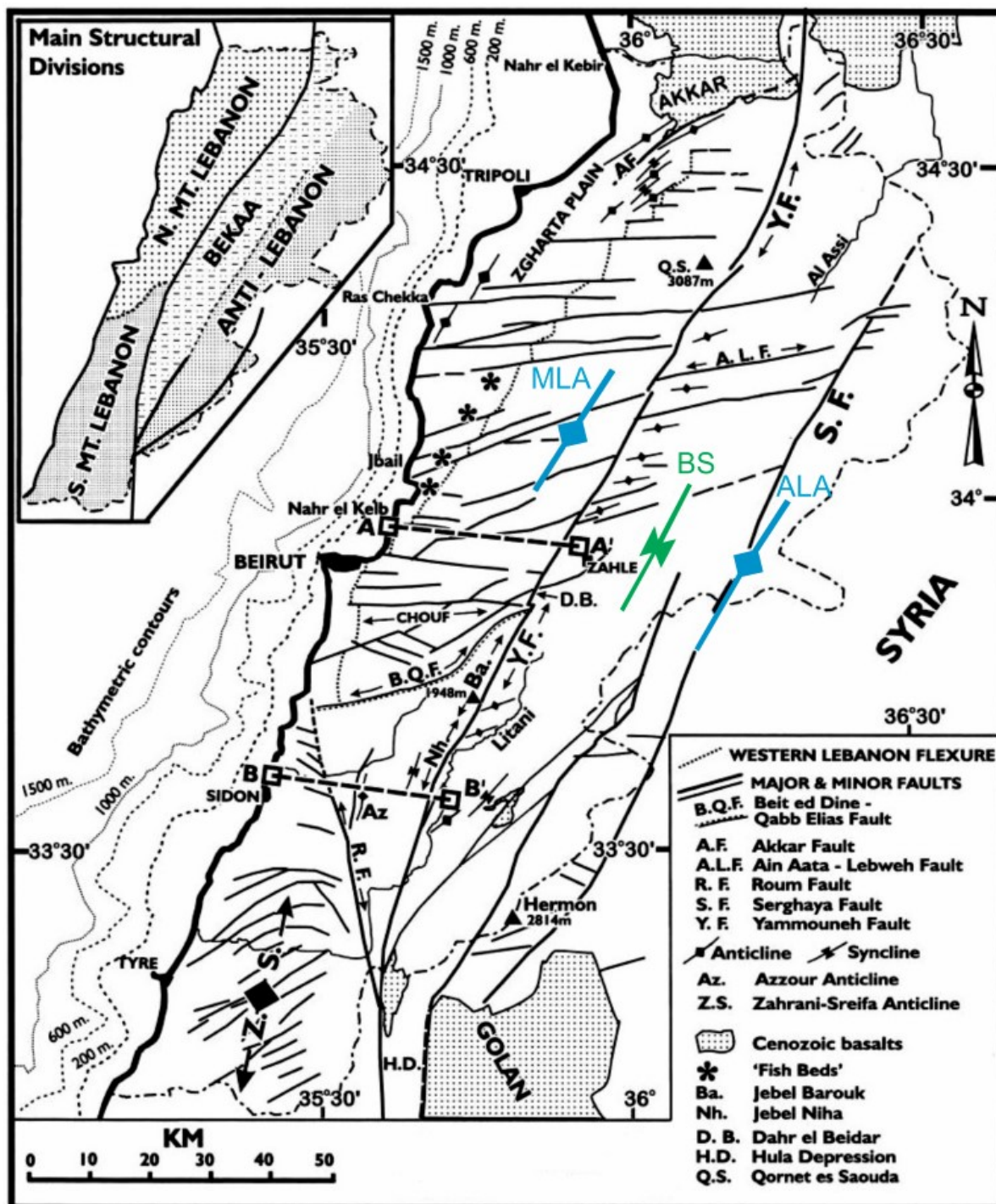


Figure 1.12: Lebanon's main geologic structures and faults: Mount Lebanon Anticline (MLA), Bekaa Syncline (BS), Anti-Lebanon Anticline (ALA), Yammounieh Fault (Y.F.). All trending NNE-SSW. Modified from Walley (1998). Cross sections A-A' and B-B' are shown in Figure 1.13.

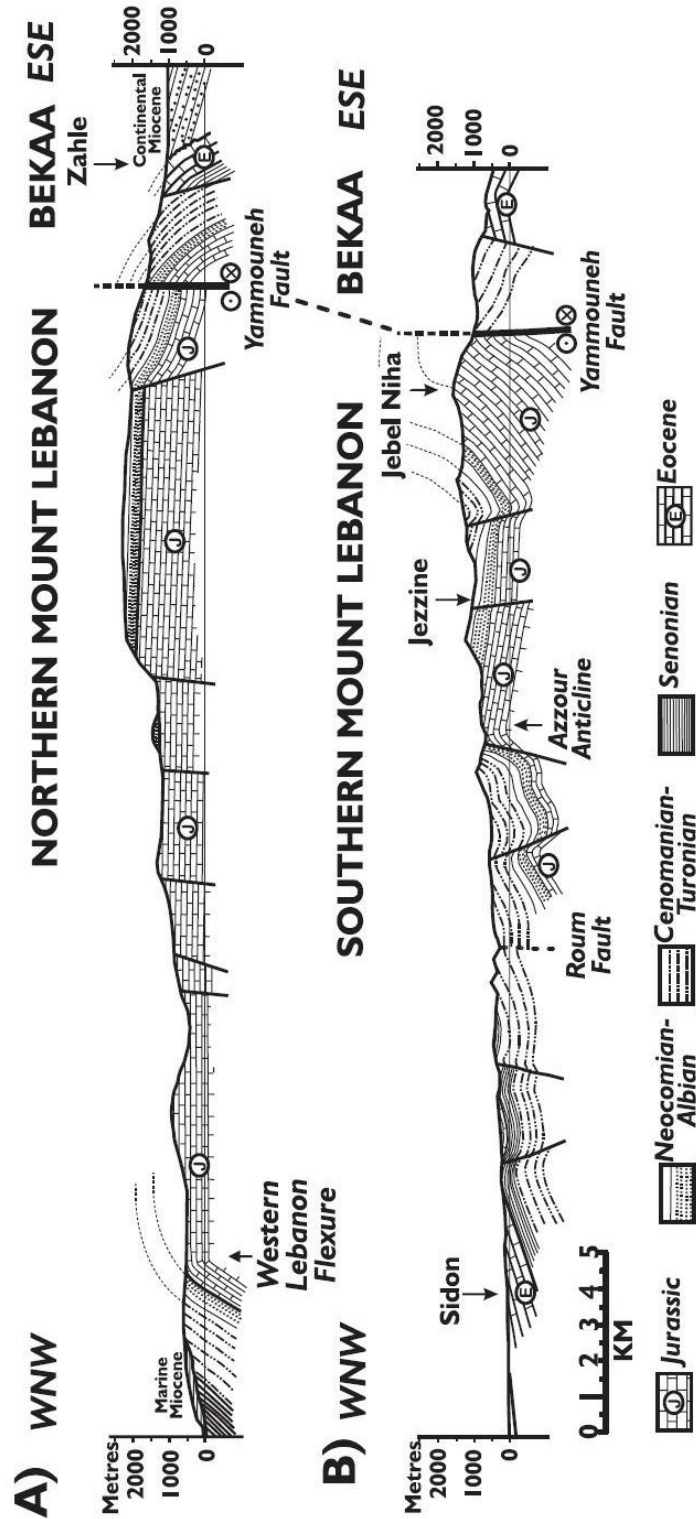


Figure 1.13: Mount Lebanon cross sections, from Walley (1998). Location shown in Figure 1.12.

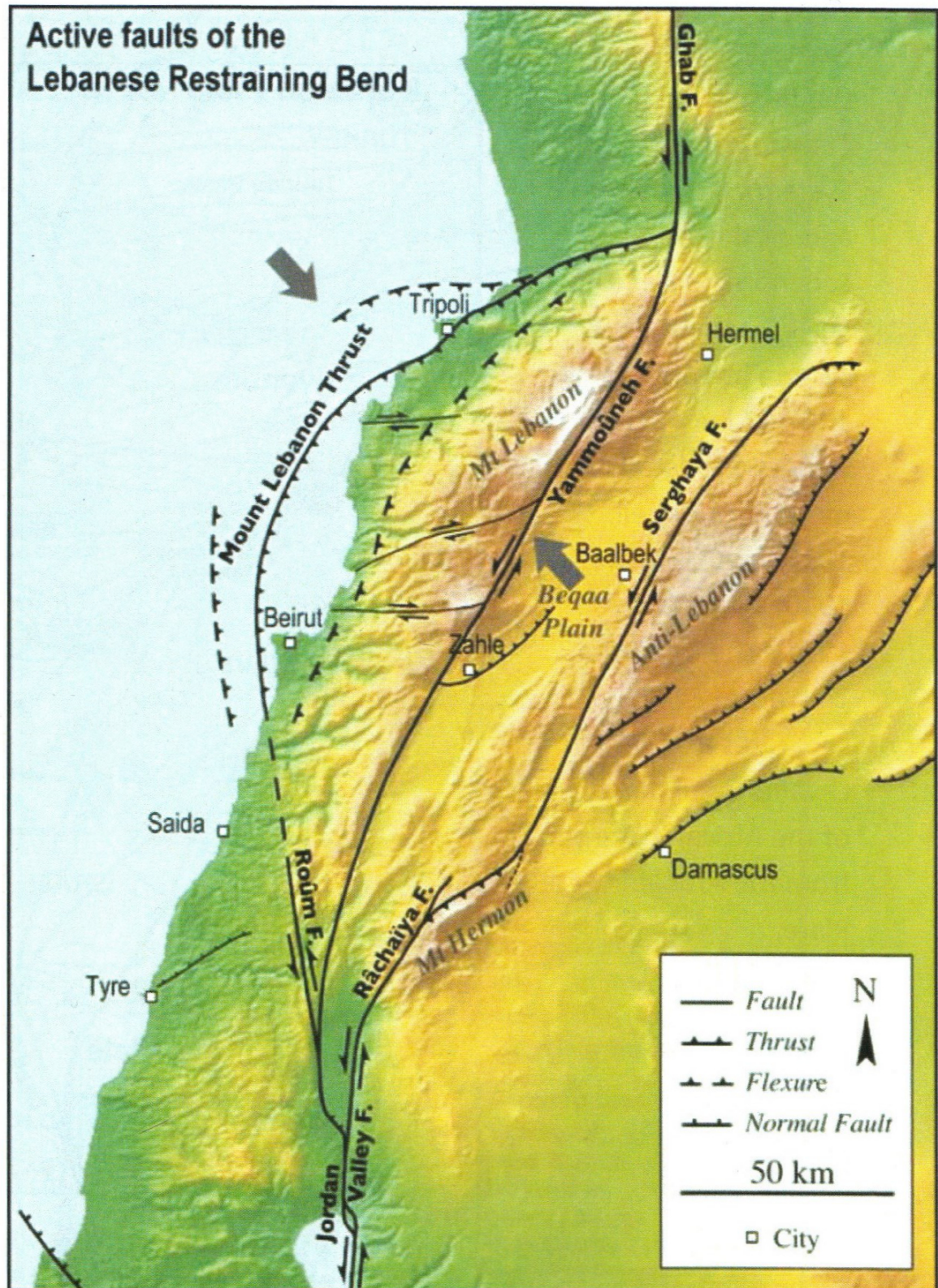


Figure 1.14: A simplified overview over the fault system in Lebanon, slightly modified from Daeron (2005).

1.2.1 The Northern Mount Lebanon area

This work focuses on the Northern Mount Lebanon and therefore the geology of this area is described in more detail. Stratigraphically this mostly over 1,000 m high area is a sequence of thick Jurassic to Palaeogene carbonates intersected by Late Jurassic to Early Cretaceous successions of basaltic volcanics, sands and clays. Structurally, the Northern Mount Lebanon zone is a box-fold-like anticline (Qartaba Anticline) (Nader and Swennen, 2004a). Its western limb is formed by a NNE-SSW-striking monocline called the Western Lebanon Flexure. The more or less horizontal lying rocks to the east mostly continue until the Yammouneh Fault. The eastern limb locally influenced by the Yammouneh fault is not that straight forward. E-W- to ENE-WSW-striking faults offset the rocks of this region (Walley, 1998). According to Gomez et al. (2007) the formation of the Qartaba Anticline started at around 11 Ma during the Late Cenozoic transpression phase of the Dead Sea Transform Fault.

Laterally the Northern Mount Lebanon area is limited by the narrow coastal plain to the west and the western margin of the Bekaa valley or Yammouneh Fault in the east. The northern boarder of this zone is the Akkar Fault, delimiting the Mount Lebanon Massif from lower lying Cenozoic basalts. The southern limit is the Beit ed Dine-Qabb Elias Fault, striking E-W in its eastern part and then turning northwards to meet the Yammouneh Fault. This border marks a significant change in stratigraphy and structures. In the Southern Mount Lebanon due to more flat-lying rocks the anticlinorium is not clearly recognisable and faults rather strike NE-SW and ESE-WNW. Late Jurassic and Early Cretaceous volcanism is less abundant in the south and both the end-Jurassic carbonates and the overlying Lower Cretaceous Chouf Sandstone Fm. thicken abruptly southwards (Walley, 1998) (see Chouf isopach model in chapter 4).

1.3 Tectonic evolution of the Lebanon area

In a regional context the most dominant fault feature is the Dead Sea Transform Fault (DSTF) separating a Levantine subplate of the African Plate from the Arabian Plate with a Neogene sinistral off-set of about 100-105 km (Quennell, 1958; Freund et al., 1970; Garfunkel, 1981). The southern segment of the DSTF in the Gulf of Aqaba and southern Jordan represents a major crustal-scale fault (Kesten et al., 2008), its northern segment in Syria (Ghab Fault system) is described as a minor left-lateral fault (Searle et al., 2010). The DSTF's central part along the Lebanese restraining bend shows active strike-slip located along the Yammouneh fault (Gomez et al., 2006). Whereas North and South of Lebanon the DSTF is striking N-S (as seen in Figure 1.15 and Figure 1.16), the Yammouneh fault follows the characteristic NNE-SSW trend of Lebanon's main structural features. Furthermore, the DSTF's northern and southern segments are transtensional, whereas the transpressional central part is the cause for the uplift of the Mount Lebanon and Anti-Lebanon ranges.

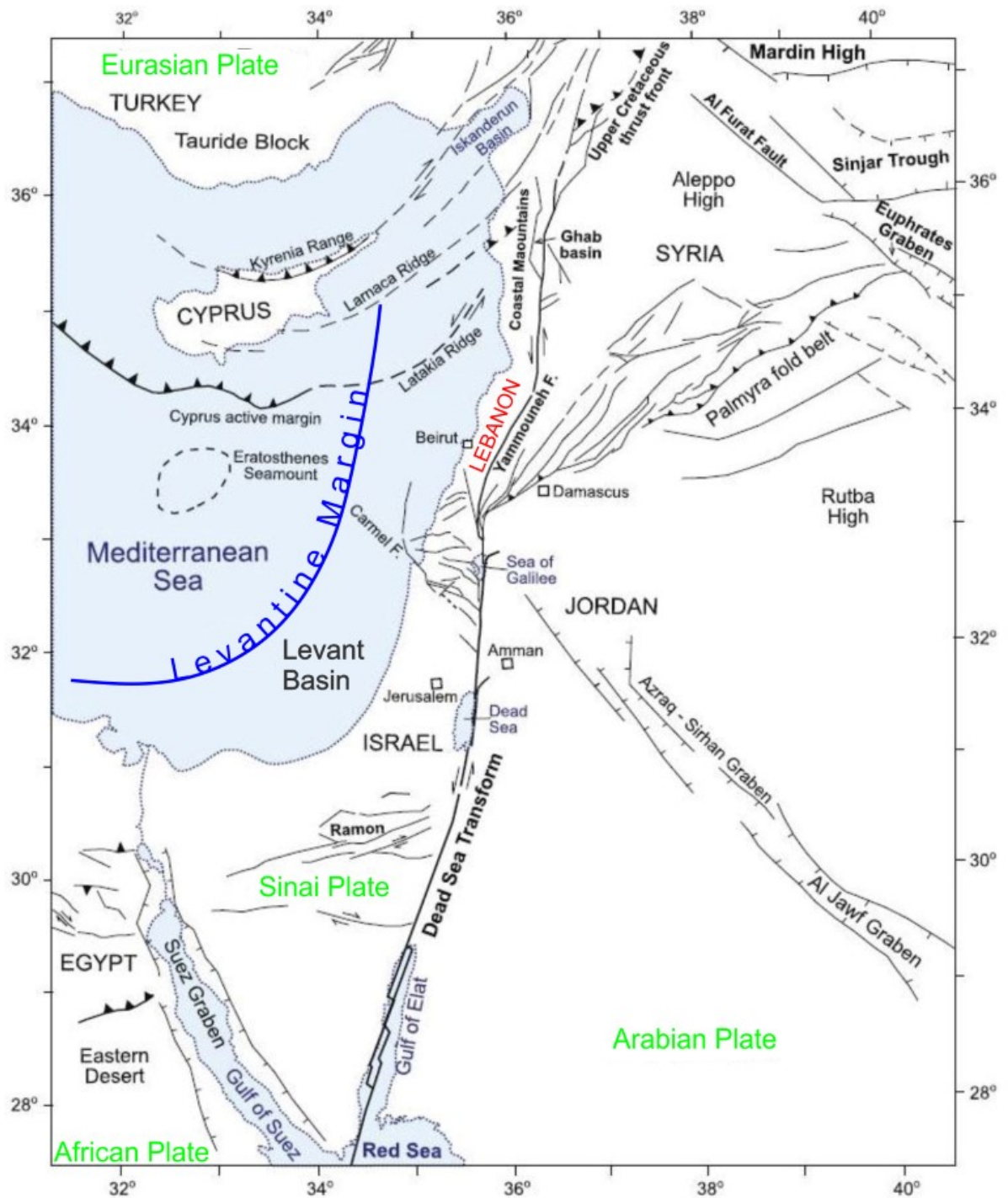


Figure 1.15: Structural geologic map of the Eastern Mediterranean region, modified from Segev (2009).

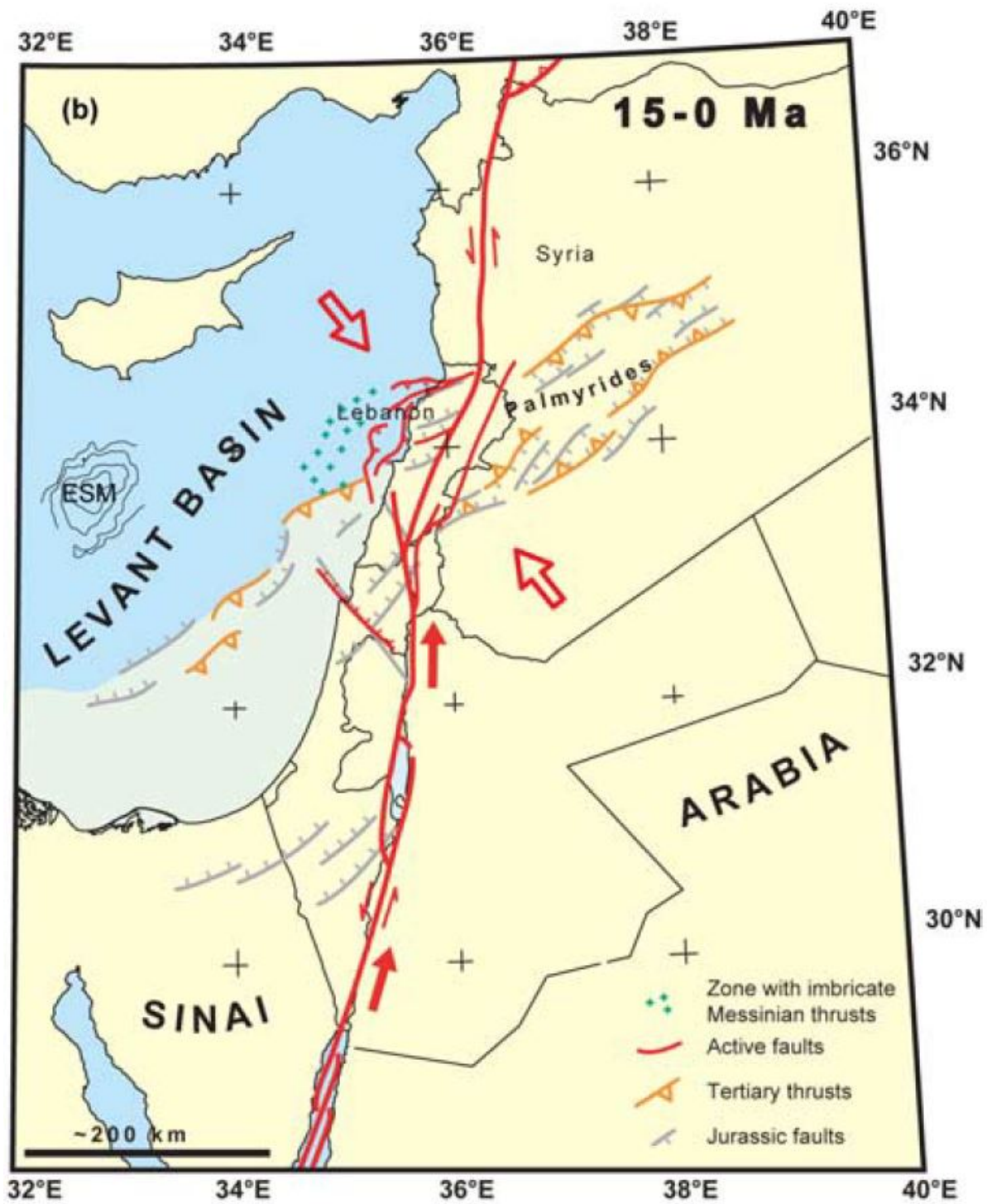


Figure 1.16: Tectonic evolution of the Levant margin, from Carton et al. (2009).

Walley (1998) puts the geologic features of Lebanon in a regional context and identifies three major tectonic phases: a two stage rifting phase from the late Palaeozoic to the early Mesozoic related to the opening of the Neotethys, a two stage compressional phase from the Upper Cretaceous to the Palaeogene (Syrian Arc events I & II, closing of the Neotethys) and the neotectonic rifting along the Dead Sea Transform Fault. Besides these Walley (2001) discusses also a later development phase of the Levantine Neo-Tethys and its multi-/single-stage and rifting/non-rifting nature. Early Cretaceous block faulting, regional uplift and alkaline basalt magmatism are caused by mantle plume activity rather than extension. Others, e.g. Homberg et al. (2009), identify a significant rifting episode during the Early Cretaceous. Collin et al. (2010) focusing on the Jurassic sedimentary evolution in Lebanon identify two major rifting phases in the Jurassic, a Triassic-Liassic and an Early Cretaceous phase, resulting in the thinning of the continental crust without formation of any oceanic crust. During the Middle and Late Jurassic (Bathonian-Kimmeridgian) a constant tectonic and geodynamic stability of the Levantine margin is suggested. Concerning the timing of the development of the DSTF there are differing ages given in Quennell (1958); Butler et al. (1998); Walley (1998). Homberg et al. (2009, 2010) reviewed the post-Palaeozoic tectonic history of the Lebanon region by mechanical analysis of meso-scale brittle faults throughout the country. Thus the tectonic evolution of the Lebanon area has been widely discussed during the last decades and the same tectonic events are not equally dated. The following summary of the tectonic history of Lebanon tries to represent the current state of research mainly based on the literature mentioned above.

1.3.1 The opening of the Neotethys

The opening of the Neotethys ocean in the late Palaeozoic triggered a series of extensional tectonic phases. A Late Permian to Mid-Triassic NE-SW aligned trend with only limited volcanism developing the Palmyrides structures reaching from the Euphrates to the Nile or even more to the West is called the Palmyrides trend. A second episode of rifting occurred in the Late Triassic to Early Jurassic and resulted in the opening of the Levantine basin and the development of the NNE-SSW trending Levantine passive margin. This NNE-SSW trend is called the Levantine trend. The latter affected a central NNE-SSW Israel/Palestine and Lebanon segment, whereas the other formed the outer NE-SW segments of the Palmyrides to the NE and the Sinai to the SW (Walley, 1998, 2001).

The Middle to Late Jurassic (Bathonian-Kimmeridgian) was a time of constant tectonic and geodynamic stability of the Levantine margin (Cohen et al., 1990; Collin et al., 2010).

1.3.2 Early Cretaceous extension

The Early Cretaceous rifting phase, detailedly described in Homberg et al. (2010), started during the Valanginian and ended at the beginning of the Cenomanian. The normal

faults developed at that time strike WNW-ESE to WSW-ENE with a mean dip of 60°. They have lengths of several kilometers to several tens of kilometers and offsets of up to several hundreds of meters. Extension was directed NNE-SSW with minor local variations and is responsible for the thickness variations in the Lower Cretaceous sedimentary sequences controlled by E-W faults. Considering the thickness variations in the Chouf Fm. the Early Cretaceous development of a WNW-ESE striking basin with a northern margin 50 km South of Tripoli is suggested. The southern margin due to burial by Palaeogene sediments can not be determined. [Collin et al. \(2010\)](#) doubt that this and the prior rifting phase in spite of significant thinning of the continental crust have led to the formation of any oceanic crust.

1.3.3 Eocene extension

Eocene normal faulting is grounded on NNE-SSW extension. Normal faults in Late Cretaceous to Palaeogene rocks can be correlated with this event. Since the extension direction resembles the one of the Early Cretaceous rifting phase, faults in pre-Late Cretaceous rocks, where tectonic development is not secured, can not be easily assigned to one of the two events ([Homburg et al., 2010](#)).

1.3.4 The closing of the Neotethys

[Walley \(1998, 2001\)](#) correlates (W)NW-(E)SE directed compressional tectonics resulting from the progressive closing of the Neotethys ocean and leading to the uplift of the Mount Lebanon and Anti-Lebanon ranges to the two Syrian Arc events dating to the Coniacian-Santonian and Eocene-Oligocene, respectively. However, more recent research on brittle tectonic features in Cretaceous to Cenozoic strata lead to a different model where a two-stage Miocene compression is suggested ([Homburg et al., 2009, 2010](#)). Compressional and transpressional deformation is related to the interaction of the African, Arabian and Eurasian plates.

Early Miocene compression

An initial folding in the Early Miocene is derived from a minor angular unconformity (less than 10°) beneath the Miocene strata. E-W compression preserved in several strike-slip and reverse faults in Early Miocene to Langhian (Middle Miocene) rocks always predates significant folding. Since this E-W compressional forces could not drive sinistral slip on the Yammouneh fault, it should not yet have existed in the Langhian.

Late Miocene compression

Local dip of the Middle Miocene units indicate that the formation of the Mount Lebanon Anticline (as well as the Bekaa syncline and Anti-Lebanon anticline) took place during the Late Miocene compressional event. A second significant unconformity separates undated, flat lying conglomerates from older Neogene conglomerates and is dipping W

at 30° along the eastern limb of the Bekaa syncline. The higher angle of the second unconformity indicates a greater importance of this tectonic event in comparison to the Early Miocene compression. Strike-slip and reverse faults from NNW-SSE directed compression both pre-dates and post-dates the folding. The clockwise rotation from E-W to NNW-SSE directed compression during the Late Miocene is interpreted as a re-organization of plate interactions in the Eastern Mediterranean and Middle East and corresponds to the initiation of the Dead Sea Transform Fault in Lebanon since the latter alignment is compatible with the kinematics of the Yammounéh fault.

1.3.5 Neotectonic rifting along the Dead Sea Transform Fault

The Dead Sea transform was another activation of the Levantine margin and started in the Miocene in response to the relative left-lateral movement between the African and Arabian plates ([Freund et al., 1970](#); [Garfunkel, 1981](#)). Tectonic motion along the sinistral Dead Sea Transform Fault (DSTF) also can be divided in two episodes. A first period of pure strike-slip motion without any transpression or transtension started between 14 and 10 Ma and lasted until 6 Ma. Then the first half of the 100-105 km of motion along the fault was transmitted straight through Lebanon along the Yammounéh Fault. In a second phase starting around 5-6 Ma with another ca. 50 km of displacement along a Lebanese restraining bend the motion pattern got more complex involving a number of fault splays and neotectonic transpressional uplift in both the Mount Lebanon and Anti-Lebanon ranges ([Walley, 1998](#); [Gomez et al., 2006, 2007](#)). However, deep-seated tectonics were not the only cause for the uplift. Investigations of [Steinberg et al. \(2014\)](#) concerning the uplift of the Judea Hills in Israel suggest that the uplift of the Mount Lebanon range after the initiation of the DSTF was not only tectonic but also for a significantly part the effect of flexural response to offshore loading in the deep Levantine Basin.

Whereas the parts of the DSTF north and south of Lebanon are striking N-S, its Lebanese section, the Yammounéh Fault, is striking NNE-SSW (see [Figure 1.16](#)). The overall displacement along the Yammounéh Fault is estimated about 47 km, the remaining 55 km of the 100-105 km of motion along the southern part of the DSTF is divided among the Serghaya Fault (ca. 20 km), shortening in the Syrian Palmyrides (15-20 km ?), the Roum Fault (max. 8 km), the Carmel-Fari'a Fault (5 km ?) and others within Lebanon and Galilee ([Walley \(1998\)](#), see [Figure 1.12](#) for location of the faults). Another aspect is the folding and faulting along the NNE-SSW trending offshore Mount Lebanon thrust ([Figure 1.14](#)). Variations in shoreline elevation indicate Late Holocene uplift activity along the Mount Lebanon thrust ([Morhange et al., 2006](#)), whereas [Homberg et al. \(2010\)](#) could not find enough evidence for significant regional onshore folding after the Early Pliocene and therefore suggest that shortening has migrated out of onshore Lebanon towards the West. However, the NNW-SSE orientated stress field should not have changed.

1.4 Lebanon's tectonic structures in a regional context

1.4.1 Mount Lebanon and the Palmyride Ranges of Syria

Walley (1998) geologically links the Mount Lebanon area with the close-by Syrian Palmyrides (Figure 1.17). The four divisions of the Palmyride area are the Northern and Southern Palmyrides and the adjacent Aleppo High to the North and the Rutbah High to the South. The Aleppo High continues westward across the Ghab Fault into the Jebel Ansariyeh Massif north of the Mount Lebanon range with no major structural differences (Ponikarov, 1967). Both the Northern Mount Lebanon and the Northern Palmyrides are dominated by NNE-trending box-folded anticlines. The Southern Palmyrides equally to the Southern Mount Lebanon area lies topographically lower than their northern counterparts and are dominated by more closely spaced narrow anticlines. The southwestward continuation of the separating Jhar Fault in Syria could be the Beit ed Dine-Qabb Elias Fault in Lebanon, although also more fault zones could be involved in a transitional zone. The southern Rutbah High's analog west of the DSTF is the central Israel/Palestine Sinea-Carmel Block south of the Carmel-Fari'a Fault (Walley, 1998).

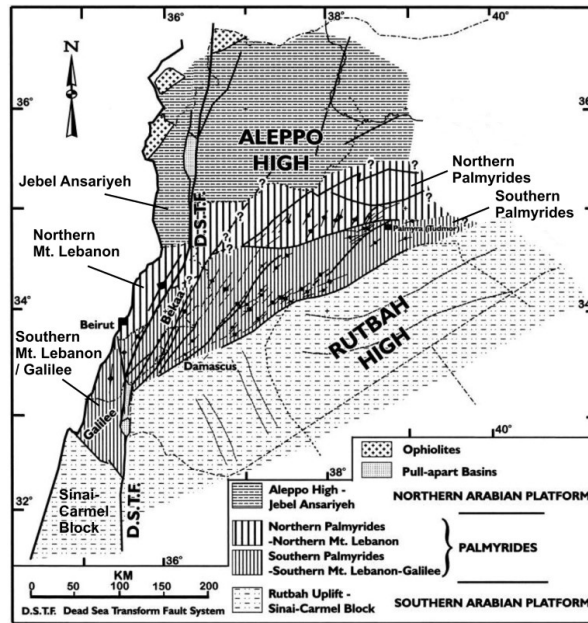


Figure 1.17: The four major tectonic divisions within the Lebanon-Syria region: Aleppo High - Jebel Ansariyeh, Northern Palmyrides - Northern Mount Lebanon, Southern Palmyrides - Southern Mount Lebanon/Galilee, Rutbah High - Sinai-Carmel Block, modified from (Walley, 1998).

1.4.2 The Levantine margin

The Lebanon flexure, a NNE-SSW-striking monoclinial flexure zone dipping westwards with a varying angle (45° to 90° , locally even overturning) can be followed for over 100 km from South of Beirut towards the northern edge of Mount Lebanon (Figure 1.13). Whereas west to the flexure pelagic sediments occur, shallow-water and peritidal sediments are found to the east. Walley (1998) concludes that prior to tectonic compression and inversion the flexure was a major Mesozoic basin margin and calls this feature the Lebanon hinge line. The folding of this older feature most probably happened in the Oligocene or little earlier coinciding with the formation of the Mount Lebanon anticline. Figure 1.18 shows the folded Cenomanian to Lower Eocene sequences separated from the Miocene rocks by an angular unconformity. The Lebanon hinge line resembles the better known, 150-km-long Mesozoic Carmel-Sinai hinge line along today's coastline of southern Israel/Palestine in age, facies development and orientation. These two could be the northern and southern parts of a Levantine margin hinge line continuing westwards with a N-E trend along the Egyptian coast (Figure 1.17).

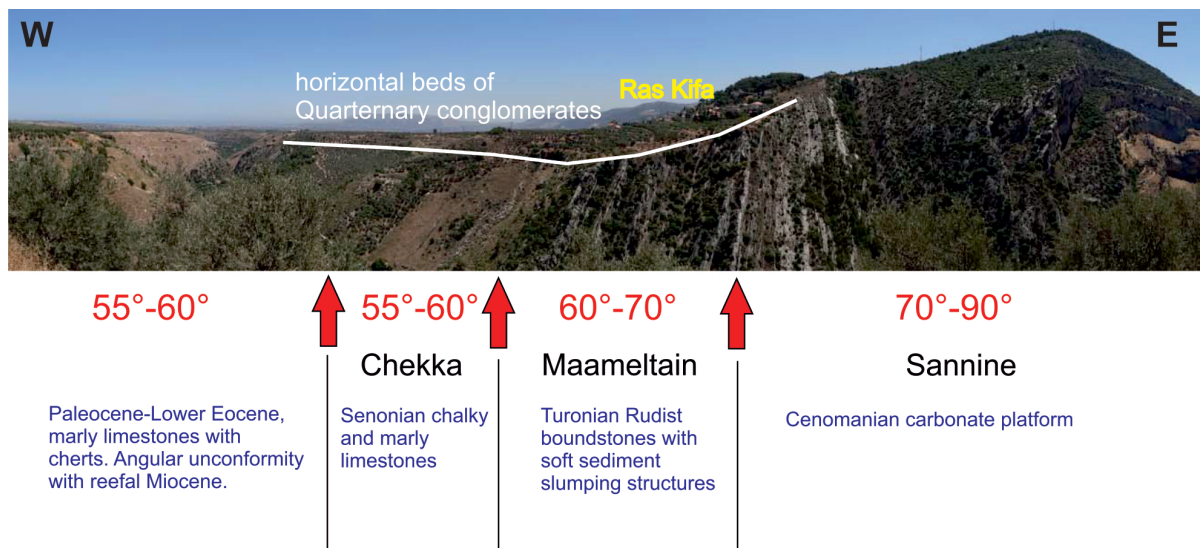


Figure 1.18: Stop 27, the Western Lebanon Flexure. Folded Cenomanian to Lower Eocene sequences unconformably overlain by Miocene rocks. The whole section is covered by horizontally bedded Quarternary conglomerates. The village of Ras Kifa is marked in yellow. A more detailed description of this section is found in Hawie et al. (2014).

1.5 Field campaign 2012

A field campaign was carried out for this study from July 4th to 9th, 2012 in the Northern Mount Lebanon area (Figure 1.19). 39 stops have been made, 6 rock samples have been taken for thin section analysis (see chapter 3) and 7 samples from the Chouf sandstone

have been taken for heavy mineral analysis (see [section 4.3](#)). The nature of the Qartaba structure has been investigated in more detail and is discussed in [chapter 2](#).

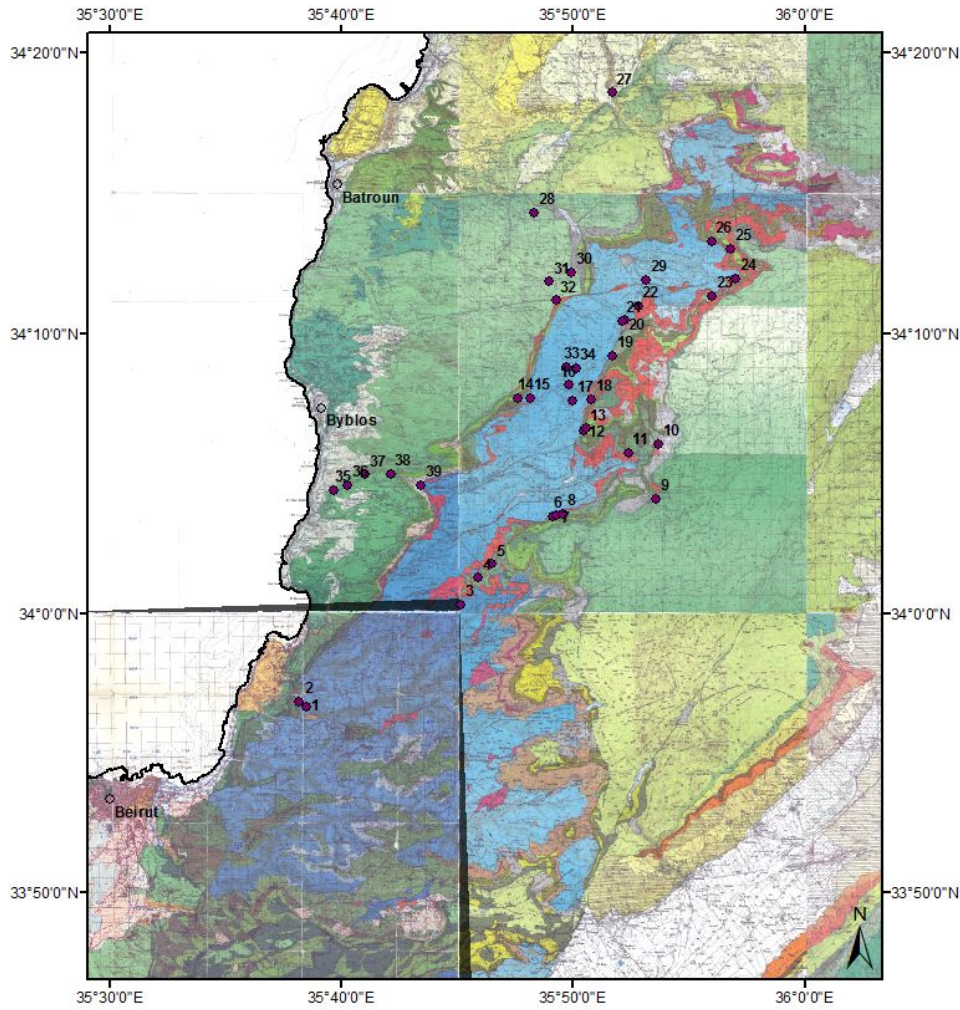


Figure 1.19: The 39 stops of the 2012 field campaign in the Northern Mount Lebanon region. Background is the geologic map 1:50000 of [Dubertret \(1975\)](#). The different sheets have slightly different nomenclature and legends. The blue color marks the Early to Middle Jurassic Kesrouane Fm. which here forms the core of the Mount Lebanon Anticline.

Methodology

Besides sampling and photo documentation the lithologies have been studied and structural analyses has been carried out. Orientations of bedding planes, fault planes, folds, joints, deformation bands and extension gashes have been measured. The data were documented for kinematic interpretations, i.e. shear sense of faults, orientation of folds, kinematics of compressional or extensional regimes and age relations between different deformation events (faulting and folding).

2 The Qartaba Structure

2.1 Location and layout of the Qartaba structure

The Qartaba horst structure covers the northern part of the NNE-SSW trending Mount Lebanon Anticline in the northern Mount Lebanon area (see description of Northern Mount Lebanon area in [subsection 1.2.1](#)) from the Nahr Ibrahim valley in the South to the Qadisha valley in the North (see [Figure 1.1](#) for location). In its central part the Jurassic rocks of the core of this box-fold like structure crops out. On its eastern and western limb rocks date from Early Cretaceous to Palaeogene (see cross section in [Figure 1.2](#)). [Nader and Swennen \(2004a,b\)](#) investigated the petroleum potential of this structure and came to a positive conclusion for that structural trap provided that its eastern contact with the Yammouneh Fault is impermeable. In that model the seal is formed by the Triassic Kurrachine evaporates known from offshore wells and seismic. A model of the Qartaba structure South of the Nahr Ibrahim valley is shown in [Figure 2.1](#). During the 2012 field campaign the nature of the Qartaba structure has been investigated but is not discussed in detail in this work. However, some overview stops are presented in this chapter.

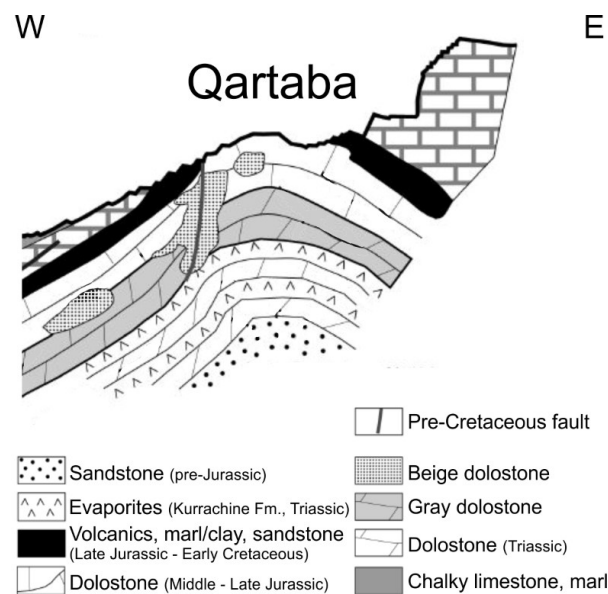


Figure 2.1: This figure shows a W-E cross section through the Qartaba horst structure South of the Nahr Ibrahim valley. Modified from [Nader and Swennen \(2004b\)](#).

2.2 Overview stops during the 2012 field campaign

2.2.1 Stop 6 - Bhassis

This view point is located near the village of Bhassis on the Eastern limb of the Qartaba Anticline. The picture in [Figure 2.2](#) is taken towards the North and shows the Eastern flanks of the Qartaba structure. The flat lying Jurassic carbonate sequences in the left bends down in a monocline in the center of the picture. The structure is highlighted by the mechanical anisotropy of the overlying Lower Cretaceous Chouf sandstone. The dm to m scale planar jointing in the limestones on the hill in the front of the picture might be anti-cracks with localisation of pressure solution cleavage, typical for axial plane cleavages in folded limestones under low grade metamorphic conditions. The dip of the proposed axial plane cleavage is $saxpl\ 115/89$.

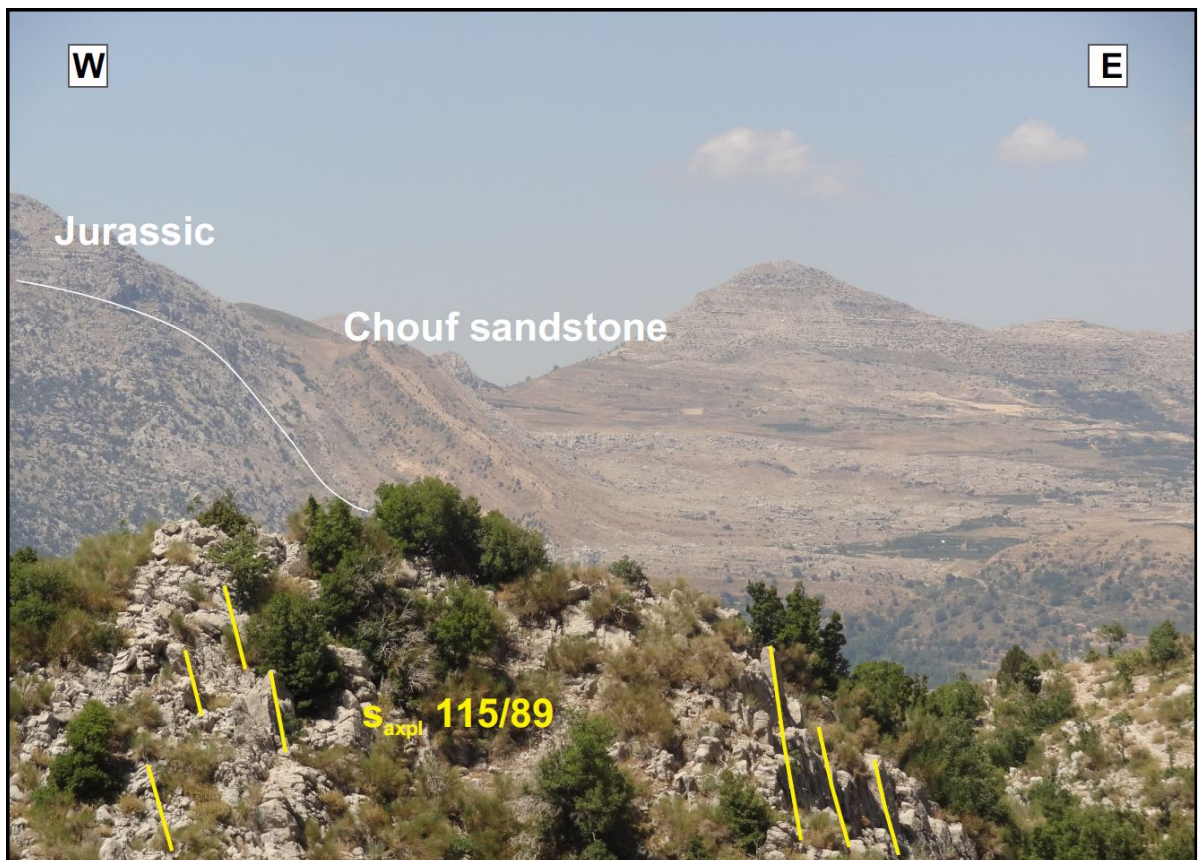


Figure 2.2: Stop 6. The Eastern flank of the Qartaba structure. Details in the text ([subsection 2.2.1](#)).

2.2.2 Stop 8 - Bhassis

This stop located about 900 m ENE of the village of Bhassis offered a great view over the Jurassic to Mid-Cretaceous sequences. [Figure 2.3](#) shows the view to the North onto

the Qartaba anticline and reveals the monoclinial shape of its Eastern limb outlining its box-fold nature. No exposed faults are associated with the folding and the deformation is most likely accommodated by the mechanical anisotropy of the stratigraphy (Yamato et al., 2011).

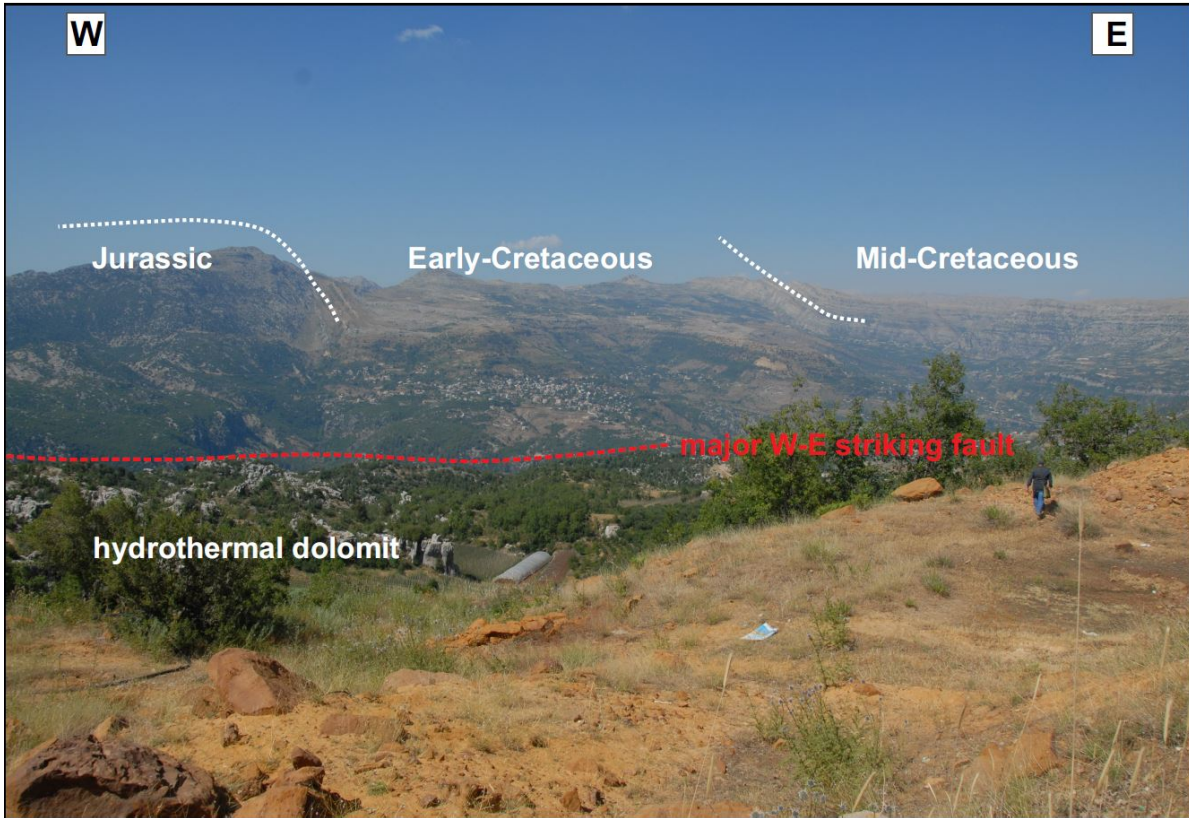


Figure 2.3: Stop 8. The Eastern flank of the Qartaba structure. Details in the text (subsection 2.2.2).

2.2.3 Stops 12 & 13 - Qartaba

These two stops are located about 2 km NNW of the village of Qartaba. Standing right on the Eastern monocline of the Qartaba structure within the Abeih and Mdairej Formations no faults, cataclasites or any evidence for flexural slip folding could be found. Stylolites with teethlengths of up to several centimeters indicate folding mainly by dissolution precipitation creep. Several generations of stylolites suggests the migration of the axial plane and the rotation of the limbs (Figure 2.4).

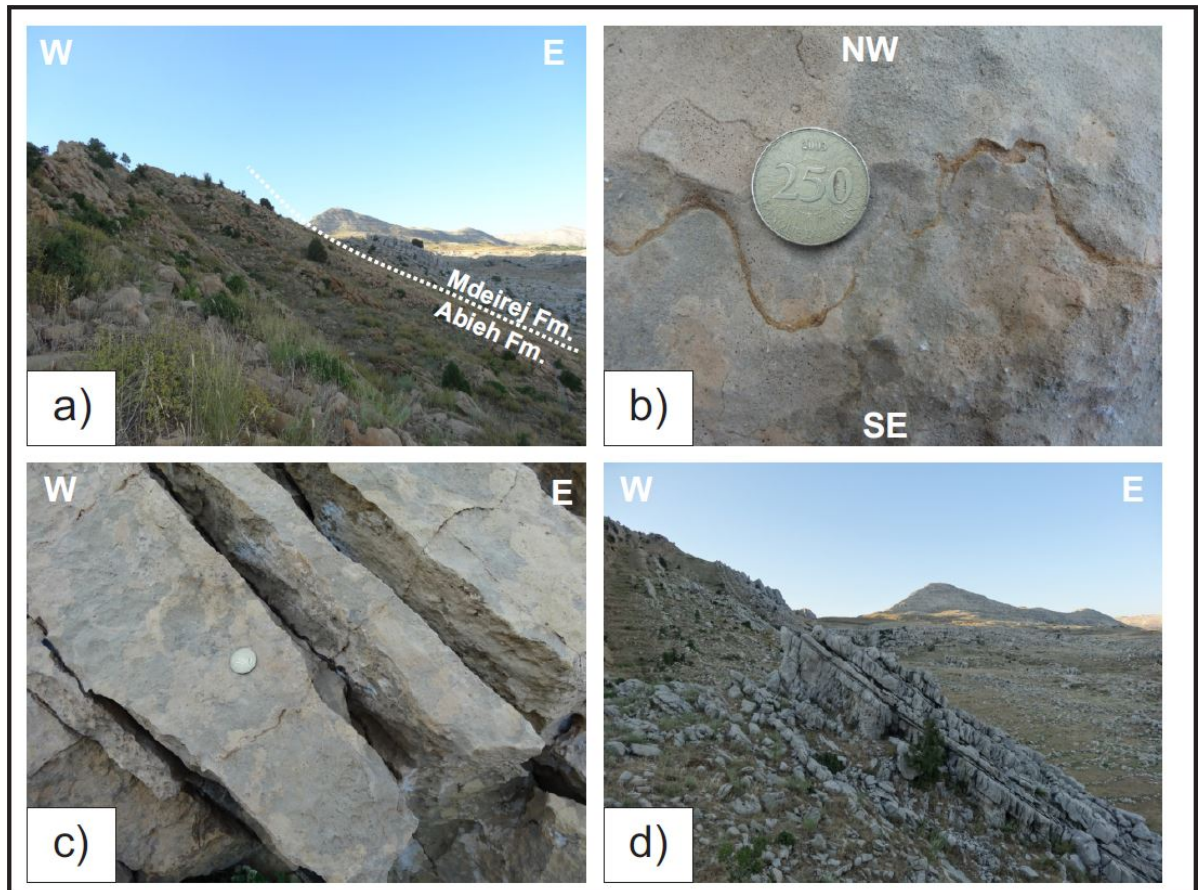


Figure 2.4: Stops 12 & 13. a) The Abeih Formation is a fossiliferous sandy limestone, of ochre yellow colour with some clay content. It is a transitional rock unit between the sandstones of the Chouf Formation and the shallow marine carbonates of the Mdairej Formation. The sedimentary bedding dips towards the east (ss 115/54). b) Stylolites within the Abeih Formation localizing along the hinge zone of the monoclinal fold of the eastern Qartaba box fold (sstyl 295/69). c) Cross cutting relationship between the stylolites (sstyl 315/55) and the bedding of the box-fold (120/54). d) Axial plane cleavage in the Mdairej Formation (ss 094/46). The axial plane cleavage (saxpl 290/69) is strongly used by surface dissolution processes and karst formation.

3 Thin section analysis

Nine thin sections of six samples from four different outcrops have been made (Table 3.1). The lithologic description and classification of the carbonate samples is based on Dunham (1962), Folk (1959, 1962) and Flügel (2004). Mechanical twinning of calcite is common in many of the investigated samples and predominantly corresponds to Type II twins in the classification of Burkhard (1993) (Figure 3.1).

Outcrop	Sample	Thin section	Lithology	Formation
14	14/01	14/01a	Limestone	Abeih Fm. (?)
14	14/02	14/02a	Limestone	Abeih Fm. (?)
18	18/01	18/01a	Limestone	Bikfaya Fm.
18	18/01	18/01b	Limestone	Bikfaya Fm.
21	21/01	21/01a	Limestone	Kesrouane Fm.
22	22/01	22/01a	Volcanoclastics	Bhannes Fm.
22	22/01	22/01b	Volcanoclastics	Bhannes Fm.
22	22/02	22/02a	Volcanoclastics	Bhannes Fm.
22	22/02	22/02b	Volcanoclastics	Bhannes Fm.

Table 3.1: Nine thin sections of six samples from four different outcrops have been examined.

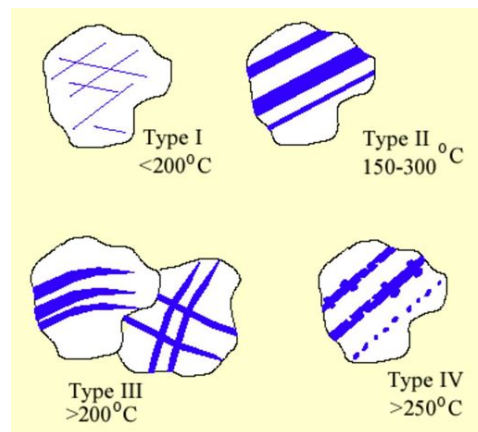


Figure 3.1: Classification of mechanical twinning in calcite, from Burkhard (1993).

3.1 Stop 14 - Abeih (?) Fm.

The outcrop at Stop 14 is an abandoned sandstone quarry (Chouf Fm.) cut by a newer road. It is located at the Eastern end of the village of Hrazmin on the Western limb of the Qartaba anticline. The nearby carbonate sequence from which samples 14/01 and 14/02 have been taken is probably part of the Lower Cretaceous (post-Chouf) Abeih Fm.

3.1.1 Sample 14/01

This sample can be macroscopically described as a greyish, ferruginous and porous limestone. [Figure 3.2](#) shows its richness in fossil fragments (bivalves, gastropods, echinoderms). Red algae indicate deposition in the photic zone. Micrite coating and cortoids are abundant, also peloids (fecal pellets) and ooids. The matrix consists of sparry cement, neomorphic spar occurs. Strain-free quartz grains with no evidence of crystal plastic deformation might be of volcanic origin. The observations indicate a high energy shallow water depositional environment. The sample can be classified as grainstone ([Dunham, 1962](#)) or unsorted biosparite ([Folk, 1962](#)), respectively. Apart from some minor veins no deformation was observed.

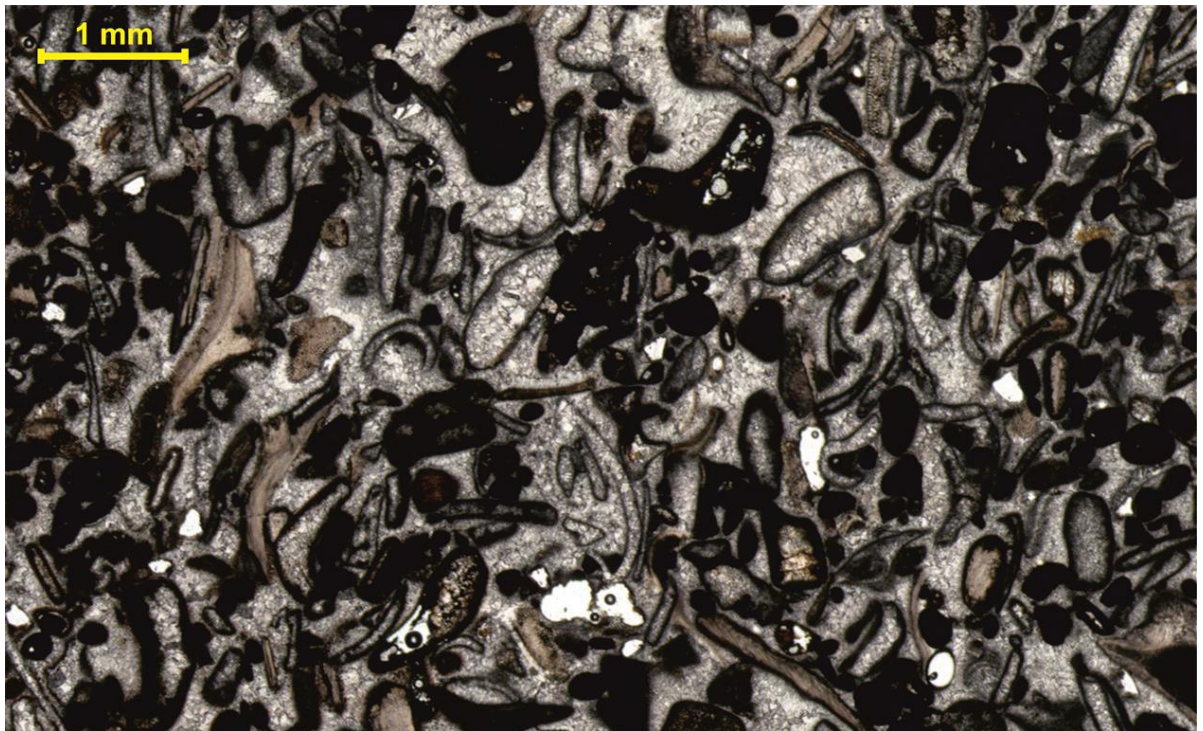


Figure 3.2: Thin section of sample 14/01a. This grainstone or unsorted biosparite consists of countless fossil fragments in a sparite matrix. Many fragments are recrystallized in sparite cement. The biodiversity comprises bivalves, gastropods, echinoderms and red algae. Cortoids, ooids and peloids (fecal pellets) are abundant.

3.1.2 Sample 14/02

The other sample from stop 14 looks already macroscopically different. It is light grey, less ferruginous and less porous. It can be classified as packstone (Dunham, 1962) or sparse biomicrite (Folk, 1962), respectively. This sample contains much less fossils. Dasycladacea and fragments of echinoderms and brachiopods(?) have been identified. The foraminifera *Kurnubia* and *Nautiloculina* confirm the Upper Jurassic age of the sample (Schlagintweit et al., 2005; Tasli, 2001). Water depth during deposition is to be set somewhat deeper than for sample 14/01. Stylolites indicate a volume loss due to pressure solution. Growth twinning in vein-calcite occurs, mechanical twinning is marginal.

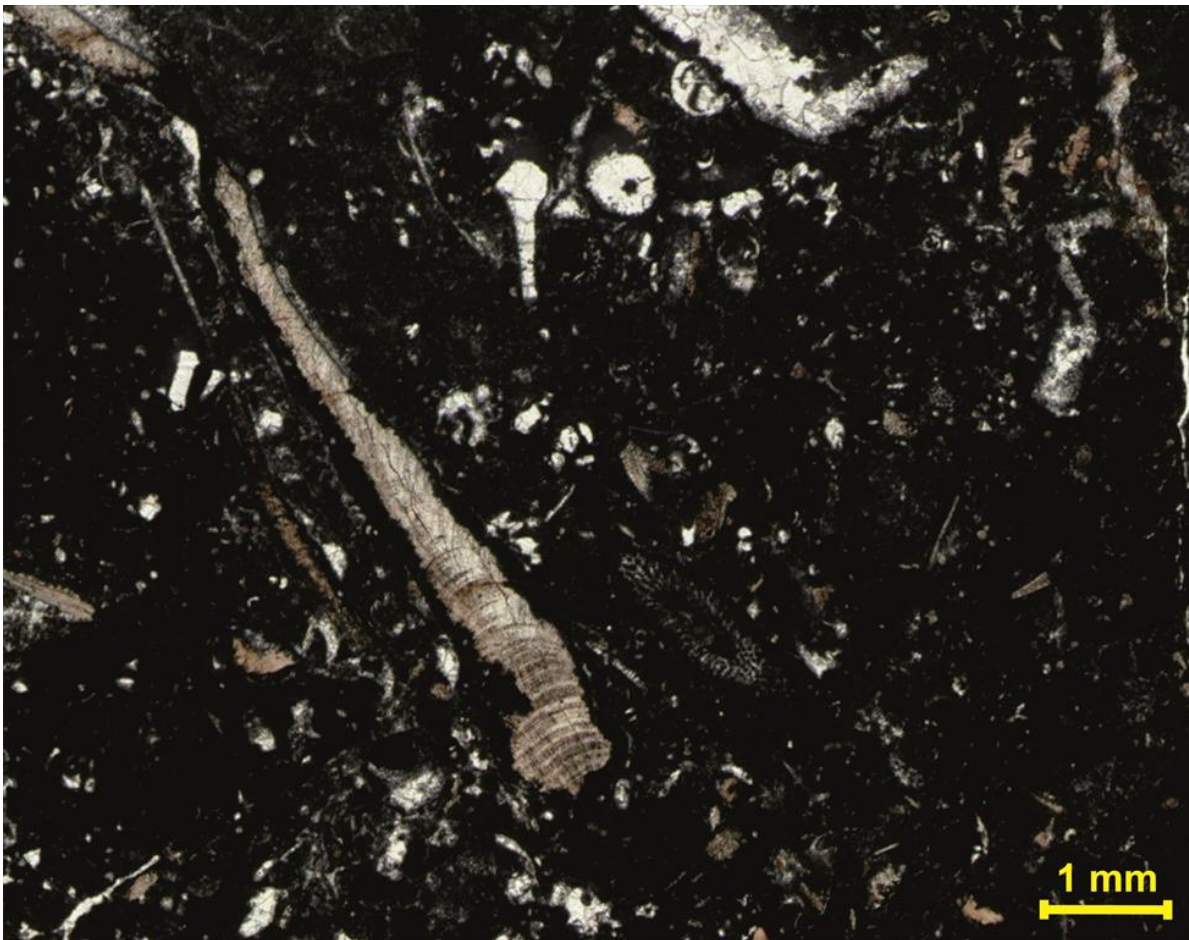


Figure 3.3: Thin section of sample 14/02a. This packstone or sparse biomicrite contains fragments of echinoderms and brachiopods (?). Green algae (Dasycladaceae) and foraminiferas have also been observed.

3.2 Stop 18 - Bikfaya Fm.

Stop 18, 500 m S of Moukhada, lies across the Qartaba Anticline nearly opposite to stop 14 on the anticline's Eastern limb. At this location the Bikfaya, Salima and Chouf Formations crop out very close to each other as NNE-SSW-striking narrow stripes. A local overthrust of the Kesrouane Fm. on the tilted Upper Jurassic and Lower Cretaceous sequences has been observed here. A rock sample has been taken from the Upper Jurassic Bikfaya Fm. which here forms the overturned limb of the Qartaba structure. The bedding is defined by syn-sedimentary pressure solution seams (stylolites) and dips steeply towards the W. The axial plane cleavage, also dipping towards the W, is defined by a pressure solution cleavage in form of wavy stylolites (Figure 3.4).

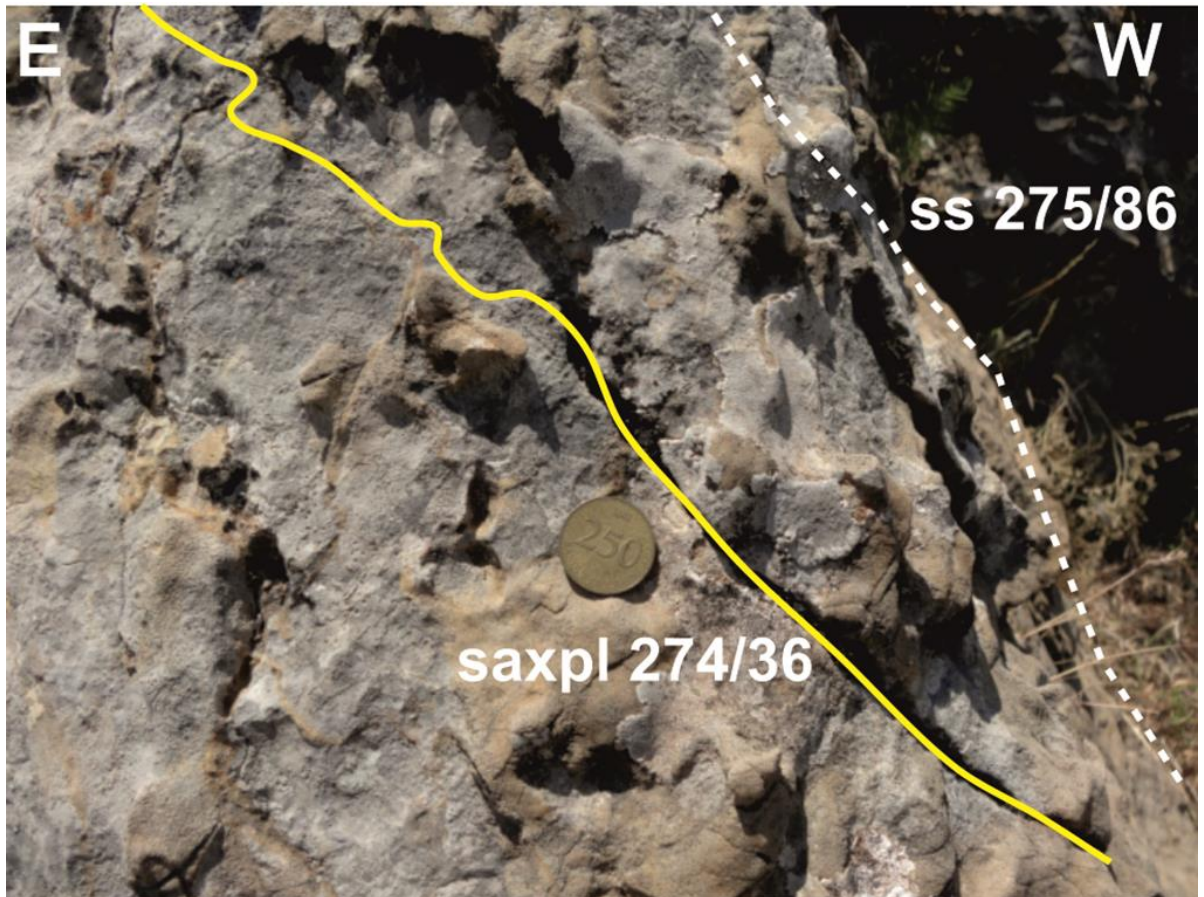


Figure 3.4: Detail of the overturned limb of the Bikfaya Formation at stop 18 of the 2012 field campaign. Sample location of sample 18/01. The bedding (ss) is defined by syn-sedimentary stylolites (white dotted line). The axial plane cleavage (saxpl) is developed in form of wavy stylolites (yellow line). See also thin section of sample 18/01 in Figure 3.5.

3.2.1 Sample 18/01

Two thin sections have been made from this micritic limestone (18/01a & 18/01b). The rock was classified as packstone ([Dunham, 1962](#)) or sparse biomicrite/poorly washed biosparite ([Folk, 1962](#)), respectively. Fossil fragments are mainly from green algae (*Dasy-cladaceae*) and some bivalves, gastropods and brachiopods. Upper Jurassic foraminiferas (*Nautiloculina*) have also been identified. Fragments are recrystallized (neomorphic spar). Calcite veins and stylolites are parallel whereas the former pre-date the latter. The veins are eroded by pressure solution. This can be explained by a consecutive change in the kinematics of deformation during folding ([Figure 3.6](#)). Mechanical twinning is abundant in the calcite veins. A marginal cataclastic overprint of the veins could be observed ([Figure 3.5](#)).



Figure 3.5: Thin section of sample 18/01b. Stylolite parallel to the calcite vein dissolves the latter. Calcite crystals in the vein show mechanical twinning. Cataclastic left part of the vein indicates brittle deformation mechanisms. Deformation responsible for the formation of the vein and the parallel stylolite is shown in [Figure 3.6](#).

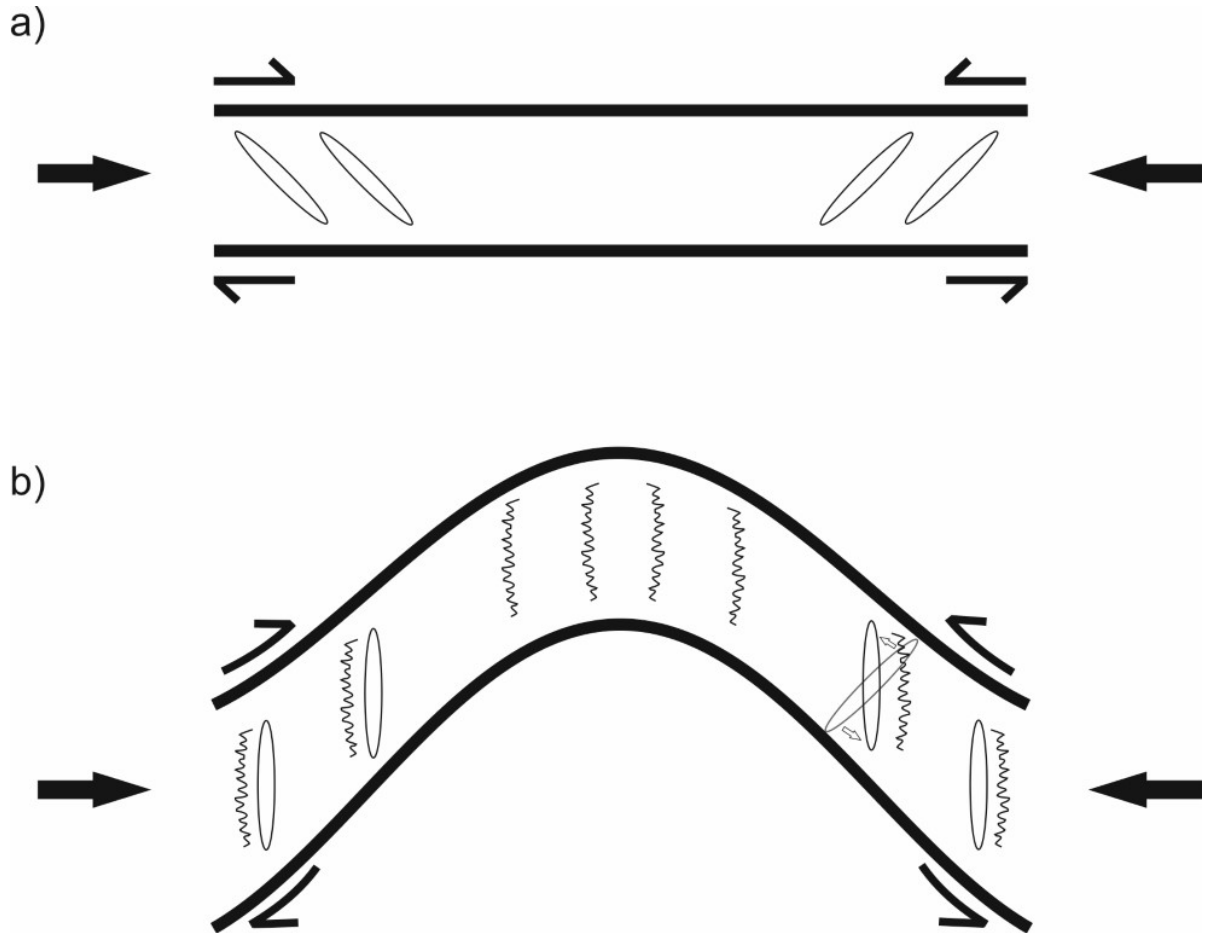


Figure 3.6: Deformation model for the Qartaba structure based on observations from stop 18 of the 2012 field campaign and thin section analysis. a) Veins opened during an initial phase of folding and flexural slip. b) During further deformation the veins are rotated and stylolites form parallel to them. In the field no brittle deformation could be observed in the hinge of the fold, only pressure solution (stylolites).

3.3 Stop 21 - Kesrouane Fm.

This stop is located 2.4 km NNE of Boaatara, W of the Boaatara potholo (also "Cave of the Three Bridges"), right on the Eastern limb of the Qartaba structure. The deformation of the Kesrouane limestone is here accommodated by the formation of a strong axial plane cleavage, which dips steeply towards E. The axial plane cleavage is formed by a pressure solution cleavage. Since only stylolites are recorded and no corresponding vein system has been observed, the folding process happened under non-isochoric conditions.

3.3.1 Sample 21/01

This limestone from the Lower to Middle Jurassic Kesrouane Fm. was classified as mudstone (Dunham, 1962) or micrite (Folk, 1962), respectively. Fossils are rare, some

coralline algae have been identified. Neomorphic spar occurs. Although stylolites forming the axial plane cleavage have been observed in the field, this thin section only shows minor stylolites and veins. No mechanical twinning in calcites was observed, thus internal deformation was low.

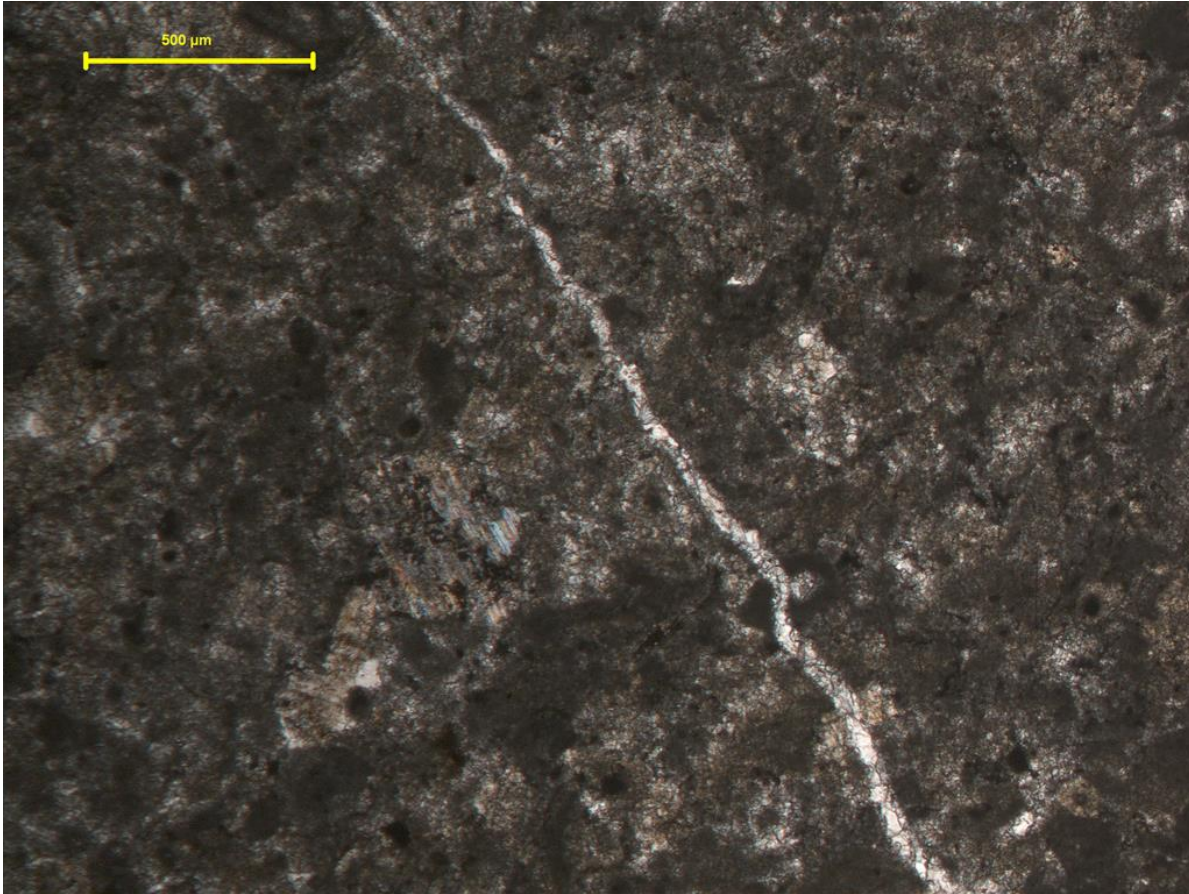


Figure 3.7: Thin section of sample 21/01a. This mudstone or micrite contains hardly any fossils. Only some coralline algae have been identified. Minor vein formation as seen in this picture occurs.

3.4 Stop 22 - Bhannes Fm.

This street outcrop is located about 400 m NNE of Meghrak on the Eastern limb of the Qartaba Anticline. Here the road cuts a major strike slip fault with an extensional component. The main fault on the geological map strikes roughly W-E and has dextral kinematics. The exposed fault, which can be clearly seen as a geomorphological lineament in the satellite image, strikes NW-SE and also has dextral strike slip kinematics. It is therefore interpreted as a synthetic Riedel fault. The fault is localized within the Upper Jurassic Bhannes Fm. along volcanoclastic rocks. Several meter thick

non-cohesive protocataclastic rocks contain organic-rich dark limestones and volcanic rocks. The cataclasites are bordered by several generations of slickensides with horizontal and vertical slickenlines. The deformation is also accommodated by pressure solution and vein formation, probably marking periods of velocity hardening alternating with periods of velocity weakening, which may represent seismic events. Two samples of the volcanoclastic fault rocks have been taken for further analysis.

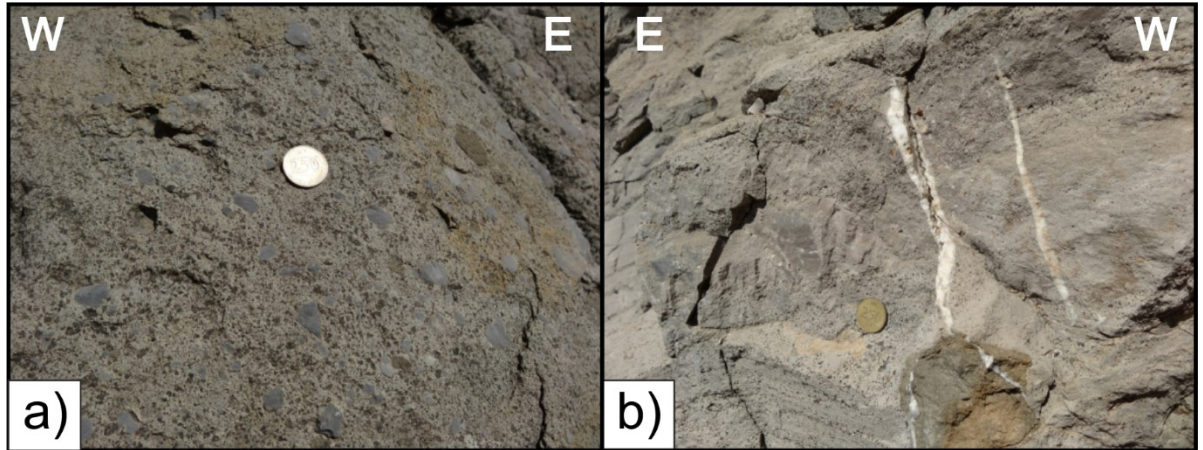


Figure 3.8: Volcanoclastic rocks at stop 22 of the 2012 field campaign. a) Volcanoclastic rock with dark, well rounded limestone clasts. b) Calcite veins cross cutting cataclasites document velocity weakening processes (cataclasites forming during seismic events) alternating with velocity hardening processes (dissolution precipitation creep). Veins and quartz micrograins with crystall preferred orientation possibly developed during a seismic event are seen in the thin sections of samples 22/01 and 22/02.

3.4.1 Sample 22/01

This sample of volcanoclastic rock contains lithoclasts of biomicrite and concretions of volcanic ash. Volcanic glasses have altered to chlorite. Minor calcite veins occur and calcite is abundant as a secondary filling of pores in volcanic glass. The matrix is a carbonate micrite. Quartz micrograins formed from a fluid occur alongside brittle fractures. Crystall preferred orientation of these quartz grains is not clear.

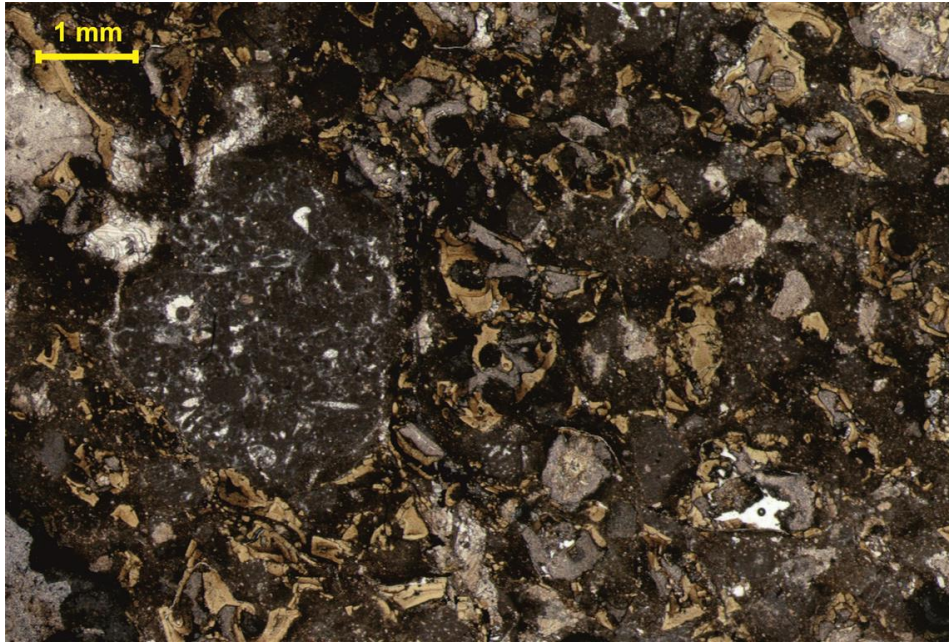


Figure 3.9: Thin section of sample 22/01b. Biomicrite lithoclast. Volcanic glass altered to chlorite (light-brown phases).

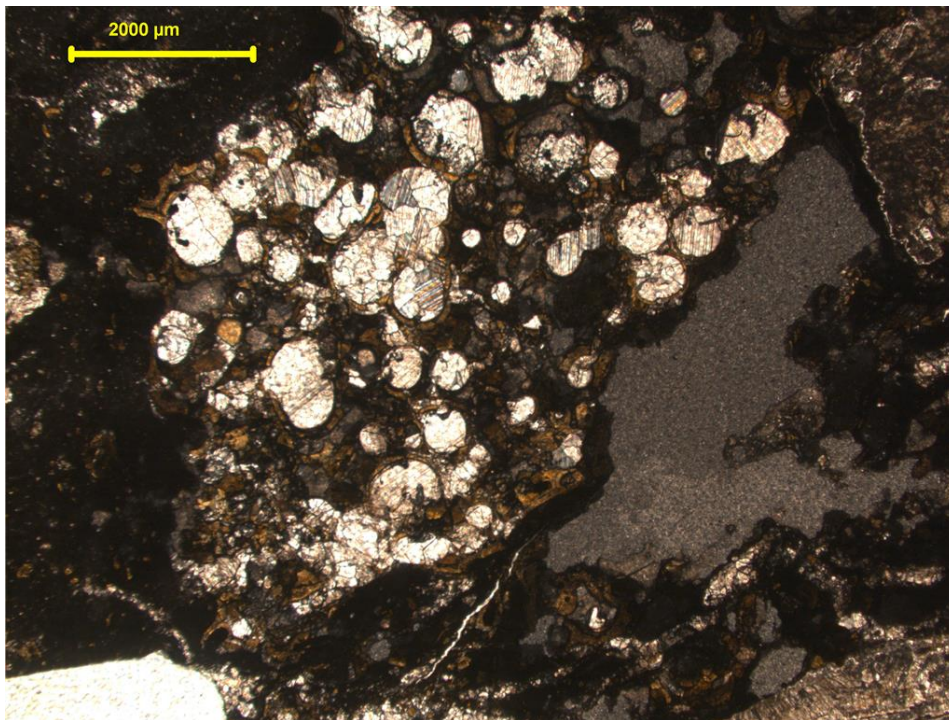


Figure 3.10: Thin section of sample 21/01a. Spherical calcite grains have grown in pores of volcanic glass.

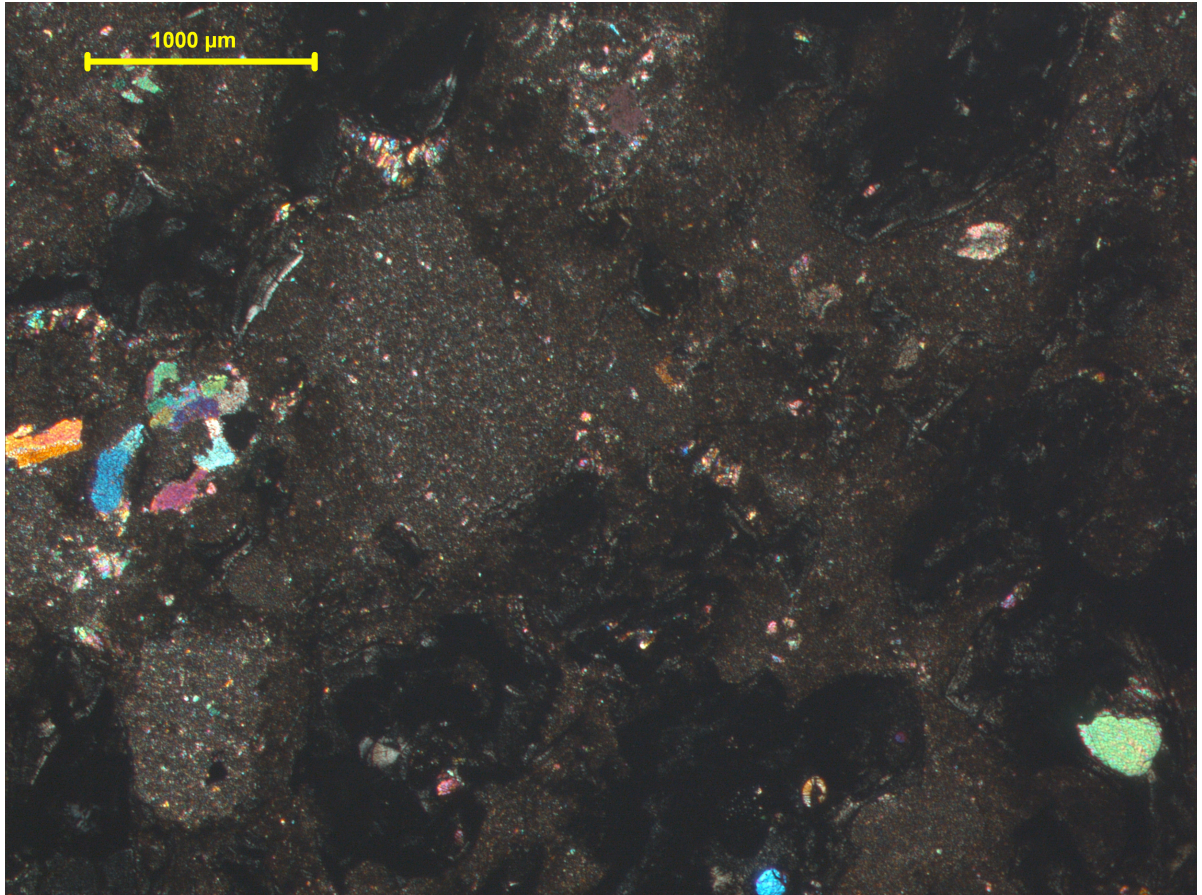


Figure 3.11: Thin section of sample 22/01b. Very fine grained volcanic ash concretion. Components have altered to calcite and chlorite. Picture was taken under crossed polarizers.

3.4.2 Sample 22/02

This sample of the strongly altered volcanoclastic rock contains a lot of lapilli altered to chlorite. A broad calcite vein is fractured by parallel faults along which quartz micrograins formed from a fluid. This dynamically recrystallized quartz grain show crystall preferred orientation whereas orientations on both sides of the fault are perpendicular to each other. Marginal parts of the vein are cataclastic and mechanical twinning of calcite is abundant in the veins. The matrix of this rock is a carbonate micrite. The fossil content comprises calcareous and silica sponges and Upper Jurassic foraminifera (Kurnubia).

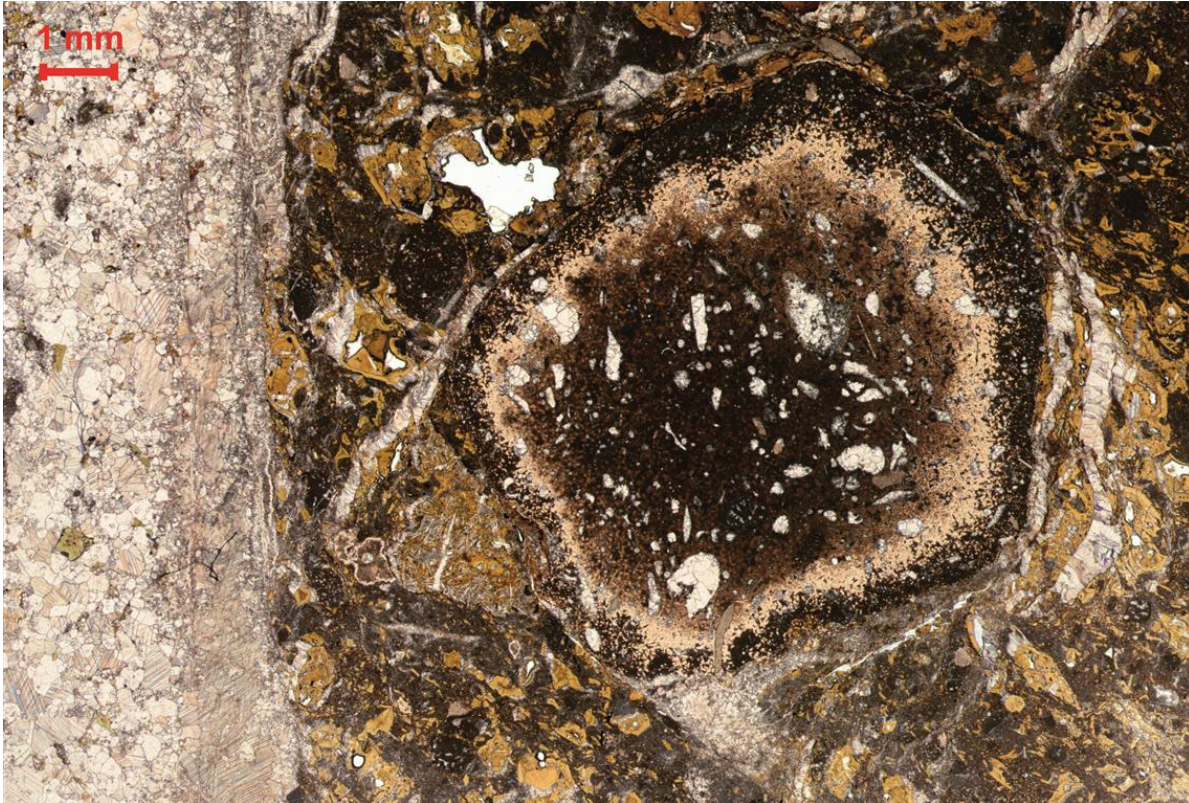


Figure 3.12: Thin section of sample 22/02a. Altered Lapilli. Secondary calcite in a micritic matrix are surrounded by a fine grained quartz rim. Calcites of the thick vein to the left show mechanical twinning.

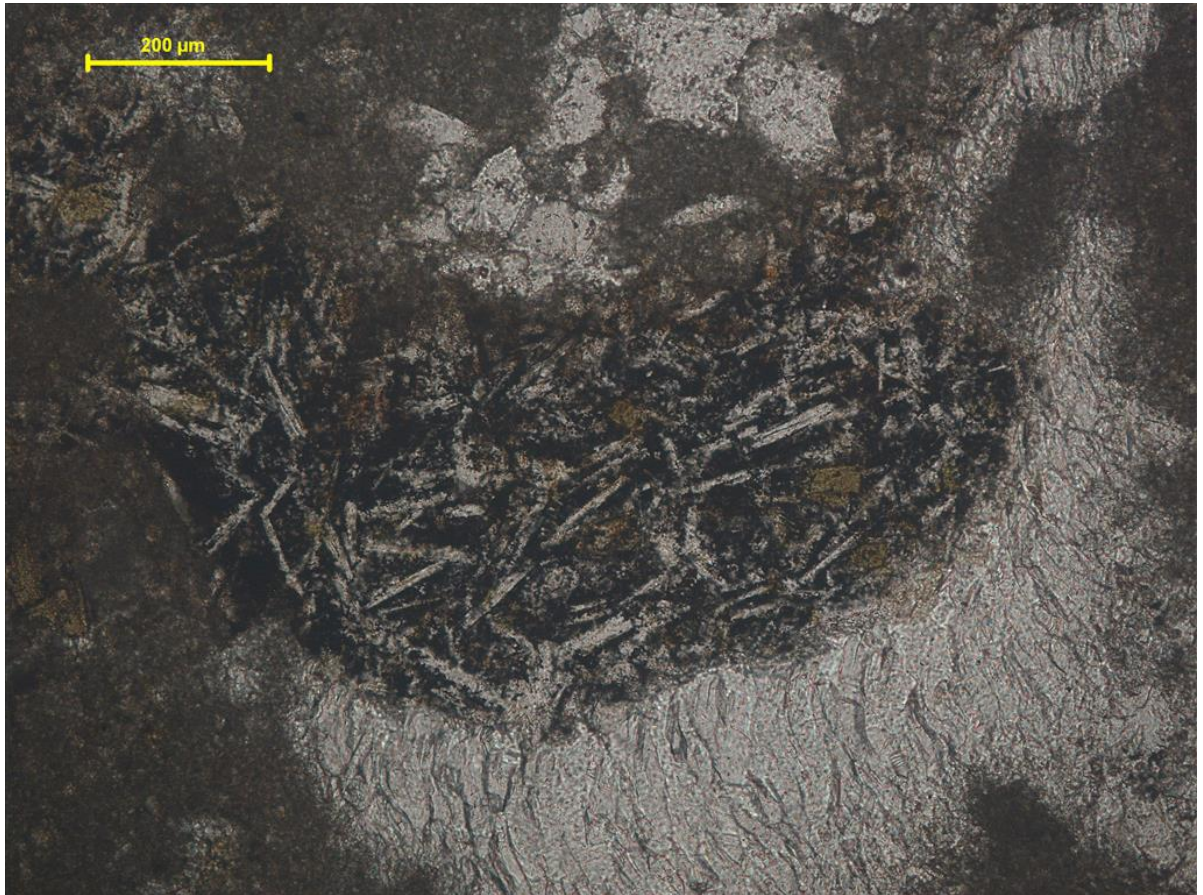


Figure 3.13: Thin section of sample 22/02a. Trachytic texture of volcanic clast.

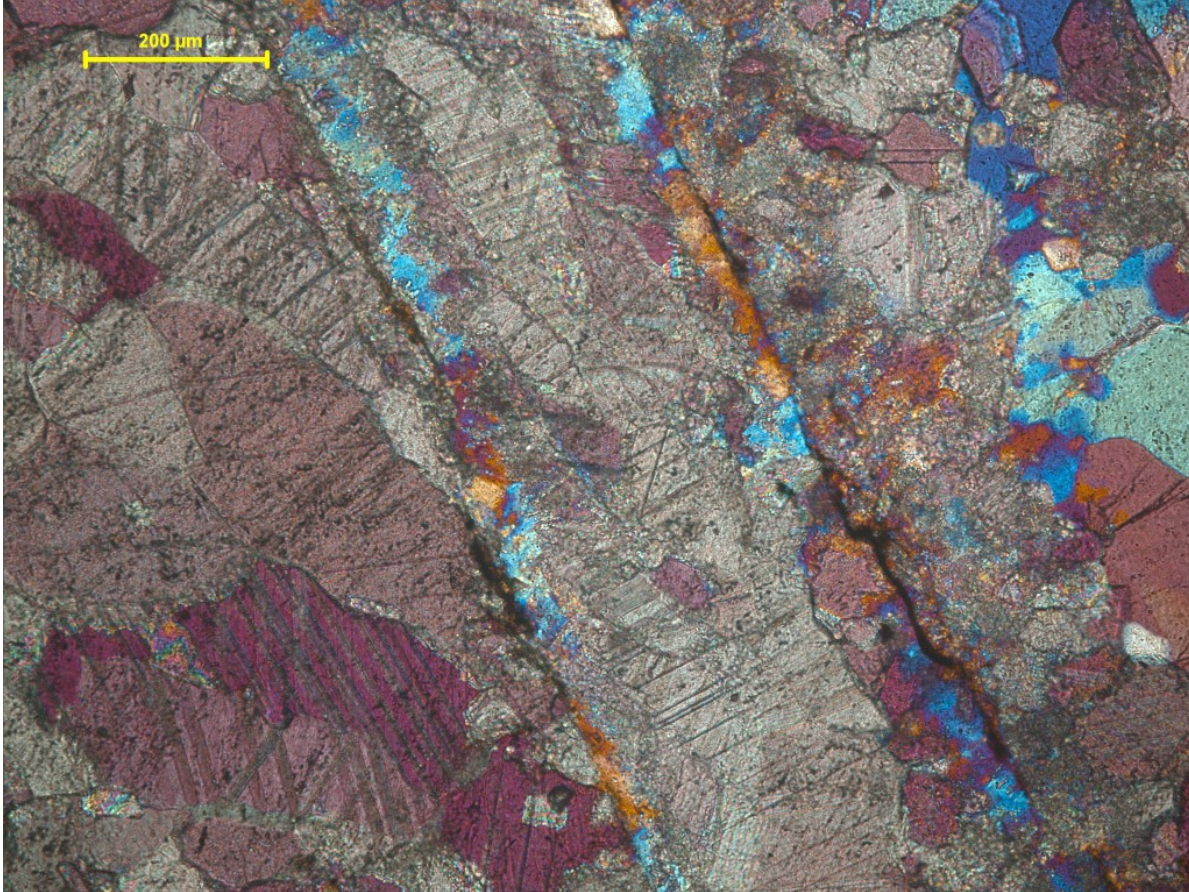


Figure 3.14: Thin section of sample 22/02a. Quartz micrograins along parallel fractures.

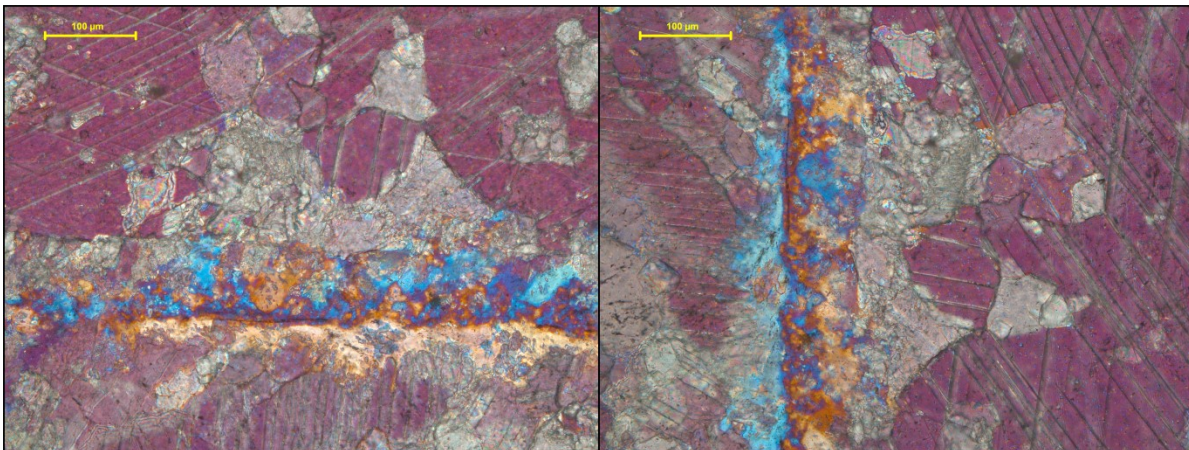


Figure 3.15: Thin section of sample 22/02a. Dynamically recrystallized quartz grains along fractures show crystal preferred orientation whereas orientations on both sides of the fault are perpendicular to each other.

3.4.3 Deposition and seismic indicators

Composition of the volcanoclastic rocks (lapilli, ash) indicate a subaerial, pyroclastic surge deposition. Carbonate lithoclasts and secondary calcite in veins and pores in the volcanics point to the general carbonate depositional environment. The documented velocity weakening processes in the cataclasites indicate seismic events. This might be supported by dynamic recrystallized quartz located alongside brittle fractures and showing low temperature bulging, which could be observed in the thin sections:

[Smith et al. \(2013\)](#) examined coseismic recrystallization of calcite during shallow earthquake slip and suggest that localized dynamic recrystallization is an important deformation process close to the principal slip surface at seismic slip rates $> 0.1 \text{ m}^{-2}$. In their experiments dynamic recrystallization of calcite occurred at distances $< 200\text{-}300 \text{ }\mu\text{m}$ from the principal slip surface. At greater distances deformation mainly lead to twinning and fracturing. In different experiments the bulk temperature along the principal slip surface after 1 m of slip was 650-900 °C. They also speculate that localized recrystallization of quartz, as described by [Bestmann et al. \(2011, 2012\)](#) at 8-10 km depth, could also occur more shallowly. In the case that the latter is possible the dynamic recrystallization and crystal preferred orientation of the quartz grains observed in sample 22/02 would count as an indicator for seismic deformation. However, temperatures and slip rates must have been higher than in the experiments described above.

4 The evolution of the Lower Cretaceous Chouf Formation

4.1 Stratigraphy and syn-depositional tectonics

The Lower Cretaceous Chouf Fm. (also Chouf Sandstone Fm. or Gès de Base) is dated to be Late Valanginian to Hauterivian in age. Due to its stratigraphic location between dominantly carbonate strata this mainly clastic sequence is easily identified in the field as it's also widely covered with pine trees. The Chouf Fm. is mainly cross bedded and comprises ferruginous (orange-)brown to white sandstone locally associated with varying amounts of clays, shales, lignites, fossilized materials (fragments of wood and coal), pyrite, marcasite and amber. Volcanics occur at its base and a fossiliferous argillaceous bed at midsection. A more detailed sedimentological analysis ([Bellos, 2008](#)) of the Chouf-Fm. in the Jezzine region in southern Lebanon identified six different microfacies: arenites, muddy quartz-rich sandstones, clayey-muddy quartz-rich sandstones, graywacke, clay and limestones. In that study also the source and reservoir properties of the Chouf Fm. regarding hydrocarbons were examined.

The depositional environment is widely agreed to be of fluvio-deltaic characteristics as both dune and fluvial structures as well as marine-dominated strata are observed. However, some studies found minor difficulties with the deltaic model as transgressions and tidal effects may locally have overprinted the deltaic character.

As origin the Nubian sandstones of Egypt, the Jordanian sandstones (Hathira Fm.) and/or the Ruthabah sandstones in Syria (Cheriffe Fm., itself originating from the Jordanian Hathira Fm.) are named ([McKee \(1963\)](#); [Kanaan \(1966\)](#); [Wakim \(1968\)](#); [Tixier \(1972\)](#); [Dubertret \(1975\)](#); [Walley \(1997\)](#) in [Bellos \(2008\)](#)).

An outcrop map of the Chouf Fm. in the Northern Mount Lebanon region is shown in [Figure 4.7](#)).

4.1.1 Stratigraphic contacts

The Chouf Fm. is marked by a major unconformity at its base where it overlies either one of the Upper Jurassic formations (Bhannes, Bikfaya, Salima Fms.) or directly the massive, mostly Lower to Middle Jurassic Kesrouane Fm. However, recent research suggests that the Kesrouane-Fm. probably extends as far as to the Early Kimmeridgian ([Collin et al., 2010](#)). The upper boundary is clear, the overlying Abeih Fm. is abundant in oysters, dated to the Barremian, and contains pisolites ([Walley, 1983](#)).

4.1.2 Syntectonic deposition

During most of the Jurassic period the Lebanon region was characterized by a subsiding but tectonically stable, shallow marine epicontinental shelf where the massive carbonates of the Kesrouane Fm. were deposited. However, during the Kimmeridgian marine regression, rifting and block faulting started. The rifting was associated with volcanic activity. The resulting continental volcanic rocks of the Bhannes Fm. vary in thickness and are found from northern to southern Lebanon today. The top of the Kesrouane Formation was locally karstified and paleosoils formed. During the Kimmeridgian-Tithonian a new transgression led to another suite of shallow marine, carbonate shelf deposits, the Bikfaya and Salima Fms. It shows rapid lateral thickness variations due to active block faulting and erosion. The end-Jurassic marine regression led to the subaerial exposure of the entire region. Intense erosion occurred, which led to the Berriasian gap in the stratigraphic record. The erosional surface, locally with incised valleys, was then buried by the unconformably overlying, mostly deltaic-fluvatile sandstones of the Lower Cretaceous Chouf Fm. (Valangian-Hauterivian) during another phase of rifting. The thickness variations of the Bhannes and Bikfaya Fms. match up. Where one is very thin or absent the same is true for the other one and their maximum extends generally coincide. Where both formations are absent the Chouf Fm., also being of variable thickness, directly overlies the top of the Kesrouane Fm. Following this argumentation [Collin et al. \(2010\)](#) suggest a Late Jurassic tilted block morphology, which was then buried by the deposition of the Chouf sandstones ([Figure 4.1](#)).

Based on brittle faults analysis [Homberg et al. \(2010\)](#) correlate the deposition of the Chouf Fm. with the Early Cretaceous rifting phase, which started during the Valanginian and ended at the beginning of the Cenomanian. The normal faults developed then strike between WNW-ESE to WSW-ENE with a mean dip of 60°. Extension was directed NNE-SSW with minor local variations and is responsible for the thickness variations in the Lower Cretaceous sedimentary sequences controlled by E-W faults. Considering the thickness variations in the Chouf Fm. they suggest the Early Cretaceous development of a WNW-ESE striking basin with a northern margin 50 km south of Tripoli. The southern margin due to burial by Palaeogene sediments can not be determined. The westward thickening implies an offshore continuation of the Lebanese basin through the Levantine basin ([Homberg et al., 2009](#)).

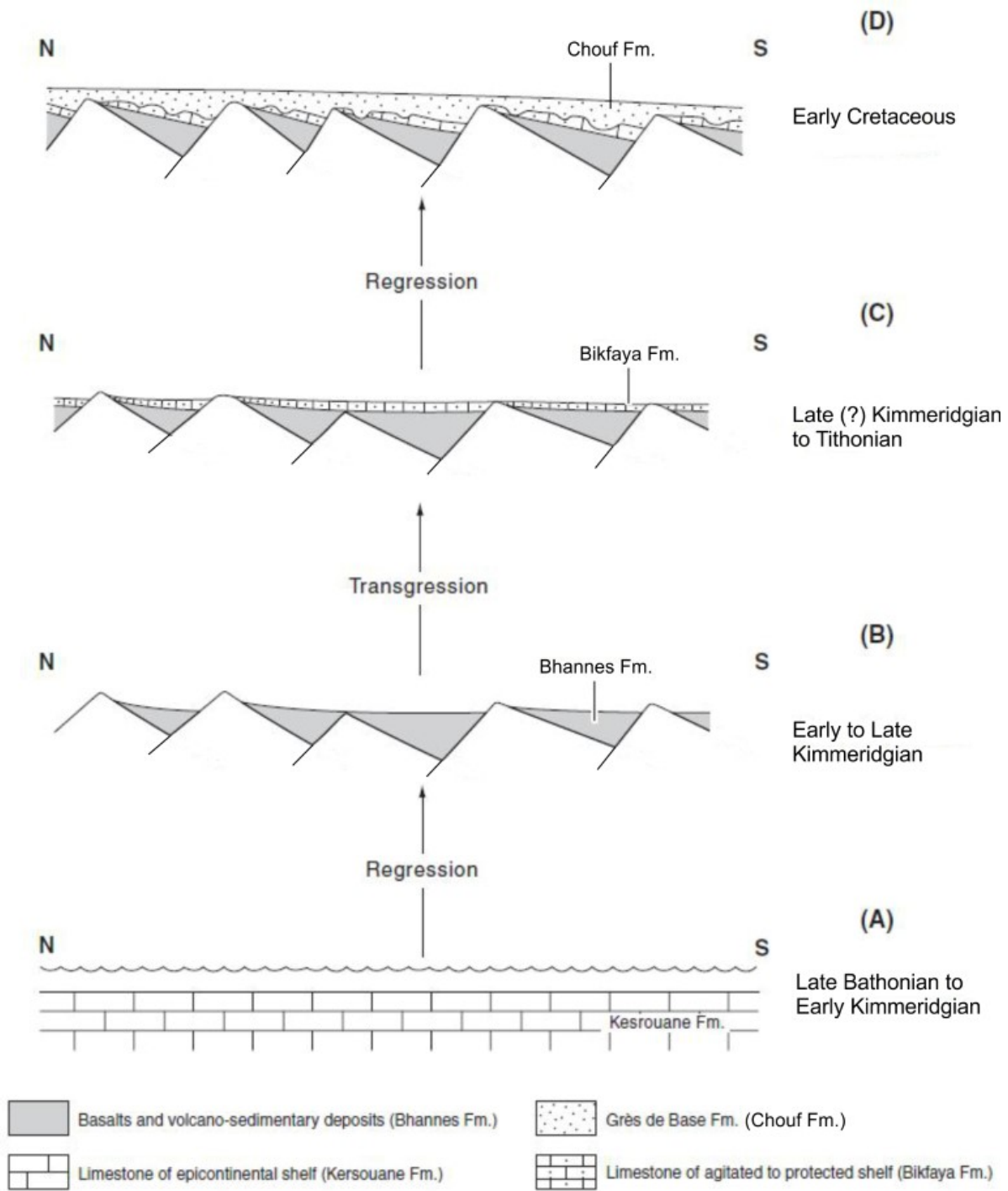


Figure 4.1: Tilted block tectonics and sedimentation from the Middle Jurassic (Bathonian) to Early Cretaceous, modified from Collin et al. (2010).

4.2 Field observations

During the 2012 field campaign eight outcrops of the Chouf Fm. have been visited (stops 2, 4, 5, 7, 14, 18, 23 and 26), whereas stop 26 was an outlook and sampling spot only. At seven of these stops samples for heavy mineral analysis have been taken (all except stop 5, see [section 4.3](#)). See [Figure 1.19](#) for outcrop locations and attached field report for further information on the outcrops including pictures and structural plots.

4.2.1 Stop 2 - Jeita Grotto

Stop 2 is located about 3 km E of Nahr El Kalb near the Jeita cave (Jeita Grotto) in the southeastern part of the Northern Mount Lebanon area. In this street outcrop the yellowish-brown to white, coarse to fine grained sandstone is well-bedded (dm-m) and records several layers with clear cross bedding ([Figure 4.2](#)). Under the hand lense the sandstone appeared well-sorted with partly coated grains by iron oxides. This coating was confirmed during heavy mineral analysis. Although the sandstone has generally been deposited in a fluvatile environment, here dunes are locally preserved. The general dip of the bedding in this outcrop is towards WSW with about 40°. Most of the cross-beds dip with a steeper dip angle as the bedding but in the same western direction. However, a few layers with cross-beds dipping to the E have been observed. About 100 m to the S a minor E-W-striking sinistral fault is offseting the stratigraphic boundary between the Chouf Fm. and the underlying Kesrouane Fm. ([Dubertret, 1955](#)). The apparent offset is about 180 m.

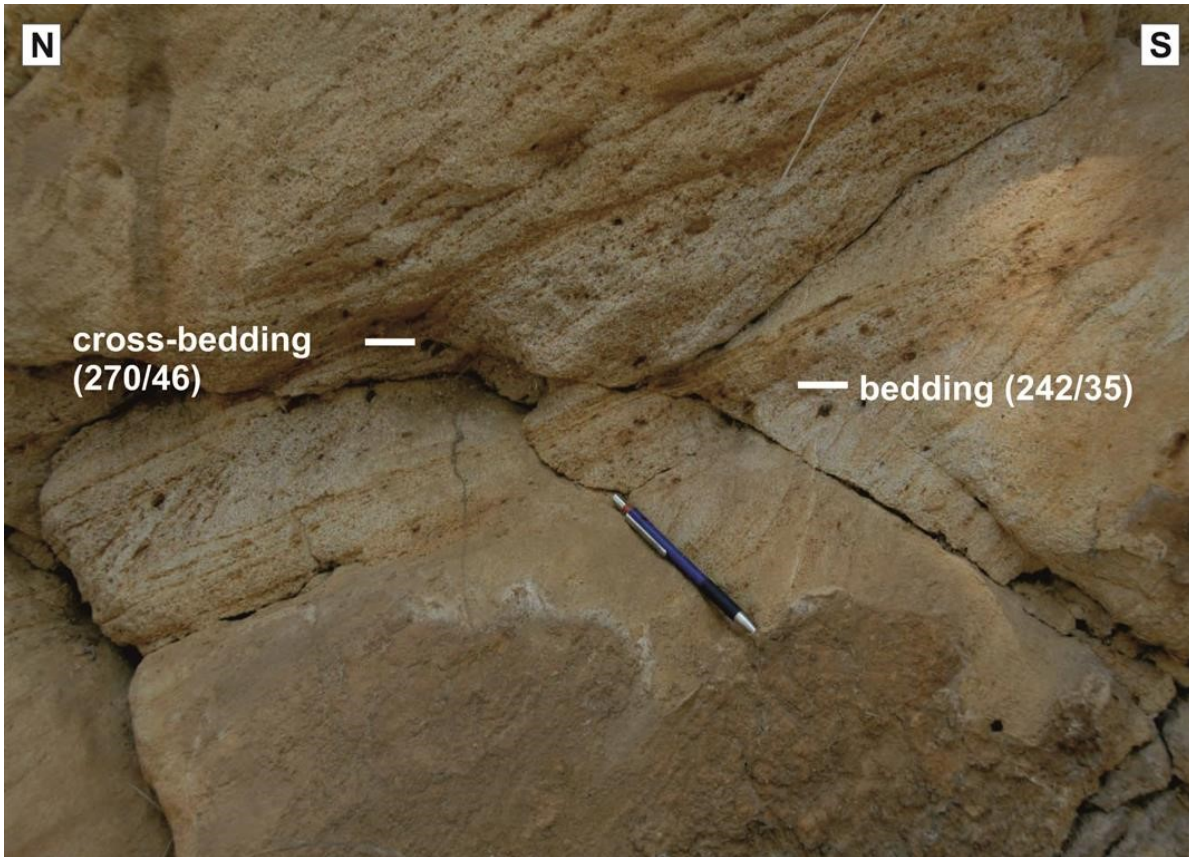


Figure 4.2: The Chouf Sandstone (bedding ss 242/35) with cross-bedding (scb 270/46) at stop 2. Although most of the cross-beds dip in a western direction like the bedding (but with a steeper dip angle), few layers with cross-beds dipping to the East (089/15) have been observed.

4.2.2 Stop 4 - Mairouba

This sand pit lies about 1 km NNW of Mairouba on the Eastern limb of the Qartaba Anticline. Here the Chouf sandstone shows white to reddish/brown sand layers with nicely developed foresets. The beds are dipping shallowly towards SW. A several dm-thick coal/clay layer serves as a marker horizon in this outcrop. Although numerous N-dipping normal faults cut through the layers with offsets up to 1 m, the marker horizon does not record any significant downthrow along the exposed section. This observation suggests that most of the faults are high angle normal faults, which were all rotating in the same direction during extension resulting in a domino or bookshelf type of deformation. The normal sense of shear indicates a roughly N-S oriented extension direction. Those sections in the outcrop which are not faulted are cut by numerous compaction bands localizing the meteoric fluids (Figure 4.3).

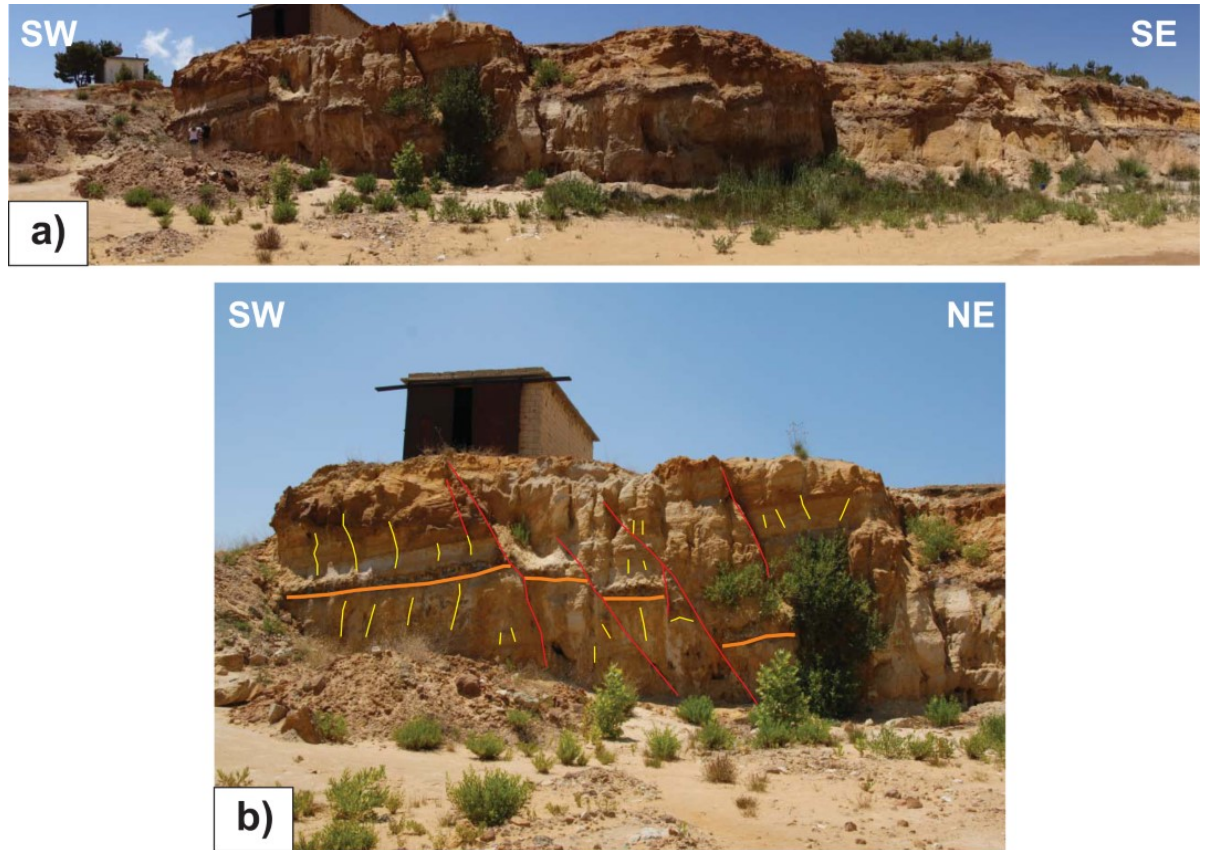


Figure 4.3: The Chouf Fm. at stop 4. a) A clay/coals marker horizon approximately in the middle of the exposed vertical section traces more or less horizontally through the outcrop although several N-dipping faults with several dm offset cut through the sequences. b) Mostly parallel and subordinated conjugate normal faults with an off-set of 30-50 cm. The general mean dip of the faults is $010/65$. The conjugate set dip $180/80$. Yellow lines: deformation bands (compaction bands); red lines: fault trace; thick orange line: marker horizon.

4.2.3 Stop 5 - Ain Ed Delbe

This stop was held at another sandpit about 700 m ENE of the village of Ain Ed Delbe. This section through the Chouf sandstone shows several local systems of eroding syn-sedimentary channels. A fluvial to deltaic and/or littoral depositional environment can be deduced. The sedimentary bedding dips shallowly towards E. Vertical joints and/or deformation bands ($290/82$) were observed.



Figure 4.4: Stop 5 is an active sand pit in the Chouf Fm. The erosive channel seen in the picture is cut perpendicular to the channel axis (looking towards E).

4.2.4 Stop 7 - Bhassis

This sandstone cliff near the villag of Bhassis is also located on the Eastern limb of the Qartaba Anticline. It shows a normal fault (sf 045/60) which offsets the marker layers for about 10 m. The fault core is composed of dm thick clay smear and acts as a significant barrier for the meteoric fluids. The sandstones in the hanging wall are differently coloured than those of the footwall due to iron oxide coating of the grains. The footwall seems almost unaffected by alterations.

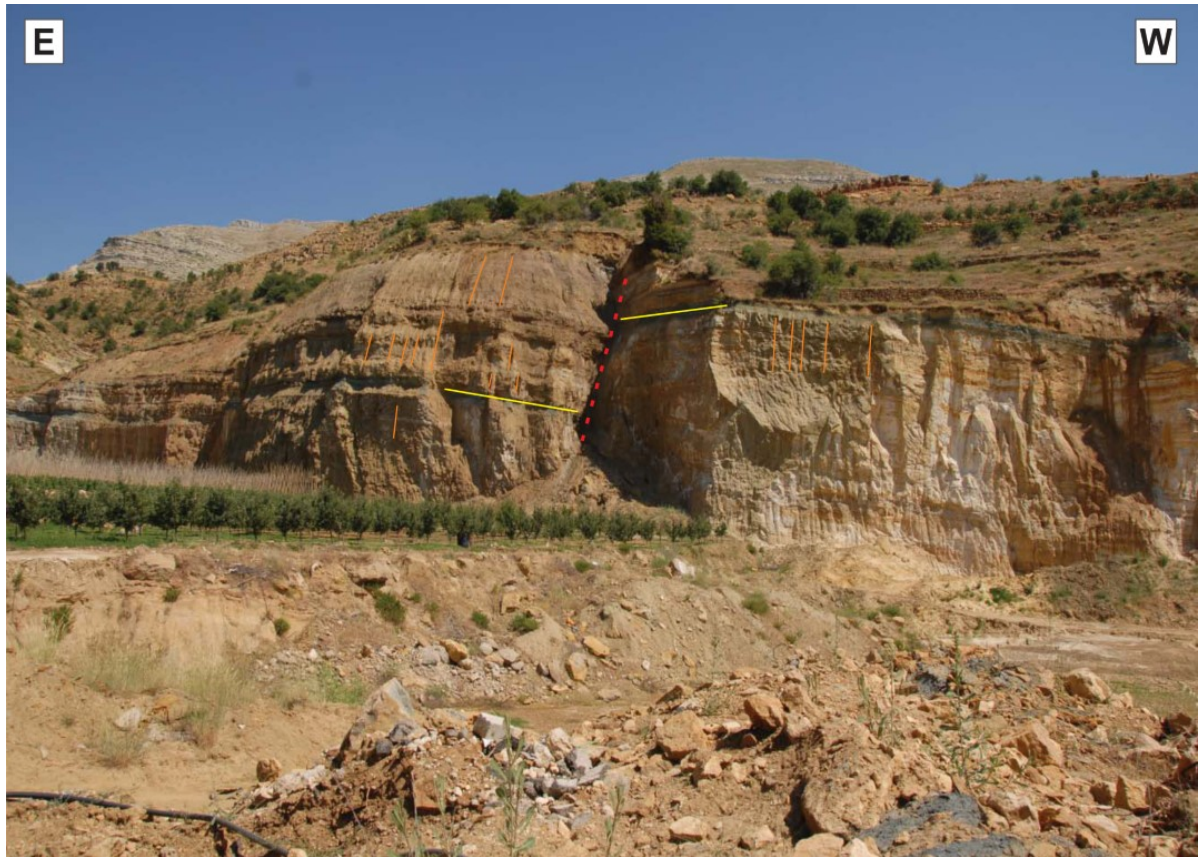


Figure 4.5: Chouf Sandstone at stop 7. Yellow line marks a layer of black clay (230/20) and an off-set of 10 meters along a normal fault (dashed red line, 045/60). Abundant vertical deformation bands (i. e. disaggregation bands) are zones of lower resistance against active erosion (orange lines, 095/85).

4.2.5 Stop 14 - Hrazmin

The outcrop at Stop 14 is an abandoned quarry cut by a quite recently built road. It is located at the Eastern end of the village of Hrazmin on the Western limb of the Qartaba anticline. The bedding dips with about 20° towards SW and the layers have varying thickness. Some prominent cross bedding structures could be observed. Right at this location the geologic map of [Dubertret \(1955\)](#) shows a minor NW-SE-striking sinistral fault offsetting the stratigraphic boundary between the Chouf Fm. and the underlying Kesrouane Fm. horizontally for about 250 m. We could indeed observe compactional shear deformation bands of several centimeter thickness dipping towards NE and SW. However, the deformation bands have almost no offset. Both conjugate sets of the contractional deformation bands are very steep and strike roughly NE-SW and NW-SE respectively. Because of the steep dip, the deformation bands cannot have formed during diagenesis but must have a tectonic origin.



Figure 4.6: Stop 14 is a road cut through an abandoned quarry. The Chouf sandstone dips with about 20° towards SW. The layers have varying thickness and some prominent cross bedding structures. Several compactional shear deformation bands of several centimeters thickness dip towards NE and SW. The deformation bands have almost no off-set.

4.2.6 Stop 18 - Moukhada

Stop 18, 500 m S of Moukhada, lies across the Qartaba Anticline nearly opposite to stop 14 on the anticline's Eastern limb. At this location the Bikfaya, Salima and Chouf Fms. crop out very close to each other as NNE-SSW-striking narrow stripes. The Chouf Fm. was not investigated here, however, it shall be mentioned that a local overthrust of the Kesrouane Fm. on the tilted Upper Jurassic and Lower Cretaceous sequences has been observed.

4.2.7 Stop 23 - Hourata

This abandoned quarry is located in Hourata in the NE part of the Northern Mount Lebanon area. The sedimentary layering of the yellow to brownish sandstone dips at shallow angles towards E. Although deformation band structures are missing in this outcrop, a vertical fault striking ENE-WSW with unknown kinematics offsets the sandstones. The geologic map of [Dubertret \(1955\)](#) shows a N-S-striking fault about 100 m E of this outcrop with an apparent dextral horizontal offset of about 200 m. A (Neptu-

nian?) dyke with unclear three dimensional orientation has been observed.

4.3 Heavy mineral analysis

At seven stops (2, 4, 7, 14, 18, 23, 26) of the 2012 field trip samples of the Chouf Fm. have been taken: S2/01, S4/02, S7/04, S14/03, S18/06, S23/07 and S26/08. These stops are distributed over the Qartaba region (Figure 4.7, see section 4.2 and field report in appendix for outcrop details). The heavy mineral spectra were obtained by analysing grain mounds using a polarisation microscope. However, the sieved fractions of samples S14/01 and S23/01 were so small and the grains were so much oxidized that they only could be analysed qualitatively using X-ray diffraction.

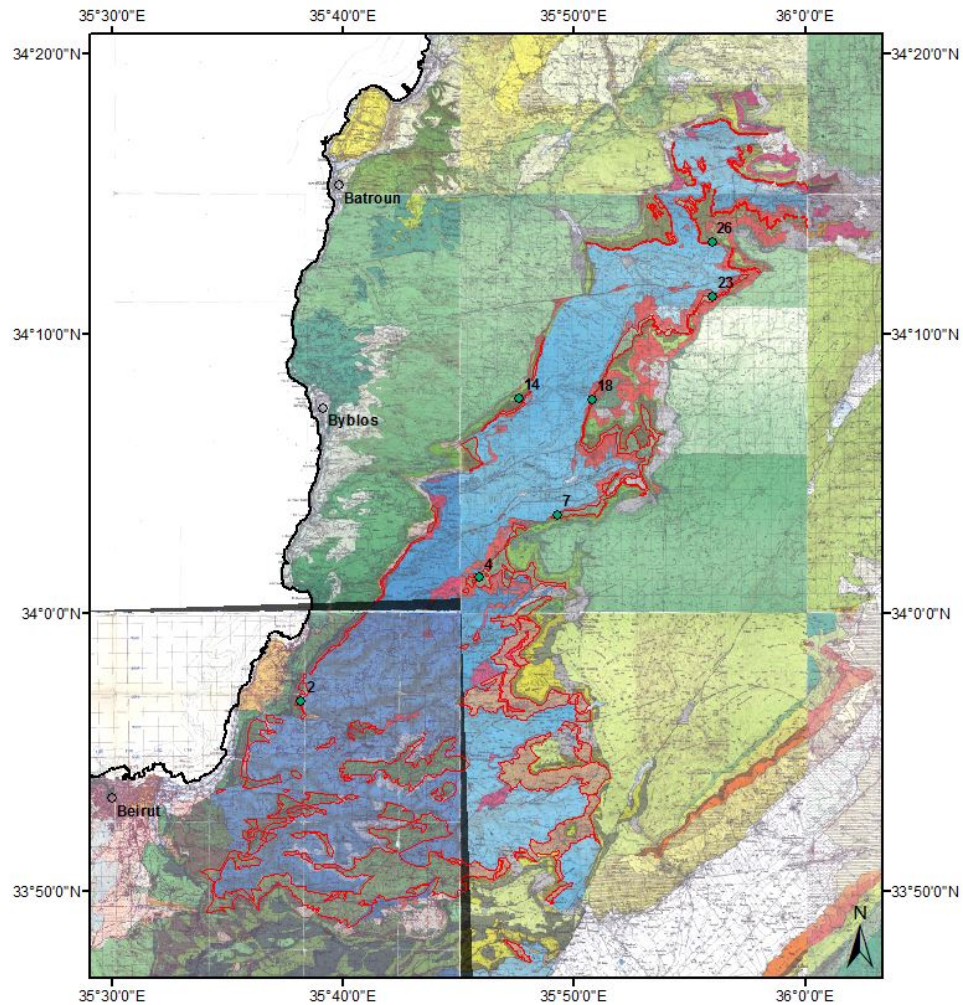


Figure 4.7: The seven Chouf sampling spots (green dots) of the 2012 field campaign in an Chouf outcrop map (red polygons). Background is the geologic map 1:50000 from Dubertret (1975).

4.3.1 Methodology

The Chouf sandstone samples have been sieved and the heavy minerals were separated by density separation using heavy liquids. Finally grain mounts of samples S2/01, S4/02, S7/04, S18/06 and S26/08 were prepared and the heavy minerals were identified and counted using a polarisation microscope.

Due to varnish coating of the grains samples S14/05 and S23/07 had to be etched using diluted hydrochloric acid. The sample was put into heated 20% dissolution for 10 min what led to precipitation of Kaolinite. Then the sample was put on a Si-body and analysed in the X-ray diffractometer (X'Pert Pro) to identify the occurring minerals.

4.3.2 Results

All samples show very similar results including only four different heavy minerals, namely Zircon, Rutile, Tourmaline and Monazite, whereupon the Tourmaline grains are highly rounded. Tourmaline and Zircon are dominating (40 – 50 %, 30 - 50 % respectively) and present in all seven samples. Rutile is also present in all samples but less abundant (10 – 20 %). Monazite was found in small amounts in samples S2/01, S4/02 and S7/04 (1 – 2 %) (Figure 4.8). X-ray diffraction analysis of sample S23/07 also detected Anatas. Kaolinite in sample S23/07 is the product of the acid treatment (Figure 4.9, Figure 4.10).

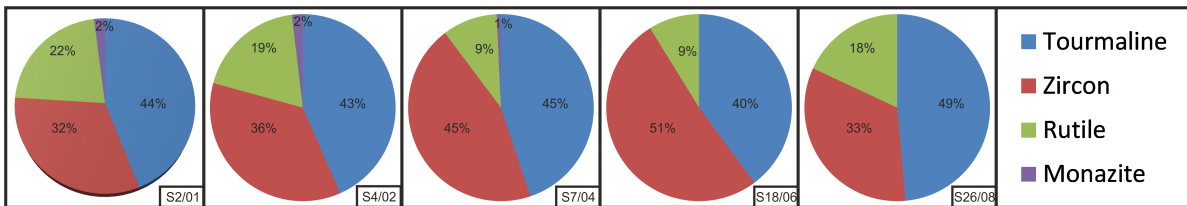


Figure 4.8: Heavy mineral spectra of the Chouf sandstone samples S2/01, S4/02, S7/04, S18/06 and S26/08.

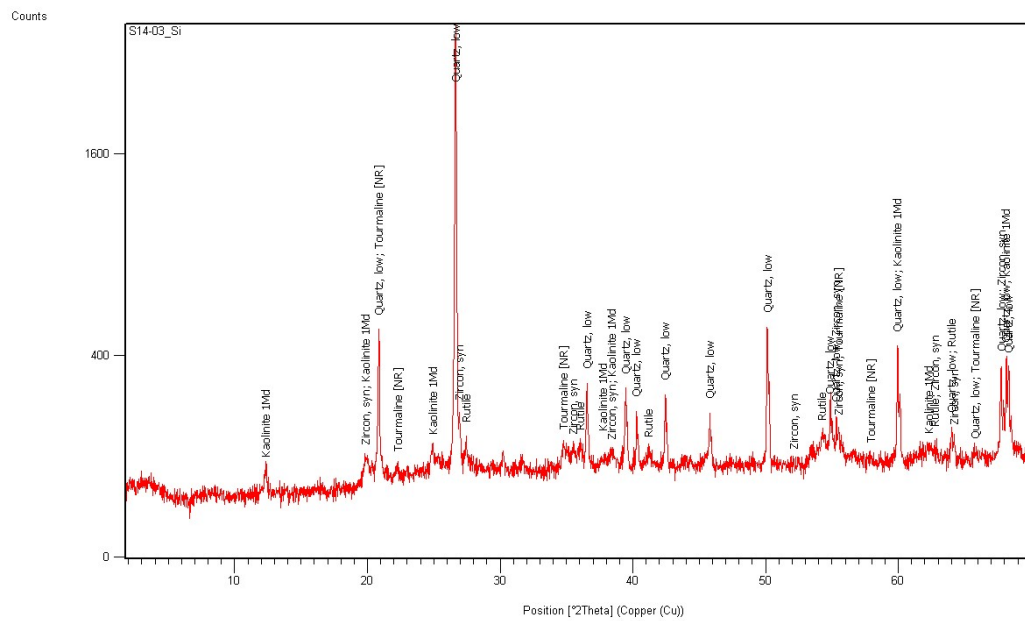


Figure 4.9: X-ray diffraction spectrum of the Chouf sandstone sample S14/03. Analysis shows Zircon, Rutile, Quartz, Tourmaline and Kaolinite.

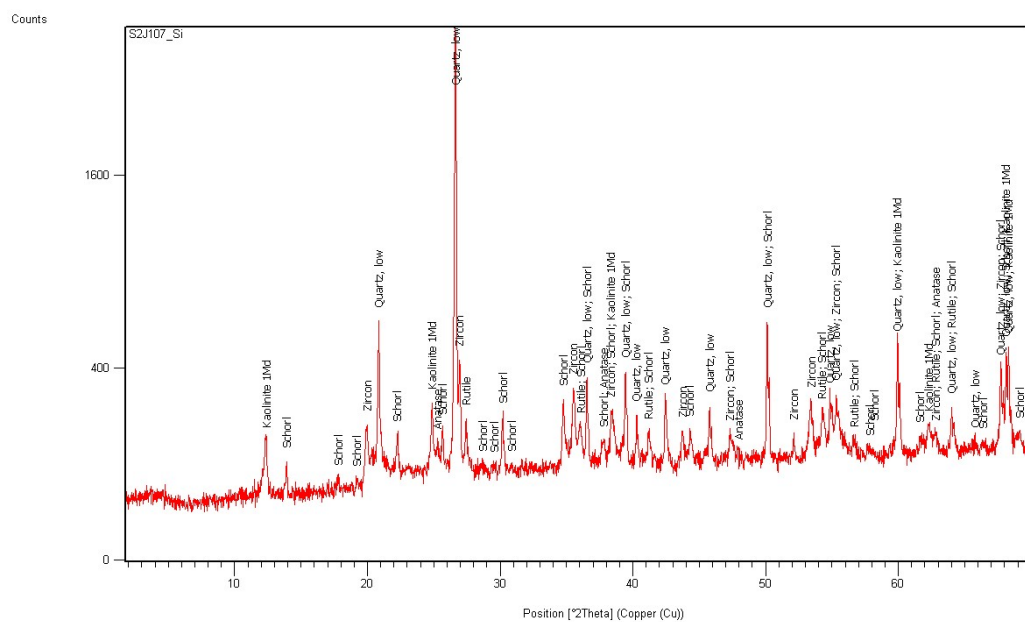


Figure 4.10: X-ray diffraction spectrum of the Chouf sandstone sample S23/07. Analysis shows Zircon, Quartz, Rutile, Schörl (Tourmaline), Kaolinite and Anatase.

4.4 Isopach model

Based on an existing isopach model from [Grasemann and Zámolyi \(2012\)](#) a more precise one (based on more data points) was created to accurately visualize the thickness variations within the Chouf Fm.

4.4.1 Previous work

[Kanaan \(1966\)](#) created two isopach maps of the "Basal Cretaceous Sandstones" in Lebanon and the whole region based on own field work and data from the literature. The regional map is shown in [Figure 4.11](#). Isopach maps of the "Grès de Base" from [Ukla \(1970\)](#) show the same elliptical form, where the thickest sequences were found in the center ([Figure 4.12](#)). It was concluded that the Chouf Fm. was deposited in an elliptical basin with the thickest deposits and the basin's center (which might be related to the Palmyride depocenter) in the Chouf region ([Figure 4.12](#)). A more recent isopach map based mostly on remote sensing data was constructed by [Grasemann and Zámolyi \(2012\)](#) ([Figure 4.13](#)). A new isopach map based on the latter was created during this study and is discussed below.

4 The evolution of the Lower Cretaceous Chouf Formation

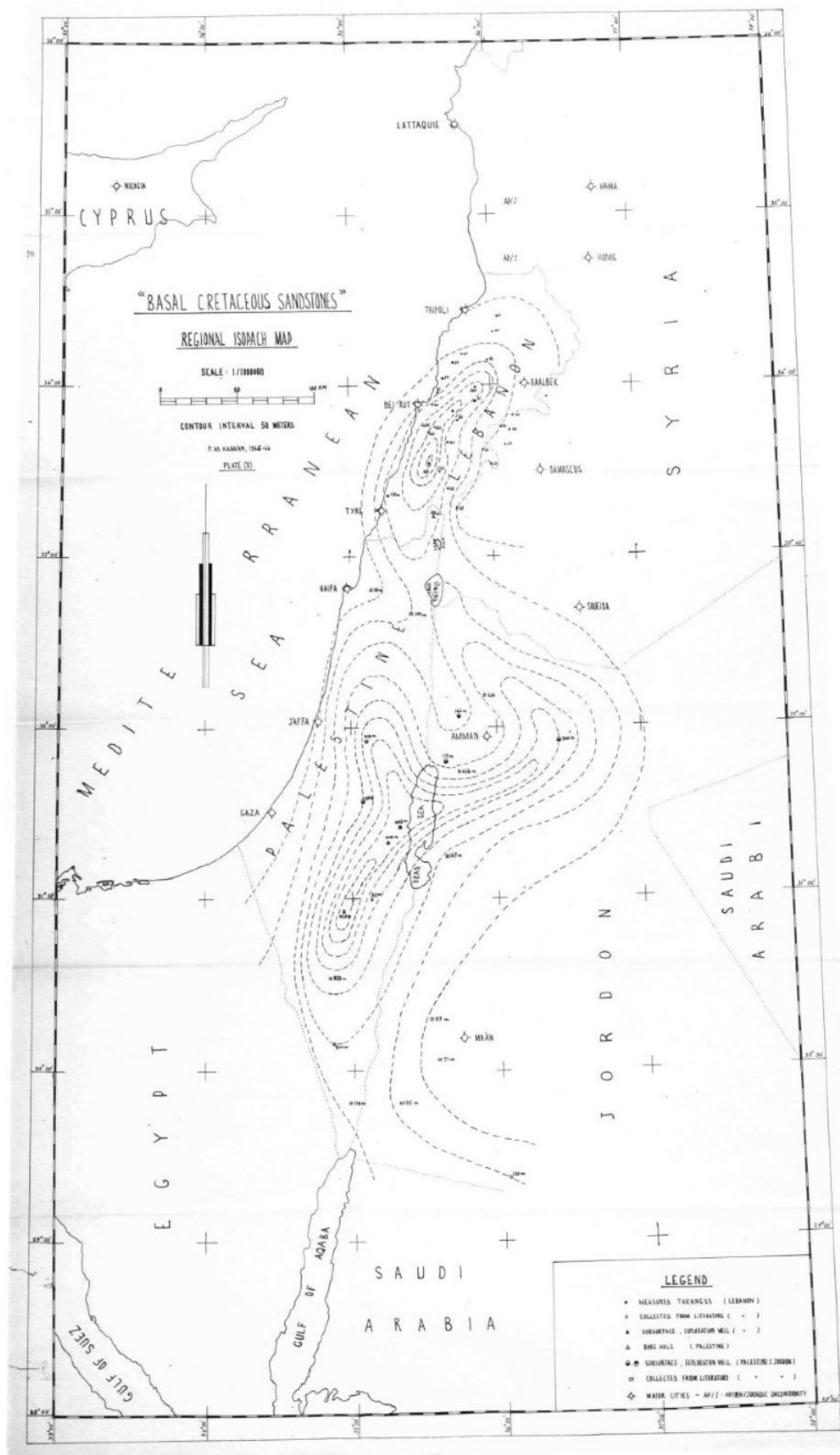


Figure 4.11: Regional isopach map of the Basal Cretaceous Sandstones from Kanaan (1966) extending from Lebanon into Syria, Egypt, Saudi Arabia and Jordan.

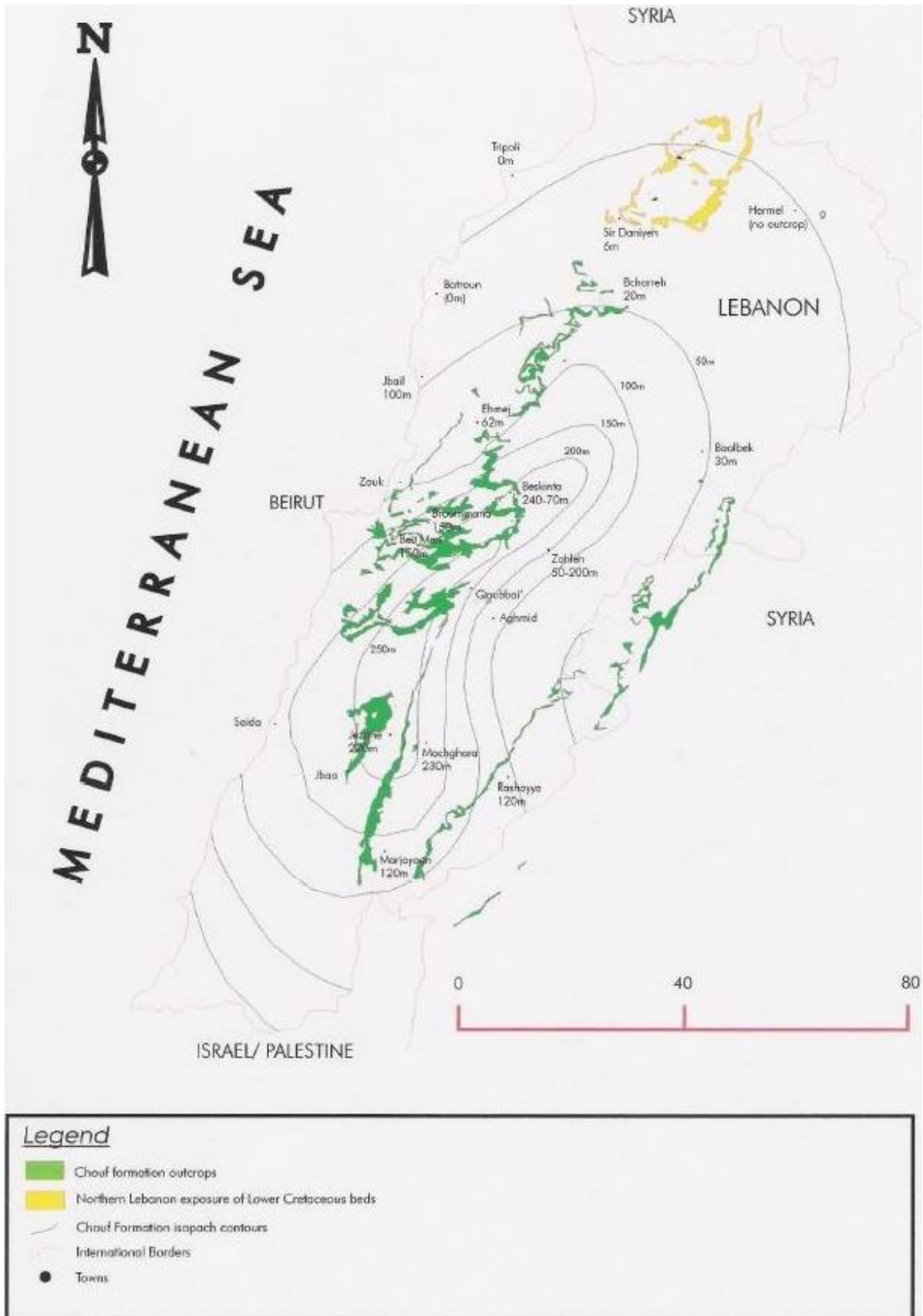


Figure 4.12: Chouf Fm. outcrop data from several sources, isopachs drawn from Ukla (1970); in Bellos (2008).

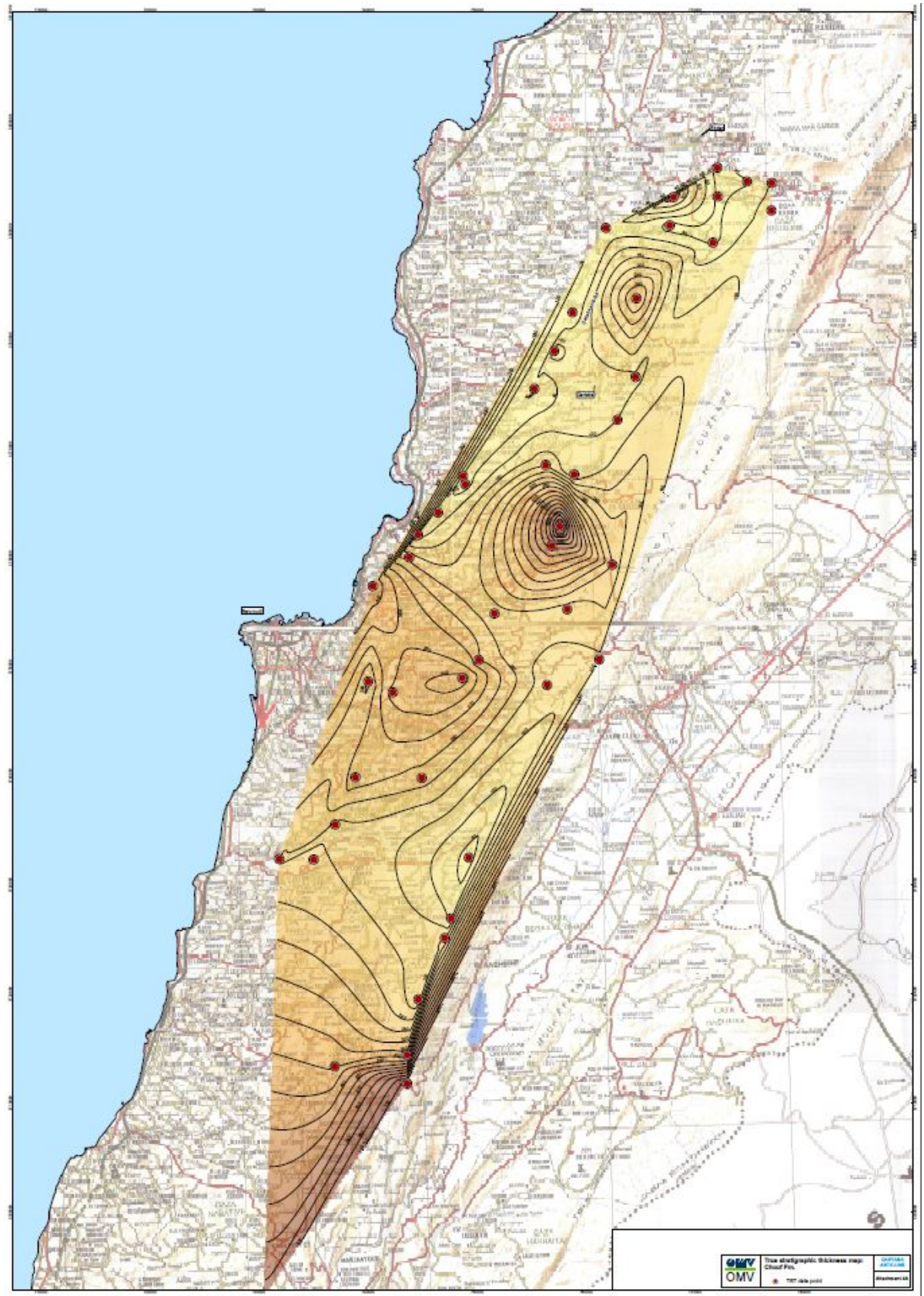


Figure 4.13: Isopach map of the Chouf Fm. based on remote sensing data ([Grasemann and Zámolyi, 2012](#)).

4.4.2 Data background and methodology

Using the data [Grasemann and Zámolyi \(2012\)](#) had been working on, their isopach model of the Chouf Fm. has been improved by increasing the number of isopach points from 47 to 190. The new points have been acquired by using field data from the ArcGIS database at hand and new field data from the 2012 field trip. More dip data was generated by using a new python tool for ArcGIS developed by Asmar (unpublished) which is solving automatically the three-point problem using Quickbird satellite images and DEMs as described by [Grasemann and Zámolyi \(2012\)](#). The isopach data was then acquired in the ArcGIS environment. Additional thickness values have been added from literature sources ([Heybroek and Dubertret, 1945](#); [Dubertret and Wetzel, 1951](#); [Dubertret et al., 1955](#); [Kanaan, 1966](#); [Walley, 1983](#); [Bellos, 2008](#)) including two well logs ([Beydoun, 1977](#)) from wells Adloun and Tell Znoub (see [Figure 1.1](#) for location).

Data background

The existing ArcGIS research database comprised remote sensing data and geologic maps provided by OMV (i, ii, iii & iv) and structural and isopach data generated by [Grasemann and Zámolyi \(2012\)](#) (v).

- (i) Quickbird composite satellite image (3 bands: RGB) covering Mount Lebanon from the Gulf of Jounieh and parts of the Nahr el Kelb up to the Syrian border with a resolution of 60 cm
- (ii) SPOT stereocorrelated digital elevation model (DEM) covering the same area with a horizontal resolution of 20 m
- (iii) SPOT stereocorrelated digital elevation model (DEM) covering the the whole Levantine region with a horizontal resolution of 100 m
- (iv) 27 geologic map sheet of 1:50,000 scale ([Dubertret, 1975](#))
- (v) Dip/strike data, isopach data points and isopach models of different stratigraphic units in the Mount Lebanon area

The coordinate system used in the ArcGIS environment was UTM Zone 36. However, it shall be noted that the Mount Lebanon region lies in both UTM Zones 36 and 37.

Dip/strike data from remote sensing

Dip/strike measurements were carried out in the ArcGIS environment (Quickbird satellite image and DEM) by solving the three-point problem ([Grasemann and Zámolyi, 2012](#)). Three points representing the three corners of a triangle were placed along a common surface line, where a geologic surface coincides with the topographic surface ([Figure 4.14](#)). The identification of the right points was favored by the layer-cake like stratigraphy along with the mediterranean vegetation and weathering conditions, although the identification of bedding planes is not as easy in the sandstones of the Chouf Fm. than e. g. in the carbonate sequences of other formations due to the sandstones' weaker resistance towards erosion. To solve the three-point problem the two of the three corner points of the triangle with the biggest difference in elevation are connected to form a dip line. The location of the third point is interpolated onto the dip line by solely

using the point's elevation. Connecting this interpolated point with the third point then provides the strike line. The dip value is derived by measuring the perpendicular distance between the strike line and the lowermost point. This calculations were carried out by [Grasemann and Zámolyi \(2012\)](#) using a MatLab script. However, to avoid having to export the values of the triangular polygon from ArcGIS into Matlab and reimport the resulting dip/strike values into ArcGIS [Asmar \(2013\)](#) recently integrated the MatLAB script into ArcGIS by programming a Python toolbox ([Figure 4.15](#)), which was also used during this study. Using this simplified workflow you first generate a shapefile containing sets of three points (the three corners of the triangles), then connect the shapefile to and run the Python toolbox, which finally returns a new shapefile containing the dip/strike values. [Grasemann and Zámolyi \(2012\)](#) give an error of the remote sensing measurements in a range of 29° for the dip direction and 25° for the dip angle.



Figure 4.14: Three-point problem: three points representing the three corners of a triangle are placed along a common surface line on the satellite image in ArcGIS.

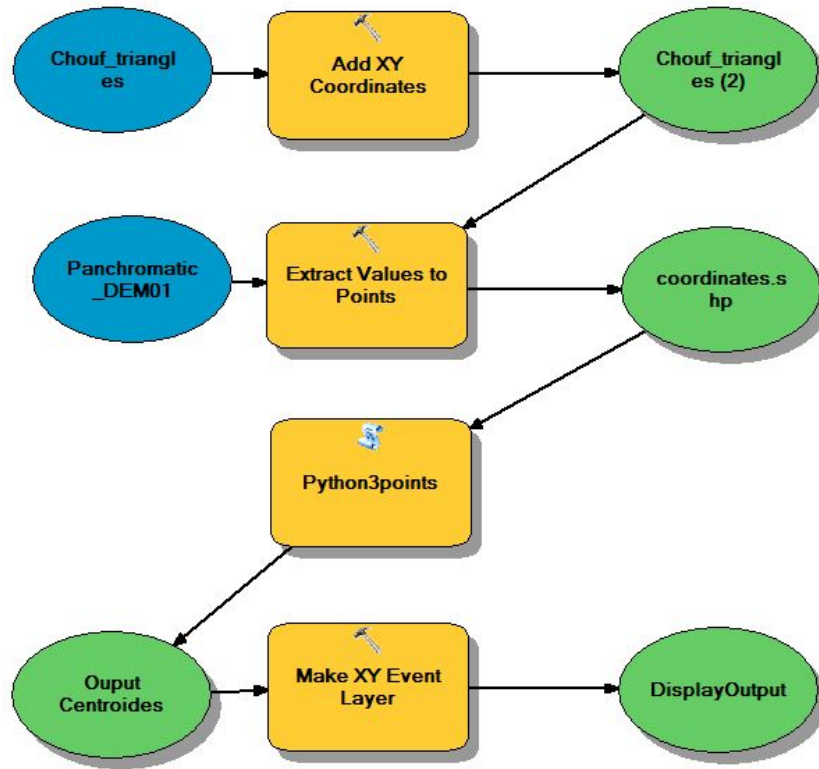


Figure 4.15: The workflow of the Python toolbox programmed by [Asmar \(2013\)](#) for solving the three-point problem directly in the ArcGIS environment.

Construction of isopach maps

Points of true stratigraphic thickness (TST) for creating the isopach maps were calculated by means of trigonometry ([Figure 4.16](#)). Dip/strike values came from the ArcGIS database ([Grasemann and Zámolyi, 2012](#)), remote-sensing, the 1:50,000 geologic map ([Dubertret, 1975](#)) and field measurements during the 2012 field campaign. Contour lines were derived from both the local DEM of the Northern Mount Lebanon region and the regional DEM of the Levantine region.

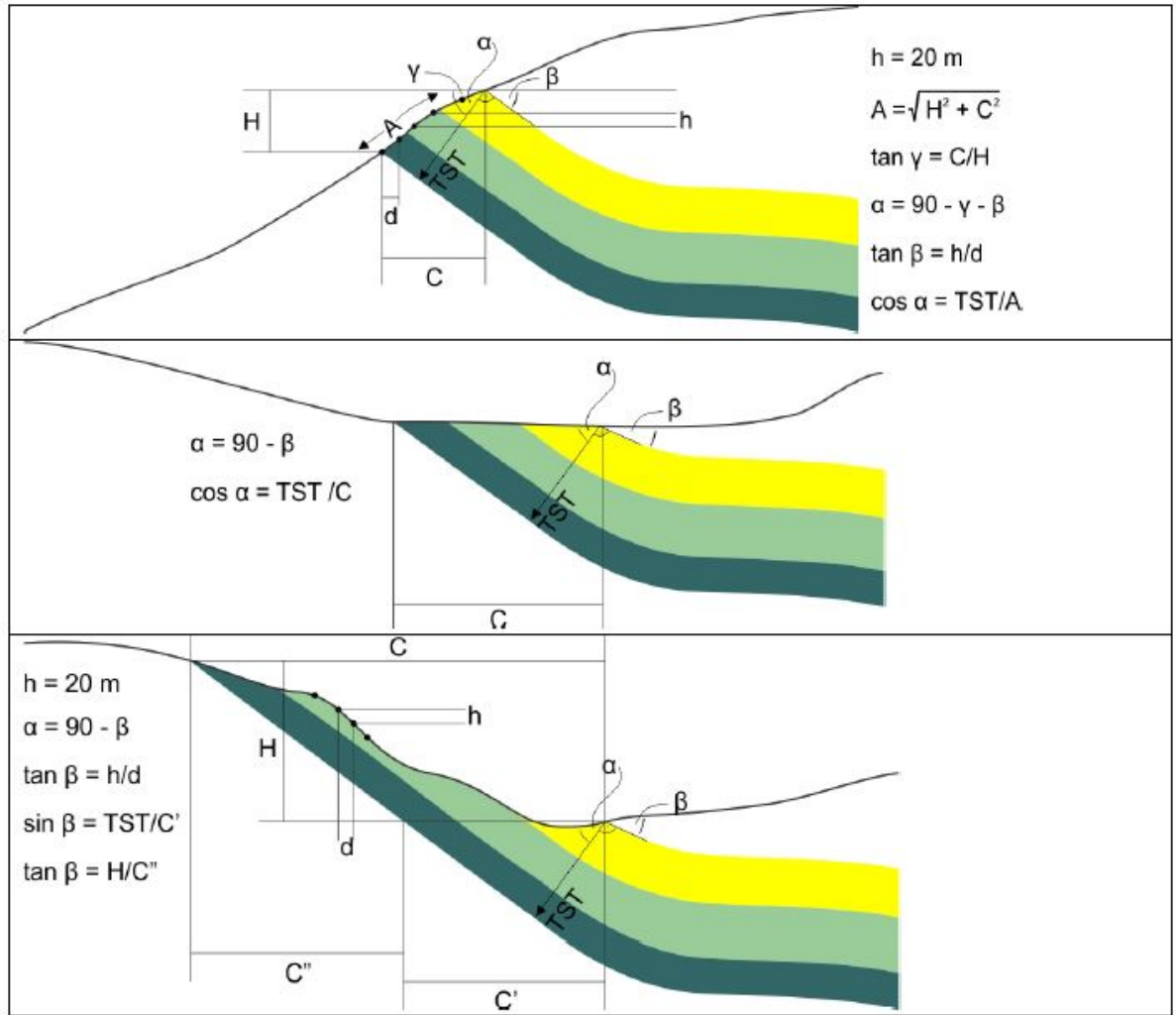


Figure 4.16: Three main cases for the calculation of true stratigraphic thickness (TST). Explanation of values used in the calculation: h = elevation difference between contour lines; d = horizontal distance between structure contours; H = elevation difference between upper and lower boundary of lithology; C , C' and C'' = horizontal distance between upper and lower boundary of lithology; α = intermittent angle necessary for TST calculation; β = bedding dip; γ = slope angle. From [Grasemann and Zámolyi \(2012\)](#).

A total of 179 TST-points from several sources have been calculated to construct an isopach map for the Chouf Fm. (Table 4.1). Since the thickness of the boundary lines in the 1:50,000 scale geologic map is about 1 mm, which equals 50 m, an error of about 40 m of TST occurs. The final isopach model can be seen in Figure 4.17. For better visualization a 2D- and 3D-model of the Chouf isopachs have been generated using MatLAB (Figure 4.19). All calculated TST values are found in the list of TST and TVT points in the appendix.

Source	Number of Points
calculated using dip/dir-data from 2012 field campaign	3
calculated using dip/dir-data from ArcGIS database	8
calculated using dip/dir-data from remote sensing	107
from ArcGIS database from Grasemann and Zámolyi (2012)	44
from literature incl. well data	17

Table 4.1: Points per source of the TST-points used for constructing the Chouf isopach model (Figure 4.17). Total number of points used for isopach model construction is 179.

4.4.3 Results

The constructed isopach contour map of the Chouf Fm. can be seen in Figure 4.17. A 2D and a 3D model of the true stratigraphic thickness can be seen in Figure 4.18 and Figure 4.19, respectively. The greatest thickness of ca. 650 m is found in the South of the study area and going NE several up-and-downs of thickness can be observed, whereas the peaks decline from about 500 m in the center of the area to about 350 m in the North. It can be seen that the overall thickness declines northwards.

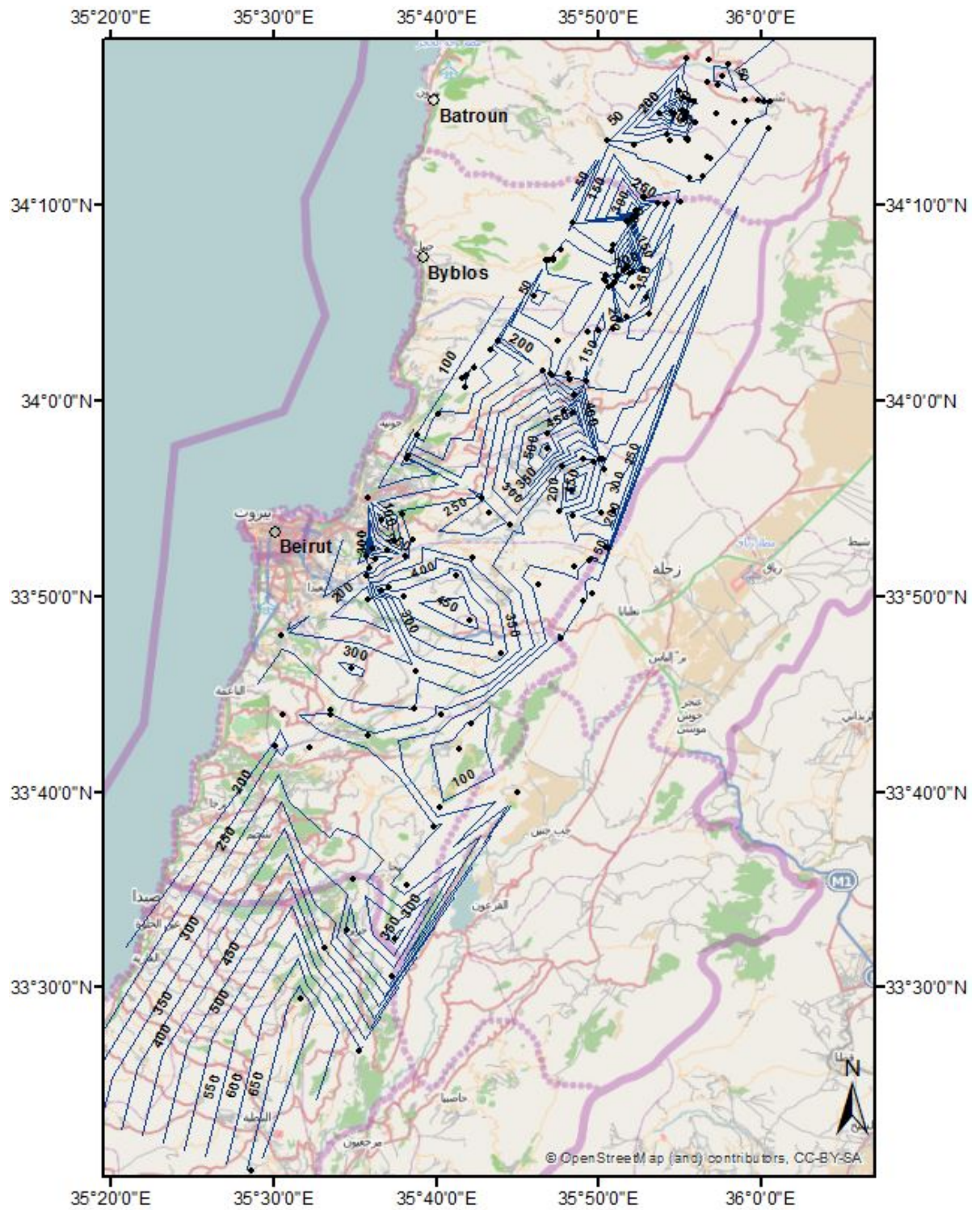


Figure 4.17: Isopach map of the Chouf Fm. Contour interval is 50 m. Black dots represent the isopach data points used for the calculation of the isopach contours. Background is from Open street map.

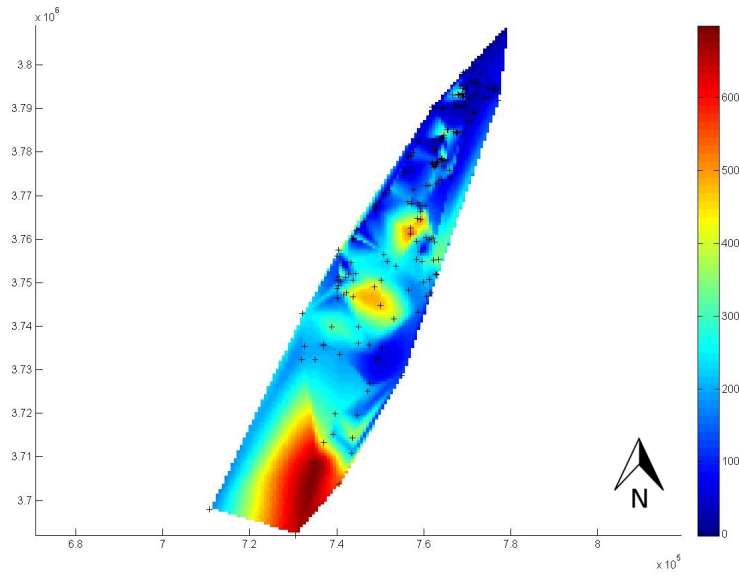


Figure 4.18: 2D isopach model of the Chouf Fm. X- and Y-axis refer to the coordinates, colors reflect the true stratigraphic thickness of the Chouf Fm. The isopach data points used for generating the contours are marked as '+'.

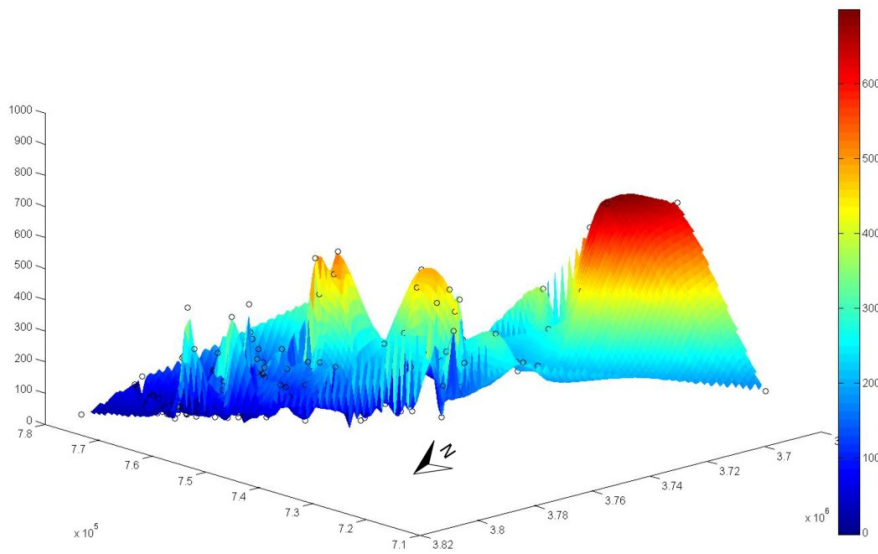


Figure 4.19: 3D isopach model of the Chouf Fm. X- and Y-axis refer to the coordinates, vertical Z-axis and colors reflect the total stratigraphic thickness of the Chouf Fm. The isopach data points used for generating the contours are marked as circles.

4.5 Isochore model

In addition to the isopach model an isochore model was calculated. Whereas isopachs display lines of true stratigraphic thickness (TST), i.e. the thickness perpendicular to the layer boundaries, an isochore map displays the true vertical thickness (TVT). The calculation of the TVT is based on the calculation of the TST and shown in [Figure 4.20](#). An isochore map is shown in [Figure 4.21](#), an isochore model visualized in MatLAB is shown in [Figure 4.22](#). The calculated TVT values are found in the list of TST and TVT points in the appendix.

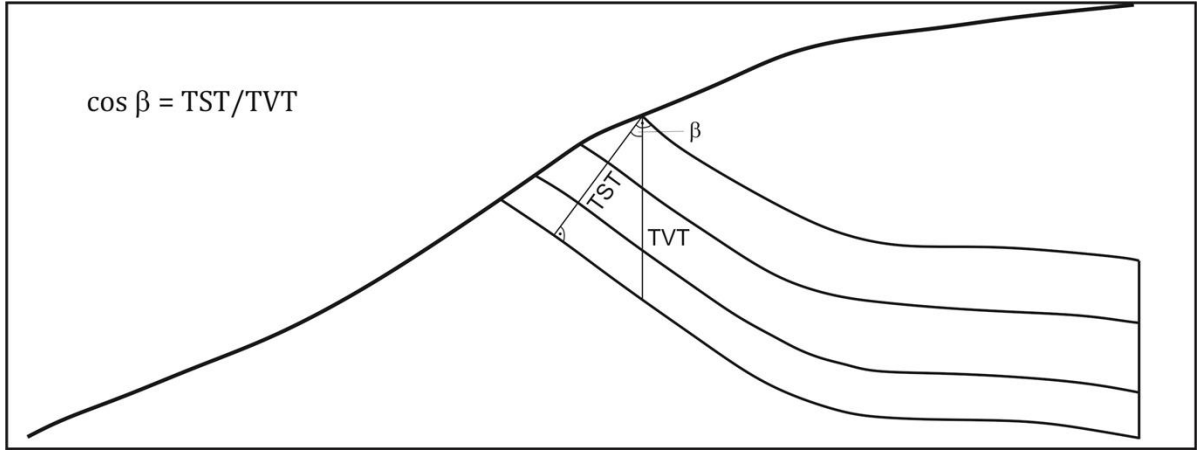


Figure 4.20: The calculation of the true vertical thickness (TVT) is based on the calculation of the true stratigraphic thickness (TST) as shown in [Figure 4.16](#). β = bedding dip.

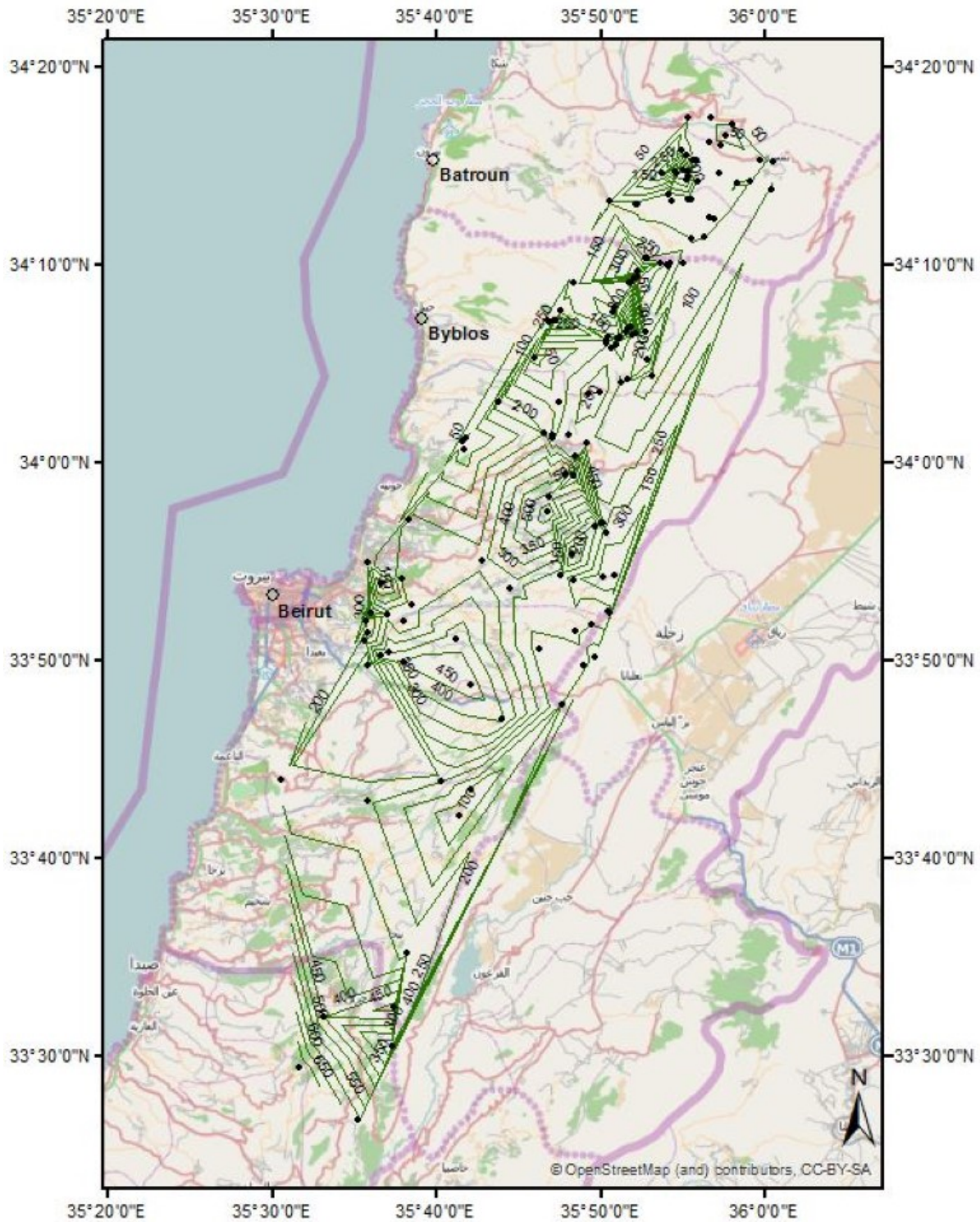


Figure 4.21: Isochore map of the Chouf Fm. displaying the variations true vertical thickness (TVT). Black dots represent the TVT data points used for the calculation of the isochore contours. Background is from Open street map.

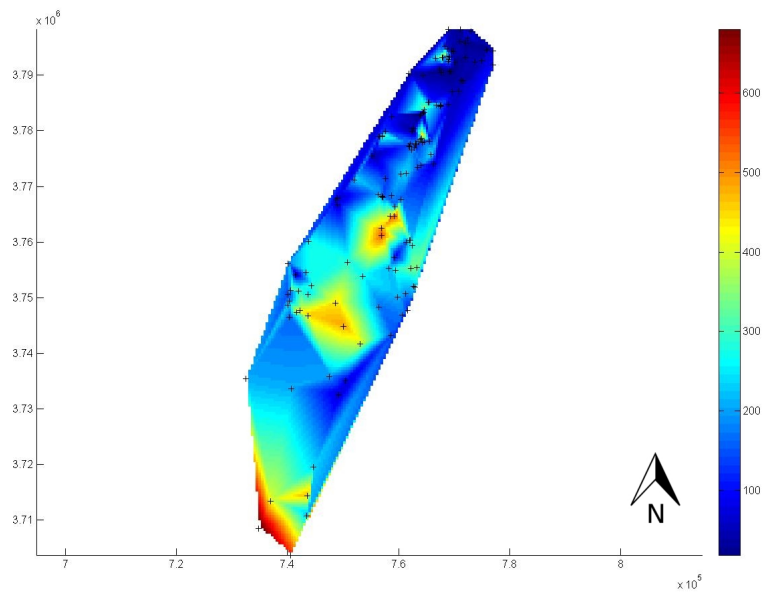


Figure 4.22: 2D isochore model of the Chouf Fm. X- and Y-axis refer to the coordinates, colors reflect the true vertical thickness of the Chouf Fm. The isochore data points used for generating the contours are marked as '+'.

4.6 Discussion

4.6.1 Heavy mineral analysis

The heavy mineral analysis ([section 4.3](#)) showed that the Chouf sandstones only comprise the most stable heavy minerals (Zircon, Rutile, Tourmaline, Monazite) of which the Tourmaline grains were highly rounded. This results indicate that the Chouf sandstones are the erosional product of an earlier sandstone and therefore support the provenance models found in the literature (see [section 4.1](#)). Monazite was found in minor quantity in the southern samples but not at all in the north ([Figure 4.23](#)).

4.6.2 Isopach model

Previous isopach models from [Kanaan \(1966\)](#) and [Ukla \(1970\)](#) ([Figure 4.11](#), [Figure 4.12](#)) have been more regional or based on less data points and therefore did indeed represent the lateral but not the internal thickness variations. The isopach model from [Grasemann and Zámolyi \(2012\)](#) did already roughly represent that ([Figure 4.13](#)). Such a model of the internal thickness variations of the Chouf Fm. inside Lebanon could now have been done more precisely. Plotting the ENE-WSW to ESE-WNW striking faults onto the isopach contours, this isopach model can support the syn-rift deposition model from [Collin et al. \(2010\)](#) ([Figure 4.24](#)).

The northern most isopach point (10 m of thickness) ENE of Tripoli fits the model of an Early Cretaceous WNW-ESE striking basin with a northern margin 50 km South of Tripoli ([Homberg et al., 2010](#)). However, a westward thickening implying an offshore continuation of that basin through the Levantine basin ([Homberg et al., 2009](#)) cannot be seen in the isopach model presented here due to its lateral limitation.

4.6.3 Isochore model

Since bedding dip angles of the Chouf Fm. are often below 10° and mostly below 20° the true vertical thickness is not much greater than the true stratigraphic thickness.

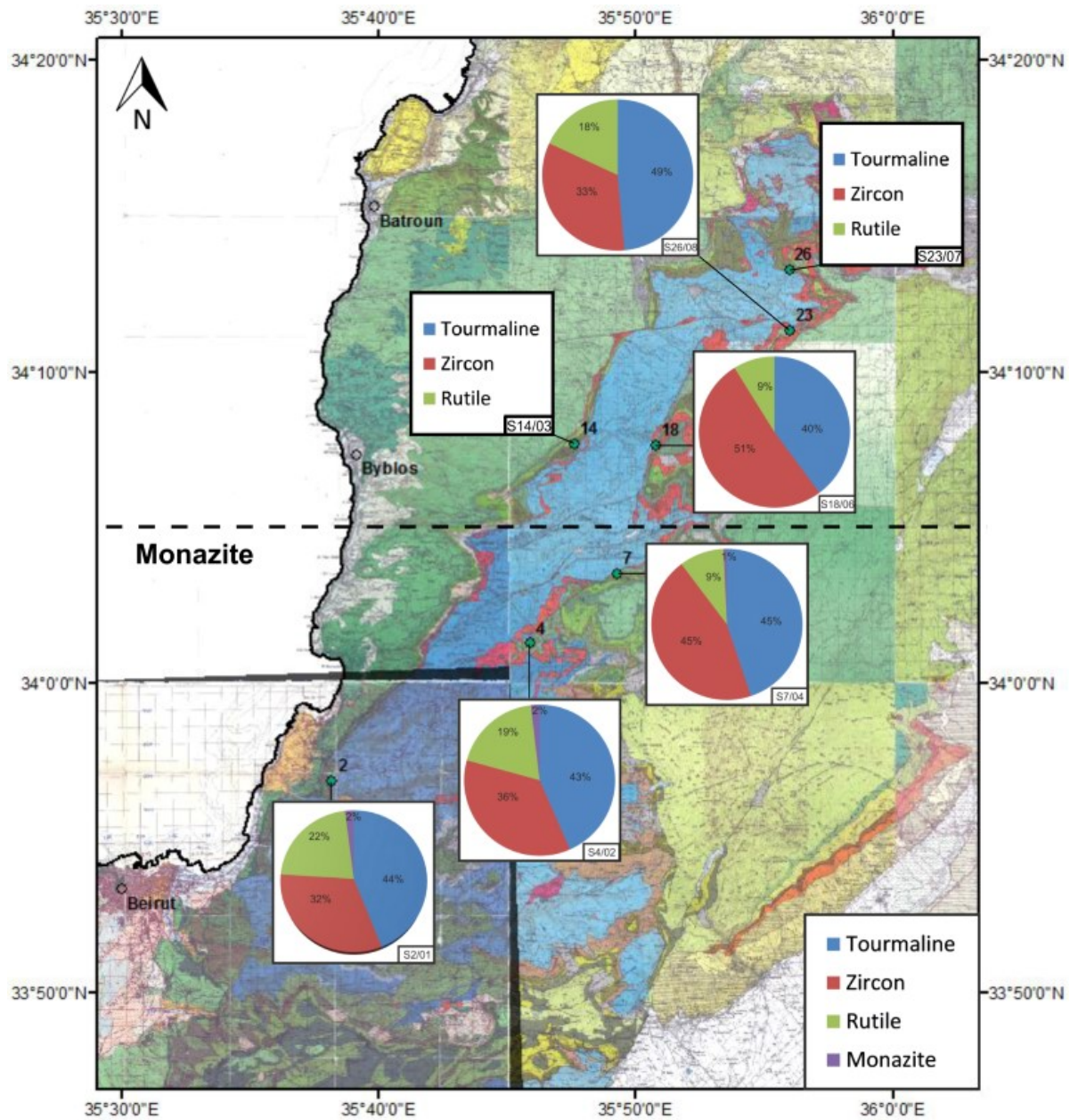


Figure 4.23: Results of the heavy mineral analysis. Samples S14/03 and S23/07 could only be analysed qualitatively. The three southern samples include Tourmaline, Zircon, Rutile and Monazite, whereas the four northern samples lack the latter. Dashed black line separates the northern part, where no Monazite has been observed, from the southern part. Inset in the bottom right corner shows the color legend for the different minerals. Background is the geologic map 1:50000 from Dubertret (1975).

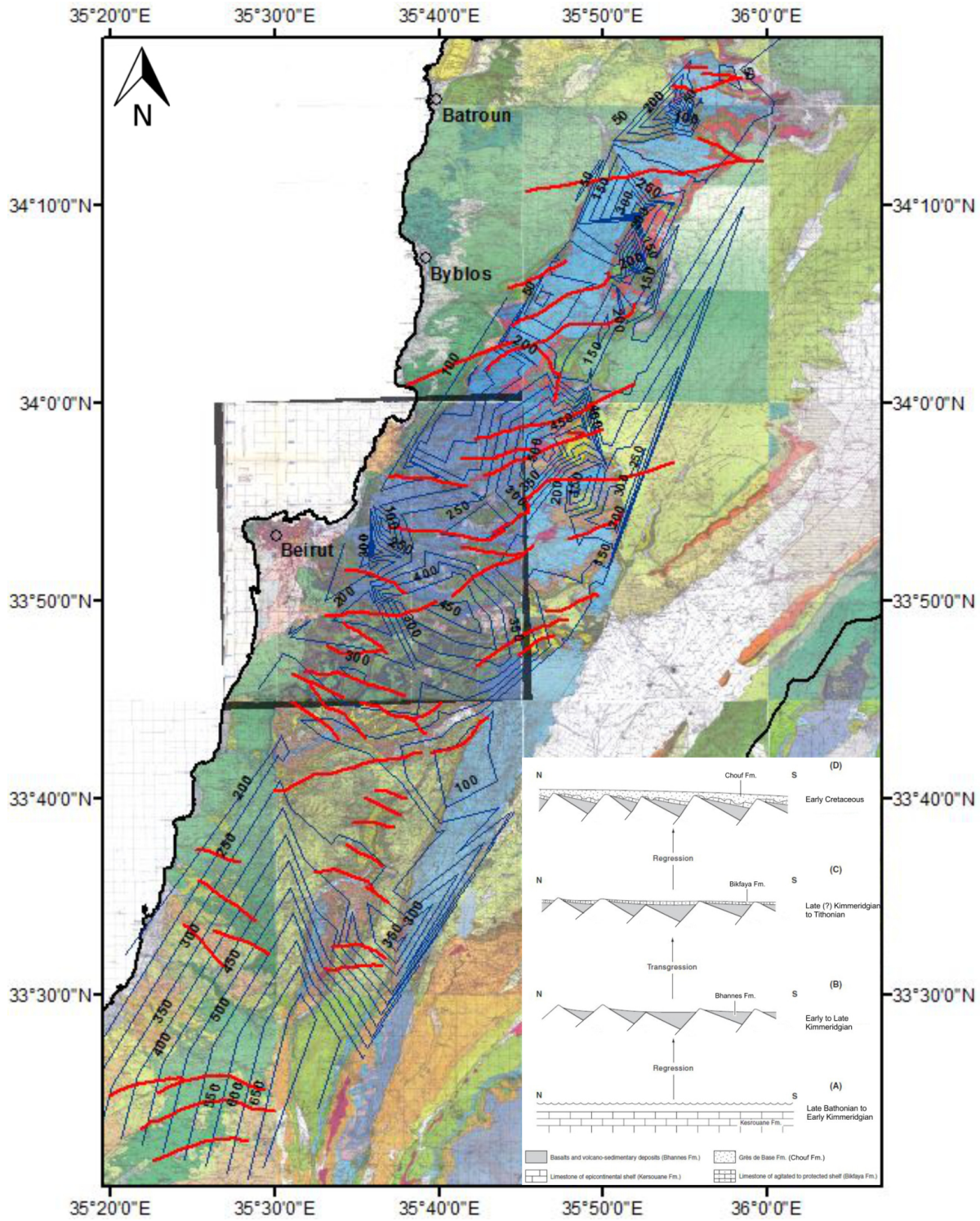


Figure 4.24: Isopach map of the Chouf Fm. Contour interval is 50 m. Primarily ENE-WSW and minor ESE-WNW striking faults in red. Background is the geologic map from [Dubertret \(1975\)](#). Black outline is the Lebanese border. Inset shows the syn-rift deposition model of the Chouf Fm. after [Collin et al. \(2010\)](#).

5 Conclusions

5.1 The Qartaba structure and thin section analysis

Thin section analysis ([chapter 3](#)) from different stratigraphic units cropping out in the Northern Mount Lebanon area gave some deeper insights into the (bio-)stratigraphical and structural characterization of those rocks.

Observations regarding rocks from the Qartaba area led to the development of a deformation model for the Qartaba structure describing the consecutive effects of extensional and compressional forces on the rocks ([Figure 3.6](#)). An initial deformation phase of folding and flexural slip accompanied by the opening of veins was followed by a second phase characterized by pressure solution processes, i.e. stylolite formation. Due to the rotation of the previous formed veins these stylolites are parallel to them. Cataclastic deformation was not observed in the hinge of the fold, where pressure solution processes clearly dominate.

The samples from the volcanoclastic rocks of the Bhannes Fm. presented a complex set-up comprising carbonate lithoclasts and different pyroclastic deposits all of which had been highly altered. Dynamical recrystallized quartz alongside brittle fractures showed crystall preferred orientation and low temperature bulging. Following the studies [Smith et al. \(2013\)](#) carried out on coseismic recrystallized calcite formed during shallow earthquake slip this supports the field study and leads to the assumption that these rocks have been deformed during seismic events.

5.2 The evolution of the Lower Cretaceous Chouf Formation

Heavy mineral analysis ([section 4.3](#)) of the Chouf Fm. in the Northern Mount Lebanon region revealed the preservation of only the most stable heavy minerals and suggests that the Chouf sandstones are the erosional product of an earlier sandstone and thus supports the provenance hypotheses found in the literature, where the Nubian sandstones of Egypt, the Jordanina sandstones and/or the Ruthabah sandstones of Syria are named. The isopach model ([section 4.4](#)) reveals the N-S trending wave-like thickness variations of the Chouf Fm. in the Mount Lebanon region. These variations are bound to ENE-WSW to ESE-WNW striking normal faults. Thus this isopach model supports the syn-rift deposition model of the Chouf sandstones as suggested by [Collin et al. \(2010\)](#). However, the new isopach model does not perfectly fit into the basin model from [Homberg et al. \(2009, 2010\)](#), although this is most probably due to its lateral limitation.

5 Conclusions

The calculation of an ischore map showed that due to the low bedding dip angles of the Chouf Fm. the true vertical thickness does not much differ from the true stratigraphic thickness.

Bibliography

- Asmar, C. (2013). Python toolbox for solving the three-point problem in the ArcGIS environment. Unpublished.
- Bauer, H., Hatzenbichler, G., and Grasemann, B. (2013). Report to OMV: Lebanon report - field-trip July 2012. Unpublished.
- Bellos, G. (2008). Sedimentology and Diagenesis of Some Neocomian-Barremian Rocks (Chouf Formation), Southern Lebanon. Master's thesis, American University of Beirut. Faculty of Arts and Sciences. Department of Geology.
- Bestmann, M., Pennacchioni, G., Frank, G., Goeken, M., and de Wall, H. (2011). Pseudotachylyte in muscovite-bearing quartzite: Coseismic friction-induced melting and plastic deformation of quartz. *Journal of Structural Geology*, 33(2):169–186.
- Bestmann, M., Pennacchioni, G., Nielsen, S., Goeken, M., and de Wall, H. (2012). Deformation and ultrafine dynamic recrystallization of quartz in pseudotachylyte-bearing brittle faults: A matter of a few seconds. *Journal of Structural Geology*, 38(SI):21–38.
- Beydoun, Z. (1977). Petroleum Prospects of Lebanon - Reevaluation. *American Association of Petroleum Geologists Bulletin*, 61(1):43–64.
- Beydoun, Z. and Habib, J. (1995). Lebanon revisited - New insights into Triassic hydrocarbon prospects. *Journal of Petroleum Geology*, 18(1):75–89.
- Burkhard, M. (1993). Calcite twins, their geometry, appearance and significance as stress-strain markers and indicators of tectonic regime - a review. *Journal of Structural Geology*, 15:351–368.
- Butler, R. W. H., Griffiths, H. M., and Spencer, S. (1998). The structural response to evolving plate kinematics during transpression: evolution of the Lebanese restraining bend of the Dead Sea Transform. *Geological Society Special Publications*, 135:81–106.
- Carton, H., Singh, S. C., Tapponnier, P., Elias, A., Briaies, A., Sursock, A., Jomaa, R., King, G. C. P., Daeron, M., Jacques, E., and Barrier, L. (2009). Seismic evidence for Neogene and active shortening offshore of Lebanon (Shalimar cruise). *Journal of Geophysical Research - Solid Earth*, 114.
- Clark, G. N. and Boudagher-Fadel, M. K. (2001). The larger benthic foraminifera and stratigraphy of the Upper Jurassic/Lower Cretaceous of Central Lebanon. *Revue de Micropaléontologie*, 44(3):215 – 232.

Bibliography

- Cohen, Z., Kaptsan, V., and Flexer, A. (1990). The Tectonic Mosaic of the Southern Levant - Implications for Hydrocarbon Prospects. *Journal of Petroleum Geology*, 13(4):437–462.
- Collin, P.-Y., Mancinelli, A., Chiocchini, M., Mroueh, M., Hamdam, W., and Higazi, F. (2010). Middle and Upper Jurassic stratigraphy and sedimentary evolution of Lebanon (Levantine margin): palaeoenvironmental and geodynamic implications. In Homberg, C and Bachmann, M, editor, *Evolution of the Levant Margin and Western Arabia Platform since the Mesozoic*, volume 341 of *Geological Society Special Publication*, pages 227–244. Geological Soc Publishing House, England.
- Courbon, P. (1989). *Atlas of the great caves of the world*. Cave Books.
- Daeron, M. (2005). *Rôle, cinématique et comportement sismique à long terme de la faille de Yammoûneh, principale branche décrochante du coude transpressif libanais*. PhD thesis, Institut de Physique du Globe de Paris.
- Dubertret, L. (1955). Carte géologique du liban au 1:200.000e. Beirut.
- Dubertret, L. (1975). *Introduction à la carte géologique à 1:50000e du Liban*. Notes et mémoires sur le Moyen-Orient. Muséum national d'histoire naturelle.
- Dubertret, L., Keller, A., Vautrin, H., Birembault, C., Heybroek, H., Canaple, G., Combaz, A., Mandersheid, G., and Renouard, G. (1955). Cartes géologiques du liban au 1/200.000e. avec notice explicative. République Libanaise, Ministère des Travaux Publics, Beyrouth.
- Dubertret, L. and Wetzel, R. (1951). Cartes géologiques du liban 1/50 000e. feuille de kartaba (avec notice explicative). République Libanaise, Ministère des Travaux Publics, Beyrouth.
- Dunham, R. J. (1962). *Memoir 1: Classification of carbonate rocks - A Symposium*, chapter Classification of carbonate rocks according to depositional texture., pages 108–121. American Association of Petroleum Geologists.
- Ferry, S., Merran, Y., Grosheny, D., and Mroueh, M. (2007). *Relations between the northern and southern margins of the Tethys ocean during the Cretaceous period*, chapter The Cretaceous of Lebanon in the Middle East (Levant) context. Carnets de Géologie / Notebooks on Geology, Brest.
- Flügel, E. (2004). *Microfacies of Carbonate Rocks: Analysis, Interpretation and Application*. Springer.
- Folk, R. L. (1959). Practical petrographical classification of limestones. *American Association of Petroleum Geologists Bulletin*, 43:1–38.

- Folk, R. L. (1962). *Memoir 1: Classification of carbonate Rocks - A Symposium*, chapter Spectral subdivision of limestone types, pages 62–84. American Association of Petroleum Geologists.
- Fossen, H., Schultz, R. A., Shipton, Z. K., and Mair, K. (2007). Deformation bands in sandstone: a review. *Journal of the Geological Society*, 164(4):755–769.
- Freund, R., Zak, I., Goldberg, M., Weissbrod, T., and Derin, B. (1970). The shear along the Dead Sea Rift. *Philos. Trans. Roy. Soc. London*, A267:107–310.
- Garfunkel, Z. (1981). Internal structure of the Dead-Sea leaky transform (rift) in relation to plate kinematics. *Tectonophysics*, 80(1-4):81–108.
- Gomez, F., Karam, G., Khawlie, M., McClusky, S., Vernant, P., Reilinger, R., Jaafar, R., Tabet, C., Khair, K., and Barazangi, M. (2007). Global Positioning System measurements of strain accumulation and slip transfer through the restraining bend along the Dead Sea fault system in Lebanon. *Geophysical Journal International*, 168(3):1021–1028.
- Gomez, F., Khawlie, M., Tabet, C., Darkal, A., Khair, K., and Barazangi, M. (2006). Late Cenozoic uplift along the northern Dead Sea transform in Lebanon and Syria. *Earth and Planetary Science Letters*, 241(3-4):913–931.
- Grasemann, B. and Zámolyi, A. (2012). Report to OMV: Structural evolution of the Qartaba Anticline, Lebanon. Unpublished.
- Hardy, C., Homberg, C., Eyal, Y., Barrier, E., and Mueller, C. (2010). Tectonic evolution of the southern Levant margin since Mesozoic. *Tectonophysics*, 494(3-4):211–225.
- Hatzenbichler, G., Bauer, H., Grasemann, B., Tari, G., Nader, F. H., Church, J., and Schneider, D. (2013). The Lower Cretaceous Chouf Sandstone of Lebanon: is it a syn-rift clastic sequence? In *EGU General Assembly Conference Abstracts*, volume 15 of *EGU General Assembly Conference Abstracts*, page 9816.
- Hawie, N., Deschamps, R., Nader, F., Gorini, C., Müller, C., Desmares, D., Hoteit, A., Granjeon, D., Montadert, L., and Baudin, F. (2014). Sedimentological and stratigraphic evolution of northern Lebanon since the Late Cretaceous: implications for the Levant margin and basin. *Arabian Journal of Geosciences*, 7(4):1323–1349.
- Hawie, N., Gorini, C., Deschamps, R., Nader, F. H., Montadert, L., Granjeon, D., and Baudin, F. (2013). Tectono-stratigraphic evolution of the northern Levant Basin (offshore Lebanon). *Marine and Petroleum Geology*, 48:392–410.
- Heybroek, M. and Dubertret, L. (1945). Cartes géologiques du liban au 1:50 000e. feuille de jezzine (avec notice explicative). République Libanaise, Ministère des Travaux Publics, Beyrouth.

Bibliography

- Homberg, C., Barrier, E., Mroueh, M., Hamdan, W., and Higazi, F. (2009). Basin tectonics during the Early Cretaceous in the Levant margin, Lebanon. *Journal of Geodynamics*, 47(4):218 – 223.
- Homberg, C., Barrier, E., Mroueh, M., Muller, C., Hamdan, W., and Higazi, F. (2010). Tectonic evolution of the central Levant domain (Lebanon) since Mesozoic time. In Homberg, C and Bachmann, M, editor, *Evolution of the Levant Margin and Western Arabia Platform since the Mesozoic*, volume 341 of *Geological Society Special Publication*, pages 245–268. Geological Soc Publishing House, England.
- Kanaan, F. (1966). Sedimentary Structures and Thickness and Facies Variation in the Basal Cretaceous Sandstones of Central Lebanon. Master's thesis, American University of Beirut. Faculty of Arts and Sciences. Department of Geology.
- Kesten, D., Weber, M., Haberland, C., Janssen, C., Agnon, A., Bartov, Y., Rabba, I., and Group, D. (2008). Combining satellite and seismic images to analyse the shallow structure of the Dead Sea Transform near the DESERT transect. *International Journal of Earth Sciences*, 97(1):153–169.
- McKee, E. (1963). Origin of the Nubian and Similar Sandstones. *International Journal of Earth Sciences*, 52.
- Morhange, C., Pirazzoli, P. A., Marriner, N., Montaggioni, L. F., and Nammour, T. (2006). Late Holocene relative sea-level changes in Lebanon, Eastern Mediterranean. *Marine Geology*, 230(1-2):99–114.
- Nader, F. and Swennen, R. (2004a). Petroleum prospects of Lebanon: some remarks from sedimentological and diagenetic studies of Jurassic carbonates. *Marine and Petroleum Geology*, 21(4):427–441.
- Nader, F. and Swennen, R. (2004b). The hydrocarbon potential of Lebanon: New insights from regional correlations and studies of Jurassic dolomitization. *Journal of Petroleum Geology*, 27(3):253–275.
- Nader, F. H. (2011). The Petroleum Prospectivity of Lebanon: An Overview. *Journal of Petroleum Geology*, 34(2):135–156.
- Passchier, C. and Trouw, R. (2005). *Microtectonics*. Number Bd. 1 in *Microtectonics*. New York.
- Ponikarov, V., editor (1967). *The Geology of Syria, Part 1: Stratigraphy, Igneous Rocks and Tectonics*. Syrian Arab Republic, Ministry of Industry, Damascus.
- Quennell, A. (1958). The structure and evolution of the Dead Sea rift. *Quarterly Journal of the Geological Society of London*, 64:1–24.
- Renouard, G. (1955). Oil prospects of Lebanon. *American Association of Petroleum Geologists Bulletin*, 39:2125–2169.

- Schlagintweit, F., Gawlick, H., and Lein, R. (2005). Mikropaläontologie und Biostratigraphie der Plassen-Karbonatplattform der Typlokalität (Ober-Jura bis Unter-Kreide, Salzkammergut, Österreich). *Mitt. Ges. Geol. Bergbaustud. Österr.*, 47:11–102.
- Schultz, R. A. and Fossen, H. (2008). Terminology for structural discontinuities. *American Association of Petroleum Geologists Bulletin*, 92(7):853–867.
- Searle, M. P., Chung, S.-L., and Lo, C.-H. (2010). Geological offsets and age constraints along the northern Dead Sea fault, Syria. *Journal of the Geological Society*, 167(5):1001–1008.
- Segev, A. (2009). Ar-40/Ar-39 and K-Ar geochronology of Berriasian-Hauterivian and Cenomanian tectonomagmatic events in northern Israel: implications for regional stratigraphy. *Cretaceous Research*, 30(3):810–828.
- Smith, S. A. F., Di Toro, G., Kim, S., Ree, J.-H., Nielsen, S., Billi, A., and Spiess, R. (2013). Coseismic recrystallization during shallow earthquake slip. *Geology*, 41(1):63–66.
- Steinberg, J., Gvirtzman, Z., and Garfunkel, Z. (2014). Flexural response of a continental margin to sedimentary loading and lithospheric rupturing: The mountain ridge between the Levant Basin and the Dead Sea Transform. *Tectonics*, 33(2):166–186.
- Tasli, K. (2001). Benthic Foraminifera of the Upper Jurassic Platform Carbonate Sequence in the Aydinçik (Icel) Area, Central Taurides, S Turkey. *Geologia Croatica*, 54/1:1–13.
- Tixier, B. (1971-1972). Le 'Grès de Base' Crétacé du Liban: Étude Stratigraphique et Granulométrique. *Notes et Mémoires sur Le Moyen-Orient, Muséum National d'Histoire Naturelle, Paris*, 12:207–213.
- Ukla, S. (1970). Subsurface Geology and Well Correlation in North and Central Lebanon. Master's thesis, American University of Beirut. Faculty of Arts and Sciences. Department of Geology.
- Van Der Pluijm, B. and Marshak, S. (2004). *Earth Structure: An Introduction to Structural Geology and Tectonics*. W W Norton & Company Incorporated.
- Wakim, S. (1968). Petrography of the Basal Cretaceous Sandstone of Central Lebanon. Master's thesis, American University of Beirut. Faculty of Arts and Sciences. Department of Geology.
- Walley, C. (1983). A revision of the Lower Cretaceous stratigraphy of Lebanon. *Geologische Rundschau*, 72(1):377–388.
- Walley, C. (1988). A braided strike-slip model for the Northern continuation of the Dead-Sea Fault and its implications for Levantine tectonics. *Tectonophysics*, 145(1-2):63–72.

Bibliography

- Walley, C. (1997). The lithostratigraphy of Lebanon: A review. *Lebanese Science Bulletin*, 10:81–108.
- Walley, C. (1998). Some outstanding issues in the geology of Lebanon and their importance in the tectonic evolution of the Levantine region. *Tectonophysics*, 298(1-3):37–62.
- Walley, C. (2001). The Lebanon passive margin and the evolution of the Levantine Neo-Tethys. In Ziegler, PA and Cavazza, W and Robertson, AHF and CrasquinSoleau, S, editor, *Peri-Tethys Memoir 6: Peri-Tethan Rift/Wrench Basins and Passive Margins*, volume 186 of *Memoires du Museum National d Histoire Naturelle*, pages 407–439. Publications Scientiques du Museum.
- Walley, C. (2011). Geology of Lebanon. In *Resource Book for OMV Trip (Unpublished)*.
- Yamato, P., Kaus, B. J. P., Mouthereau, F., and Castelltort, S. (2011). Dynamic constraints on the crustal-scale rheology of the Zagros fold belt, Iran. *Geology*, 39(9):815–818.

List of Figures

1.1	Lebanon geology - overview	9
1.2	Lebanon cross section	10
1.3	The layer-cake stratigraphy of Lebanon	11
1.4	Stratigraphic chart of Lebanon	12
1.5	Karstification of the Kesrouane Fm. Stop 20 - Bataara sinkhole.	14
1.6	Bhannes Fm. at stop 22	15
1.7	Bikfaya Fm. at stop 24	16
1.8	Abeih Fm. at stop 19	18
1.9	Transition zone between Mdairej and Hammana Fms. at stop 38	19
1.10	Sannine Fm. at stop 36	20
1.11	Stratigraphy of the Cretaceous (Ferry et al., 2007)	22
1.12	Lebanon's main geologic structures and faults	24
1.13	Northern Lebanon cross sections	25
1.14	A simplified overview over the fault system in Lebanon	26
1.15	Structural geologic map of the Eastern Mediterranean region	28
1.16	Tectonic evolution of the Levant margin	29
1.17	Major tectonic divisions within the Lebanon-Syria region	33
1.18	Western Lebanon Flexure	34
1.19	Stops of the 2012 field campaign	35
2.1	Qartaba structure - cross section	37
2.2	Stop 6 overview	38
2.3	Stop 8 overview	39
2.4	Stops 12 & 13 overview	40
3.1	Classification of mechanical twinning in calcite	41
3.2	Thin section of sample 14/01a	42
3.3	Thin section of sample 14/02a	43
3.4	Stop 18 - overturned limb of Bikfaya Formation	44
3.5	Thin section of sample 18/01b	45
3.6	Stop 18. Deformation model.	46
3.7	Thin section of sample 21/01a	47
3.8	Stop 22 - volcanoclastic rocks	48
3.9	Thin section of sample 22/01b	49
3.10	Thin section of sample 22/01a	49
3.11	Thin section of sample 22/01b	50
3.12	Thin section of sample 22/02a	51

List of Figures

3.13	Thin section of sample 22/02a	52
3.14	Thin section of sample 22/02a	53
3.15	Thin section of sample 22/02a	53
4.1	Tilted block tectonics and sedimentation from the Middle Jurassic to Early Cretaceous	57
4.2	Chouf Fm. at stop 2	59
4.3	Chouf Fm. at stop 4	60
4.4	Chouf Fm. at stop 5	61
4.5	Chouf Fm. at stop 7	62
4.6	Chouf Fm. at stop 14	63
4.7	Chouf outcrop map and sampling spots	64
4.8	Heavy mineral spectra of the Chouf sandstone samples	65
4.9	X-ray diffraction spectrum, Chouf sandstone sample S14/03	66
4.10	X-ray diffraction spectrum, Chouf sandstone sample S23/07	66
4.11	Regional isopach map of the Basal Cretaceous Sandstones from Kanaan (1966)	68
4.12	Chouf Fm. outcrop and isopach map from Bellos (2008)	69
4.13	Chouf Fm. isopach map from Grasemann and Zámolyi (2012)	70
4.14	ArcGIS: three-point problem	72
4.15	Python toolbox for solving the three-point problem	73
4.16	Three main cases for the calculation of true stratigraphic thickness (TST)	74
4.17	Isopach map of the Chouf Fm.	76
4.18	2D isopach model of the Chouf Fm.	77
4.19	3D isopach model of the Chouf Fm.	77
4.20	Calculation of the TVT	78
4.21	Isochore map of the Chouf Fm.	79
4.22	2D isochore model of the Chouf Fm.	80
4.23	Results of the heavy mineral analysis	82
4.24	Isopach map of the Chouf Fm.	83

List of Tables

3.1	Thin sections	41
4.1	TST-points used for the Chouf isopach model	75

Appendix

I. Zusammenfassung

Das engere Forschungsgebiet umfasst das nördliche Libanon-Gebirge zwischen Beirut und Tripoli, wo die Exkursion und Probennahme stattfanden. Das erweiterte Forschungsgebiet für Fernerkundung und Isopachenstudien setzt sich etwas gegen Süden fort.

Die Untersuchung von Dünnschliffen von Gesteinsproben verschiedener stratigraphischer Einheiten konzentrierte sich auf die (bio-)stratigraphische Klassifizierung und strukturgeologische Interpretation dieser Gesteine. Zu den Ergebnissen zählt ein Deformationsmodell für die Qartaba-Struktur, welches zwei Deformationsphasen beschreibt: auf eine erste Faltungsphase inklusiver Schichtgleitfaltung, welche zur Bildung zahlreicher Adern führte, folgte eine zweite, von Drucklösungsprozessen gekennzeichnete Phase (Bildung von Stylolithen). Die Beobachtung von möglicherweise bei Erdbeben gebildetem, dynamisch rekristallisiertem Quarz in Dünnschliffen von vulkanoklastischen Gesteinen der Bhannes-Formation deutet auf die seismische Deformation dieser Gesteine hin.

Das Hauptaugenmerk dieser Arbeit liegt jedoch auf der Entwicklung der unterkre-tazischen Chouf-Formation, deren tektonischen Ablagerungsbedingungen aufgrund ihrer starken Mächtigkeitsschwankungen in der Vergangenheit viel diskutiert wurden. Eine Analyse der Schwerminerale zeigte, dass nur die stabilsten Schwerminerale erhalten sind, was auf einen präexistenten Sandstein als Muttergestein hindeutet und somit die Herkunftsmodelle zum Chouf-Sandstein aus der Literatur unterstützt. Das unter Verwendung von Feld- und Fernerkundungsdaten entwickelte Isopachen-Modell veranschaulicht die mehrmals von Nord nach Süd auftretenden Mächtigkeitsunterschiede der Chouf-Fm. In Anbetracht der gleich alten, O-W streichenden Abschiebungen wird, wie schon von [Collin et al. \(2010\)](#) vorgeschlagen, von einer Ablagerung in einer aktiven Riftzone ausgegangen. Eine ebenfalls erstellte Isochorenkarte unterscheidet sich aufgrund des seichten Schichteinfallens der Chouf-Fm. nur wenig von der Isopachenkarte.

II. Lists and field report

- A. List of field stops
- B. List of TST (total stratigraphic thickness) and TVT (total vertical thickness) points
- C. Field report of the 2012 field campaign - Chouf stops

List of field stops

Stop	UTM (Zone 36)		Elevation m a.s.l.	Formation	Sample	Location
	N	E				
Day 1 / 1	3759080	744104	94	Kesrouane		Jeita Grotto
2	3759430	743657	113	Chouf	S2/01	Jeita Grotto
3	3766144	754202	1322	Kesrouane		Ain Ej Jorn
4	3767938	755335	1403	Chouf	S4/02	Mairouba
5	3768883	756226	1472	Chouf		Ain Ed Delbe
6	3772125	760143	1466	Chouf		Bhassis
7	3772226	760428	1447	Chouf	S7/03, S7/04	Bhassis
8	3772346	760843	1468	(overview stop)		Bhassis
9	3773493	766968	1149	Sannine		Afqa cave
10	3777101	767089	1263	Hammana, Sannine		Majdel
11	3776499	765091	145	Kesrouane - Sannine		Mghaira
12	3777858	762071	1528	Abeih, Mdairej		Qartaba
13	3778018	762199	1535	Abeih, Mdairej		Qartaba
Day 2 / 14	3779901	757627	1261	Chouf	14/1, 14/2, S14/05	Hrazmin
15	3779923	758440	1253	Bhannes, Bikfaya		Bqarta
16	3780852	761001	1452	Kesrouane		Moukhada
17	3779847	761266	1628	Kesrouane		Moukhada
18	3779958	762510	1620	Bikfaya, Salima, Chouf	18/1, S18/06	Moukhada
19	3782860	763842	1681	Abeih		Boaatara
20	3785231	764554	1542	Kesrouane		Baatara pothole
21	3785205	764422	1559	Kesrouane, Bhannes	21/1	Boaatara
22	3786198	765443	1439	Bhannes	22/1	Meghrak
23	3787013	770316	1752	Chouf	S23/07	Hourata
24	3788181	771851	1726	Bhannes, Bikfaya		Harissa
25	3790170	771471	1741	Bhannes		Tannourine
26	3790607	770199	1720	Kesrouane, Bhannes, Chouf	S26/08	Tannourine
27	3800219	763323	224	Sannine, Maameltain, Chekka		Kousba
Day 3 / 28	3792183	758379	668	(overview stop)		Bsetine el Osse
29	3787962	765947	1111	Kesrouane		Ouadi Tannourine
30	3788279	760991	1221	Kesrouane - Sannine		Ouadi Tannourine
31	3787642	759476	1178	Sannine		Tartij
32	3786403	759974	1096	Sannine, volcanics		Tartij
33	3782062	760768	1668	Kesrouane		Jajj Cedar Park
34	3781965	761448	1813	Kesrouane		Jajj Cedar Park
Day 4 / 35	3773492	745603	138	Sannine, Maameltain		Nahr Ibrahim valley
36	3773816	746515	85	Sannine		Nahr Ibrahim valley
37	3774566	747644	88	Hammana, Sannine		Nahr Ibrahim valley
38	3774667	749332	169	Mdairej, Hammana, Sannine		Nahr Ibrahim valley
39	3773980	751386	322	Kesrouane - Sannine		Nahr Ibrahim valley

List of TST and TVT points

Point	UTM (Zone 36)		(in meters)		Source
	N	E	TST	TVT	
1	3772226	760428	163	230	Dip/dir-data from 2012 field campaign
2	3779901	757627	144	124	Dip/dir-data from 2012 field campaign
3	3779958	762510	41	18	Dip/dir-data from 2012 field campaign
4	3784399	767546	149	151	Dip/dir-data from Grasemann & Zámolyi (2012) database
5	3784664	767638	154	159	Dip/dir-data from Grasemann & Zámolyi (2012) database
6	3777273	761886	116	149	Dip/dir-data from Grasemann & Zámolyi (2012) database
7	3790620	769480	20	20	Dip/dir-data from Grasemann & Zámolyi (2012) database
8	3782809	764019	29	29	Dip/dir-data from Grasemann & Zámolyi (2012) database
9	3782815	763868	16	16	Dip/dir-data from Grasemann & Zámolyi (2012) database
10	3785075	765376	131	134	Dip/dir-data from Grasemann & Zámolyi (2012) database
11	3793198	767863	373	430	Dip/dir-data from Grasemann & Zámolyi (2012) database
12	3777660	762044	151	168	Dip/dir-data from remote sensing
13	3777113	761969	141	145	Dip/dir-data from remote sensing
14	3776933	762810	108	113	Dip/dir-data from remote sensing
15	3777562	763003	227	309	Dip/dir-data from remote sensing
16	3777730	763066	153	160	Dip/dir-data from remote sensing
17	3778189	763717	257	285	Dip/dir-data from remote sensing
18	3778448	763952	278	310	Dip/dir-data from remote sensing
19	3778596	764129	369	479	Dip/dir-data from remote sensing
20	3779044	757028	94	96	Dip/dir-data from remote sensing
21	3778986	756361	86	129	Dip/dir-data from remote sensing
22	3768176	757039	156	169	Dip/dir-data from remote sensing
23	3768184	757050	152	163	Dip/dir-data from remote sensing
24	3768293	757048	136	140	Dip/dir-data from remote sensing
25	3768079	757127	148	150	Dip/dir-data from remote sensing
26	3790620	769480	18	18	Dip/dir-data from remote sensing
27	3790662	769480	18	18	Dip/dir-data from remote sensing
28	3792867	769063	92	92	Dip/dir-data from remote sensing
29	3792509	768930	209	210	Dip/dir-data from remote sensing
30	3784508	767460	111	111	Dip/dir-data from remote sensing
31	3785089	765491	102	103	Dip/dir-data from remote sensing
32	3790003	764388	32	32	Dip/dir-data from remote sensing
33	3790071	764417	30	31	Dip/dir-data from remote sensing
34	3787030	769681	48	48	Dip/dir-data from remote sensing
35	3787047	769658	49	49	Dip/dir-data from remote sensing
36	3778037	764592	147	149	Dip/dir-data from remote sensing
37	3783243	764356	137	138	Dip/dir-data from remote sensing
38	3783264	764458	238	252	Dip/dir-data from remote sensing
39	3783342	764661	293	305	Dip/dir-data from remote sensing
40	3783318	764686	255	262	Dip/dir-data from remote sensing
41	3764633	759214	509	541	Dip/dir-data from remote sensing
42	3762532	756947	464	470	Dip/dir-data from remote sensing
43	3759989	761325	185	186	Dip/dir-data from remote sensing
44	3760280	761939	301	309	Dip/dir-data from remote sensing
45	3760267	762158	217	218	Dip/dir-data from remote sensing
46	3757228	759263	80	80	Dip/dir-data from remote sensing

47	3754874	759489	286	287	Dip/dir-data from remote sensing
48	3755357	763357	342	344	Dip/dir-data from remote sensing
49	3751962	762749	224	224	Dip/dir-data from remote sensing
50	3751869	762951	251	251	Dip/dir-data from remote sensing
51	3798264	769015	38	38	Dip/dir-data from remote sensing
52	3798286	771143	32	33	Dip/dir-data from remote sensing
53	3797831	773074	44	48	Dip/dir-data from remote sensing
54	3796654	772490	77	81	Dip/dir-data from remote sensing
55	3795256	768408	58	59	Dip/dir-data from remote sensing
56	3794690	768863	54	55	Dip/dir-data from remote sensing
57	3794373	769505	12	12	Dip/dir-data from remote sensing
58	3794311	769868	53	53	Dip/dir-data from remote sensing
59	3793268	769195	48	53	Dip/dir-data from remote sensing
60	3793070	766618	247	252	Dip/dir-data from remote sensing
61	3791069	767399	39	40	Dip/dir-data from remote sensing
62	3796053	771062	28	31	Dip/dir-data from remote sensing
63	3794545	775894	23	23	Dip/dir-data from remote sensing
64	3792569	774989	50	52	Dip/dir-data from remote sensing
65	3792349	773743	48	51	Dip/dir-data from remote sensing
66	3792323	770103	20	20	Dip/dir-data from remote sensing
67	3793362	768731	208	212	Dip/dir-data from remote sensing
68	3790676	769258	17	18	Dip/dir-data from remote sensing
69	3789110	771276	42	46	Dip/dir-data from remote sensing
70	3787172	770883	49	50	Dip/dir-data from remote sensing
71	3784740	768931	65	66	Dip/dir-data from remote sensing
72	3784604	766752	213	224	Dip/dir-data from remote sensing
73	3780469	762673	51	53	Dip/dir-data from remote sensing
74	3776587	762362	168	178	Dip/dir-data from remote sensing
75	3778147	765570	109	113	Dip/dir-data from remote sensing
76	3777921	764293	150	154	Dip/dir-data from remote sensing
77	3777573	763192	195	218	Dip/dir-data from remote sensing
78	3775694	765824	214	246	Dip/dir-data from remote sensing
79	3774096	766256	75	79	Dip/dir-data from remote sensing
80	3773771	764081	170	199	Dip/dir-data from remote sensing
81	3773450	763370	140	144	Dip/dir-data from remote sensing
82	3772394	761410	223	237	Dip/dir-data from remote sensing
83	3778929	756530	112	116	Dip/dir-data from remote sensing
84	3771211	752021	210	230	Dip/dir-data from remote sensing
85	3771369	757588	125	127	Dip/dir-data from remote sensing
86	3768338	758704	186	187	Dip/dir-data from remote sensing
87	3767637	760393	144	159	Dip/dir-data from remote sensing
88	3766365	759284	161	163	Dip/dir-data from remote sensing
89	3764704	758445	396	406	Dip/dir-data from remote sensing
90	3750118	759823	214	216	Dip/dir-data from remote sensing
91	3747639	761605	105	110	Dip/dir-data from remote sensing
92	3767878	749023	46	47	Dip/dir-data from remote sensing
93	3755209	762243	338	347	Dip/dir-data from remote sensing
94	3756058	740028	176	184	Dip/dir-data from remote sensing
95	3754029	741360	62	62	Dip/dir-data from remote sensing
96	3754593	743356	263	267	Dip/dir-data from remote sensing

97	3756403	750830	256	280	Dip/dir-data from remote sensing
98	3753845	753571	259	260	Dip/dir-data from remote sensing
99	3751340	740517	338	347	Dip/dir-data from remote sensing
100	3750530	740027	138	141	Dip/dir-data from remote sensing
101	3749420	740302	155	161	Dip/dir-data from remote sensing
102	3751202	741991	264	284	Dip/dir-data from remote sensing
103	3752173	744320	265	278	Dip/dir-data from remote sensing
104	3750583	743679	239	247	Dip/dir-data from remote sensing
105	3746779	743688	444	458	Dip/dir-data from remote sensing
106	3747274	741597	424	431	Dip/dir-data from remote sensing
107	3746429	740267	155	160	Dip/dir-data from remote sensing
108	3744753	750011	472	484	Dip/dir-data from remote sensing
109	3746865	760682	173	176	Dip/dir-data from remote sensing
110	3743236	758638	148	149	Dip/dir-data from remote sensing
111	3741709	753085	372	405	Dip/dir-data from remote sensing
112	3735758	747507	184	202	Dip/dir-data from remote sensing
113	3735026	750379	88	90	Dip/dir-data from remote sensing
114	3733615	740641	193	207	Dip/dir-data from remote sensing
115	3735435	732494	205	206	Dip/dir-data from remote sensing
116	3708476	734835	676	697	Dip/dir-data from remote sensing
117	3703705	740553	558	563	Dip/dir-data from remote sensing
118	3710782	743504	207	210	Dip/dir-data from remote sensing
119	3748348	756430	173	173	Isopach points from Grasemann & Zámolyi (2012) database
120	3732381	731871	195		Isopach points from Grasemann & Zámolyi (2012) database
121	3759387	762408	281	283	Isopach points from Grasemann & Zámolyi (2012) database
122	3767662	758919	120		Isopach points from Grasemann & Zámolyi (2012) database
123	3795814	772052	19	19	Isopach points from Grasemann & Zámolyi (2012) database
124	3793155	772059	32	33	Isopach points from Grasemann & Zámolyi (2012) database
125	3791878	776994	102	104	Isopach points from Grasemann & Zámolyi (2012) database
126	3794418	777024	83	84	Isopach points from Grasemann & Zámolyi (2012) database
127	3794549	774751	33		Isopach points from Grasemann & Zámolyi (2012) database
128	3775525	755263	32	34	Isopach points from Grasemann & Zámolyi (2012) database
129	3767524	748719	71	81	Isopach points from Grasemann & Zámolyi (2012) database
130	3766749	748929	53	70	Isopach points from Grasemann & Zámolyi (2012) database
131	3778983	757073	139	310	Isopach points from Grasemann & Zámolyi (2012) database
132	3782528	758761	41	80	Isopach points from Grasemann & Zámolyi (2012) database
133	3790292	761825	43	46	Isopach points from Grasemann & Zámolyi (2012) database
134	3790522	767682	17	17	Isopach points from Grasemann & Zámolyi (2012) database
135	3793118	768020	231	235	Isopach points from Grasemann & Zámolyi (2012) database
136	3788933	771636	31	31	Isopach points from Grasemann & Zámolyi (2012) database
137	3783827	764622	338	343	Isopach points from Grasemann & Zámolyi (2012) database
138	3776621	764553	110		Isopach points from Grasemann & Zámolyi (2012) database
139	3772684	762881	120		Isopach points from Grasemann & Zámolyi (2012) database
140	3764163	746428	105		Isopach points from Grasemann & Zámolyi (2012) database
141	3755290	758281	218	219	Isopach points from Grasemann & Zámolyi (2012) database
142	3750690	761208	194	196	Isopach points from Grasemann & Zámolyi (2012) database
143	3739867	738854	310		Isopach points from Grasemann & Zámolyi (2012) database
144	3735537	736993	190		Isopach points from Grasemann & Zámolyi (2012) database
145	3732325	735026	210		Isopach points from Grasemann & Zámolyi (2012) database
146	3739811	744948	260		Isopach points from Grasemann & Zámolyi (2012) database

147	3750649	750155	280		Isopach points from Grasemann & Zámolyi (2012) database
148	3748991	748643	430	437	Isopach points from Grasemann & Zámolyi (2012) database
149	3748660	740021	231	236	Isopach points from Grasemann & Zámolyi (2012) database
150	3747658	742274	383	394	Isopach points from Grasemann & Zámolyi (2012) database
151	3754911	751610	220		Isopach points from Grasemann & Zámolyi (2012) database
152	3761112	756885	533	540	Isopach points from Grasemann & Zámolyi (2012) database
153	3768545	756304	197	200	Isopach points from Grasemann & Zámolyi (2012) database
154	3762132	744590	84		Isopach points from Grasemann & Zámolyi (2012) database
155	3760066	743803	225	266	Isopach points from Grasemann & Zámolyi (2012) database
156	3714400	743594	369	472	Isopach points from Grasemann & Zámolyi (2012) database
157	3719519	744633	166	235	Isopach points from Grasemann & Zámolyi (2012) database
158	3713344	736961	395	400	Isopach points from Grasemann & Zámolyi (2012) database
159	3725130	747054	208		Isopach points from Grasemann & Zámolyi (2012) database
160	3726932	747638	105		Isopach points from Grasemann & Zámolyi (2012) database
161	3732502	749254	60	63	Isopach points from Grasemann & Zámolyi (2012) database
162	3692019	730471	660		Isopach points from Grasemann & Zámolyi (2012) database
163	3715147	739104	225		Isopach points from Literature
164	3759502	758323	250		Isopach points from Literature
165	3809001	779151	10		Isopach points from Literature
166	3719902	739589	275		Isopach points from Literature
167	3751991	742688	150		Isopach points from Literature
168	3776658	762567	150		Isopach points from Literature
169	3735920	737027	220		Isopach points from Literature
170	3794494	776589	10		Isopach points from Literature
171	3760335	760422	240		Isopach points from Literature
172	3742846	732100	259		Isopach points from Literature
173	3736187	745007	250		Isopach points from Literature
174	3770368	751238	86		Isopach points from Literature
175	3768586	749731	89		Isopach points from Literature
176	3759864	743661	85		Isopach points from Literature
177	3750231	740859	150		Isopach points from Literature
178	3697929	710804	170		Isopach points from Literature
179	3728591	754982	128		Isopach points from Literature

LEBANON REPORT - FIELD-TRIP JULY 2012



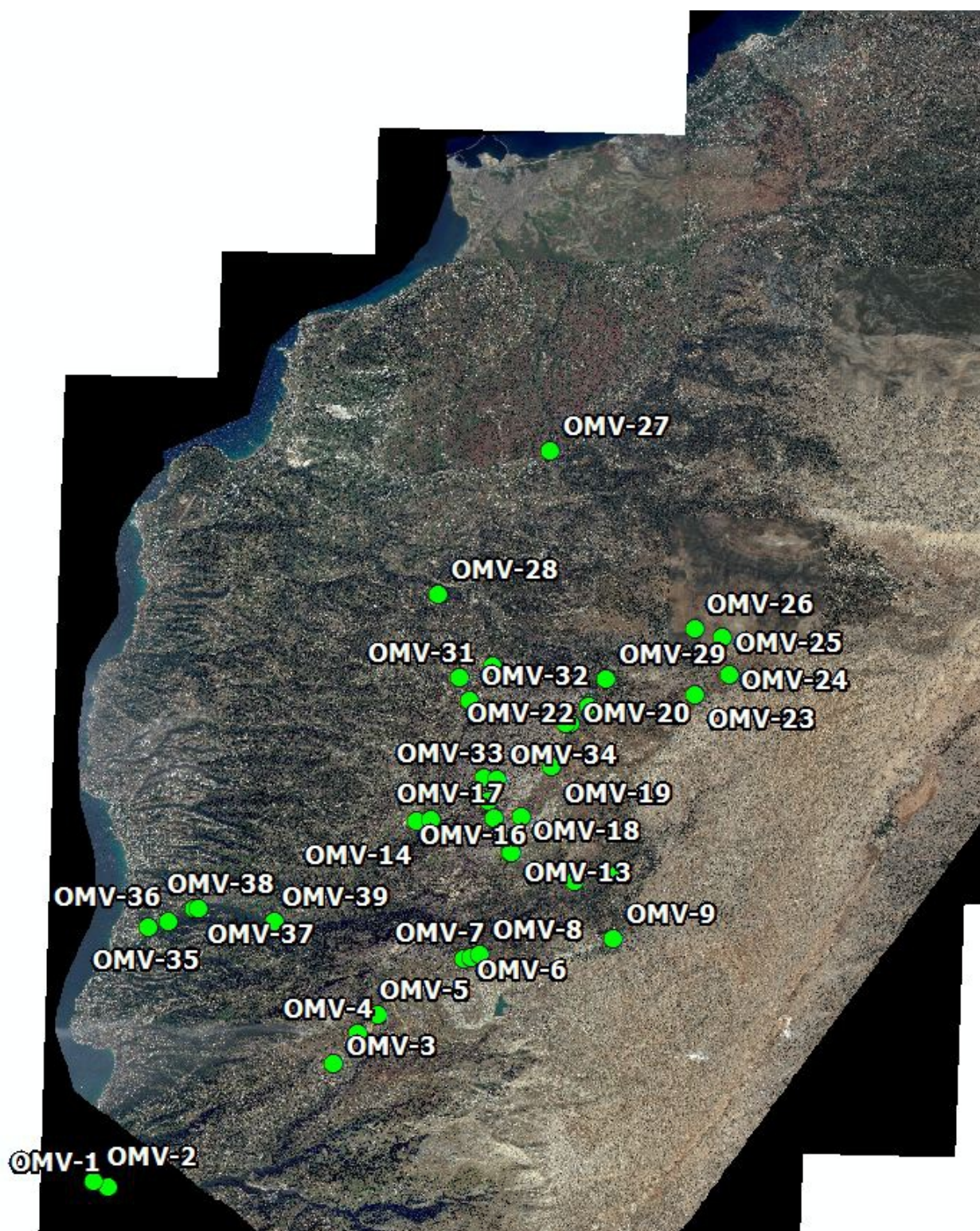
4. - 9. 7. 2012

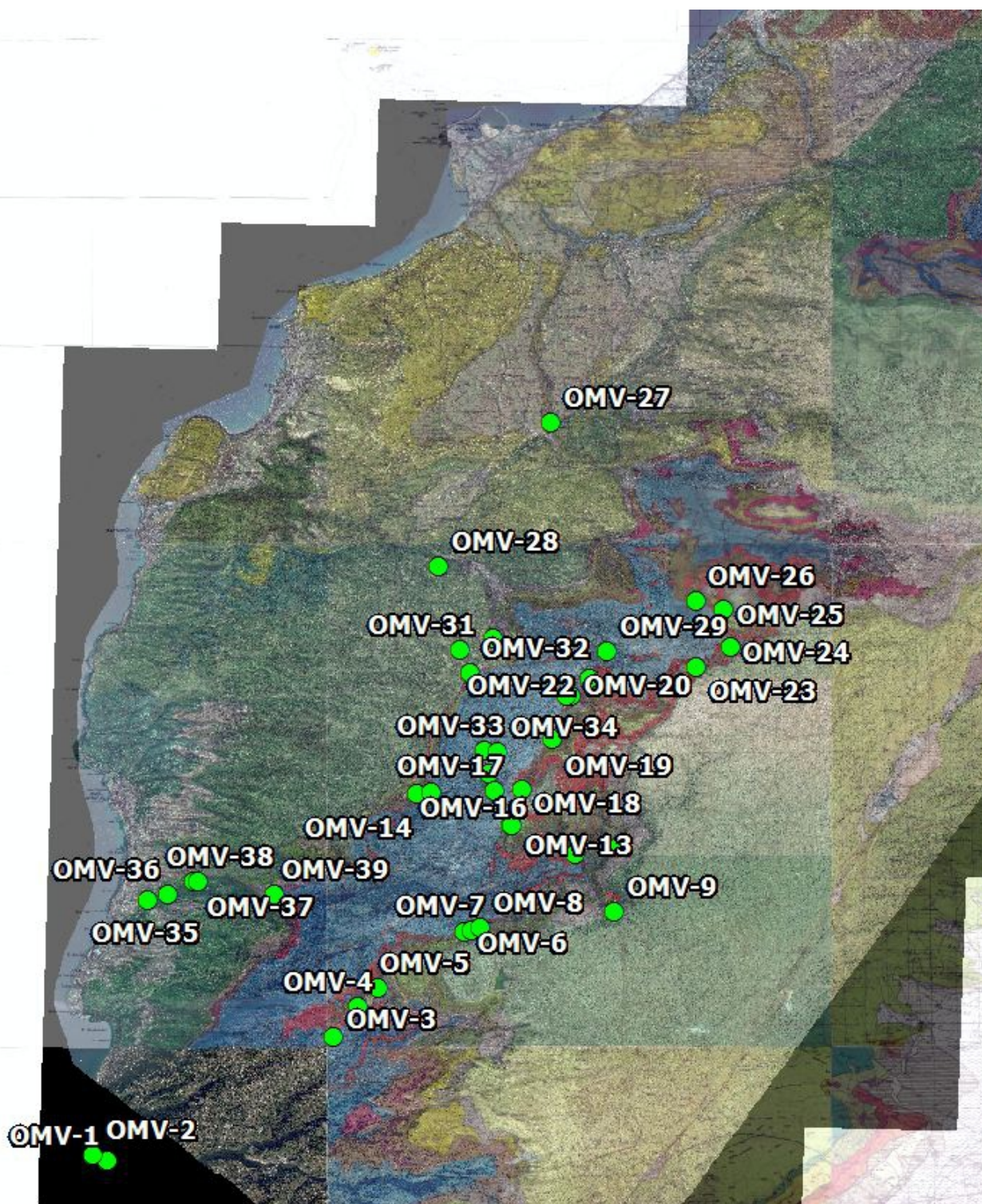
**HARALD BAUER
BERNHARD GRASEMANN
GEORG HATZENBICHLER**

Department of Geodynamics and Sedimentology



**universität
wien**





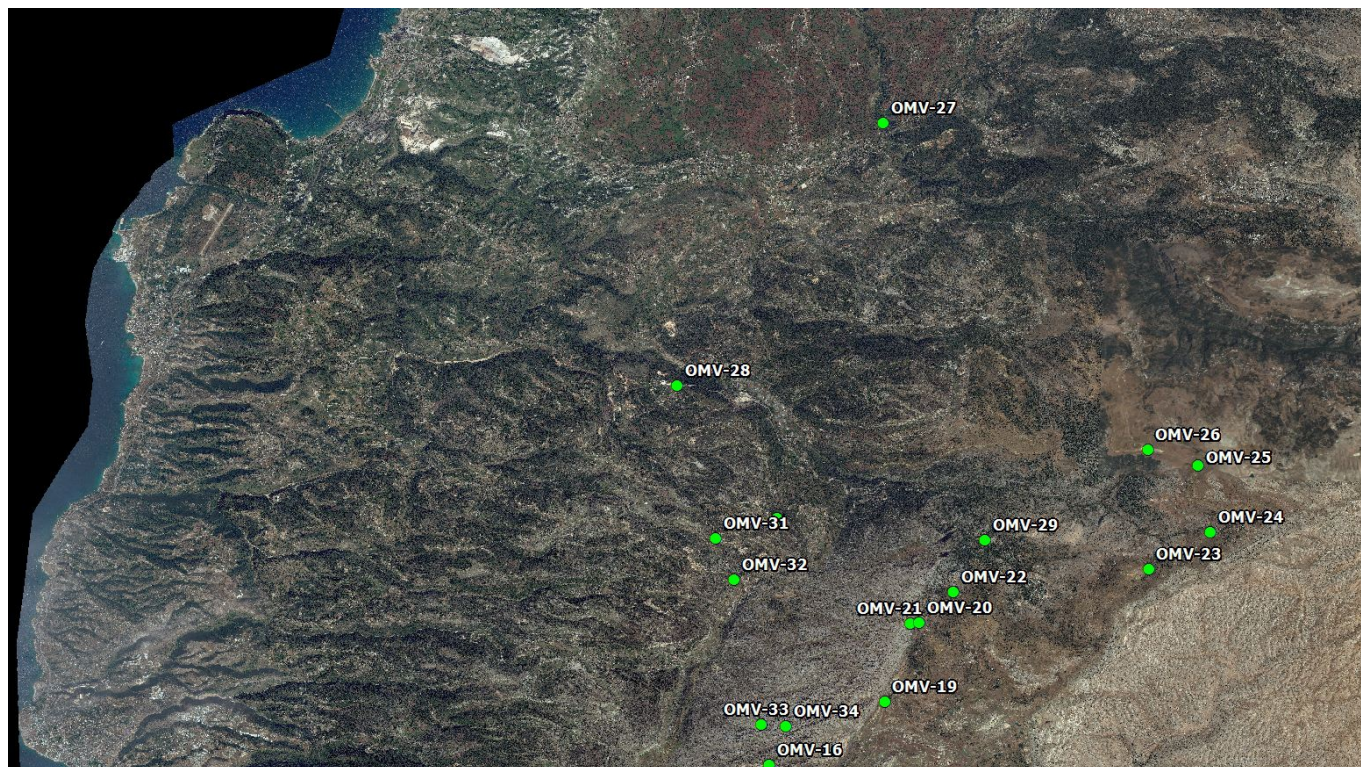


Photo QuickBird image - overview north 1:100,000

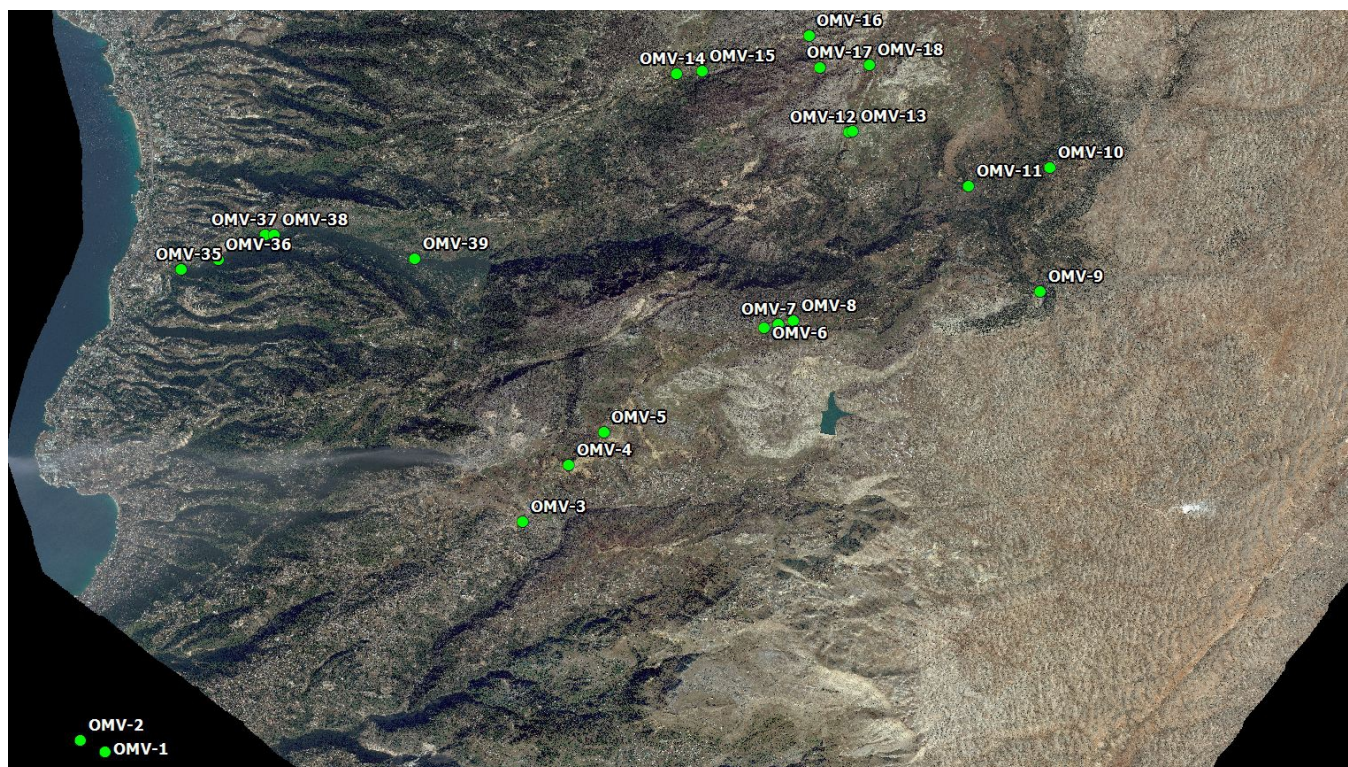


Photo QuickBird image - overview south 1:100,000

Structural Outcrop Analyses		Stop02
Outcrop No.		
Page		1

		UTM 36	
Locality	Jeita Grotto	E	743657
		N	3759430
Outcrop type	Street Outcrop	Elevation	112 m

Interpreter	Bauer, Grasemann, Hatzenbichler
Date	6.7.2012

Tectonic unit	
Lithostratigraphic unit	Chouf Sandstone Fm.
Stratigraphic age	Lower Cretaceous
Lithology	Brown to white, coarse to fine sandstone with clays and lignites

References	Walley (1998): Tectonophysics 298, 37-62.
	Walley (1983): Geologische Rundschau 72, 377-388.
	Hombert et al. (2009): Journal of Geodynamics 47, 218-223.

Outcrop description



Photo	DSC_0079 Hatzenbichler	Stop 02: Next to the Jeita Grotto
-------	------------------------	-----------------------------------

Structural Outcrop Analyses			Stop02
Outcrop No.			
Page			2
			UTM 36
Locality	Jeita Grotto	E	743657
		N	3759430
Outcrop type	Street Outcrop	Elevation	112 m

Location of the Outcrop

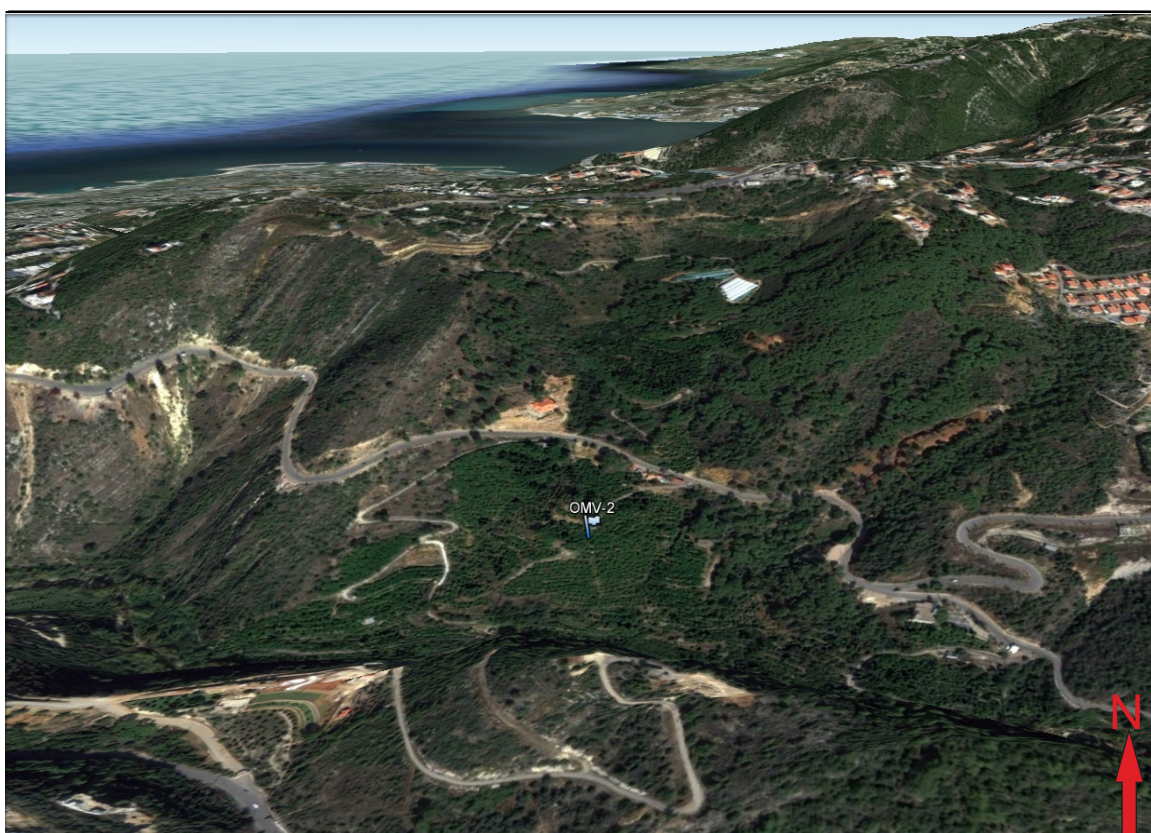


Photo Google Earth

Description

In this outcrop the yellowish-brown to white, coarse to fine grained sandstone is well bedded (dm-m) and records several layers with clear cross-bedding. Under the hand lense the sandstone appears well-sorted with grains partly coated by iron oxides. Generally the sandstone has been deposited in a fluvialite environment but here, locally dunes are preserved. The general dip of the bedding is towards WSW with about 40°.

The outcrop was sampled (S2/01) with the aim to constrain the heavy mineral spectra und to date zircon and apatite with either fission tracks and/or (U-Th)/He.

Structural Outcrop Analyses			Stop02
Outcrop No.			
Page			3
			UTM 36
Locality	Jeita Grotto	E	743657
		N	3759430
Outcrop type	Street Outcrop	Elevation	112 m

Location in the geological map

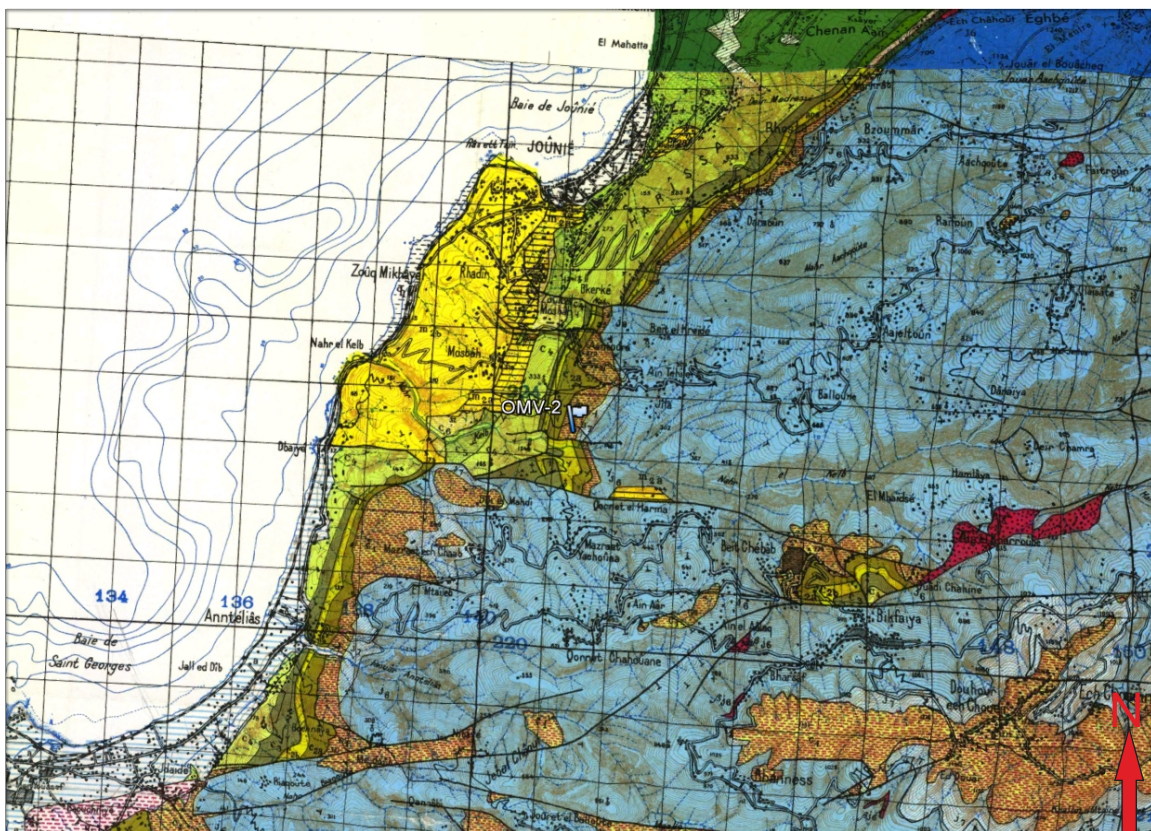


Photo Geological map of Lebanon, orig. 1:50 000 (Ministere des Travaux Publics, Beyrouth)

Structural Outcrop Analyses		Stop02
Outcrop No.		
<i>Page</i>		4
UTM 36		
Locality	Jeita Grotto	E 743657
		N 3759430
Outcrop type	Street Outcrop	Elevation 112 m

Stratigraphic interpretation

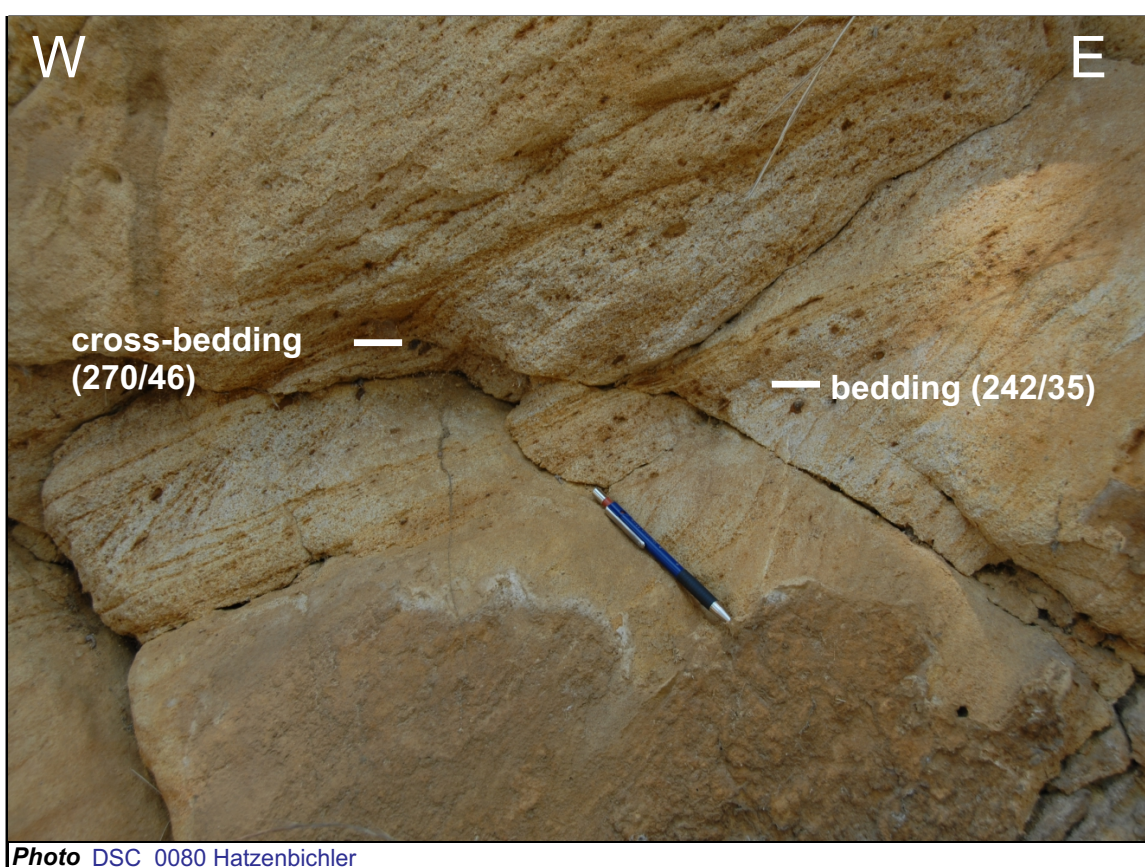


Photo DSC_0080 Hatzenbichler

Description

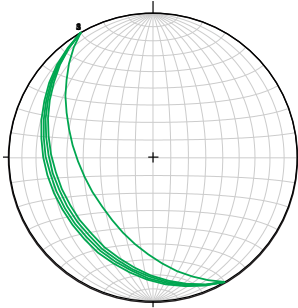
The Chouf Sandstone (bedding ss 242/35) with cross-bedding (scb 270/46). Although most of the cross-beds also dip like the bedding in a western direction (but with a steeper dip angle), a few layers with cross-beds, which dip to the E (089/15) have been observed.

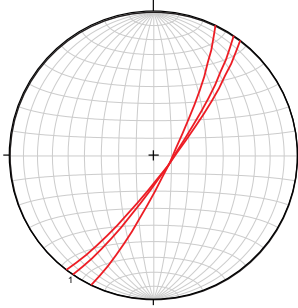
Structural Outcrop Analyses		Stop02
Outcrop No.		
	Page	5

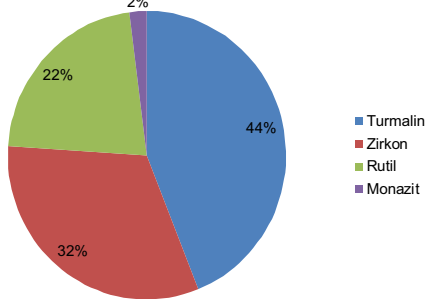
UTM 36

Locality	Jeita Grotto	E	743657
		N	3759430
Outcrop type	Street Outcrop	Elevation	112 m

Structural data interpretation

B	Bedding	
	Consistent bedding planes (ss 240/30).	

DB	Deformation Bands	
	Shear enhanced deformation bands (sdb 138/80).	

S	Sample S2/01	
	Chouf Sandstone heavy mineral spectrum: Dominated by turmaline, zircon and rutile	

Structural Outcrop Analyses		Stop04
Outcrop No.		
Page		1

		UTM 36	
Locality	Mairouba	E	755335
		N	3767938
Outcrop type	Sand pit	Elevation	1403 m

Interpreter	Bauer, Grasemann, Hatzenbichler
Date	6.7.2012

Tectonic unit	
Lithostratigraphic unit	Chouf Sandstone Fm.
Stratigraphic age	Lower Cretaceous
Lithology	Brown to white, coarse to fine sandstone with clays and lignites

References	Walley (1998): Tectonophysics 298, 37-62.
	Nader (2011): Journal of Petroleum Geology 34, 135-156.
	Homberg (2009): Journal of Geodynamics 47, 218-223.

Outcrop description



Photo	DSC_0101 Hatzenbichler	Stop 04: Sandpit
-------	------------------------	------------------

Structural Outcrop Analyses			Stop04
Outcrop No.			
Page			2
			UTM 36
Locality	Mairouba	E	755335
		N	3767938
Outcrop type	Sand pit	Elevation	1403 m

Location of the Outcrop

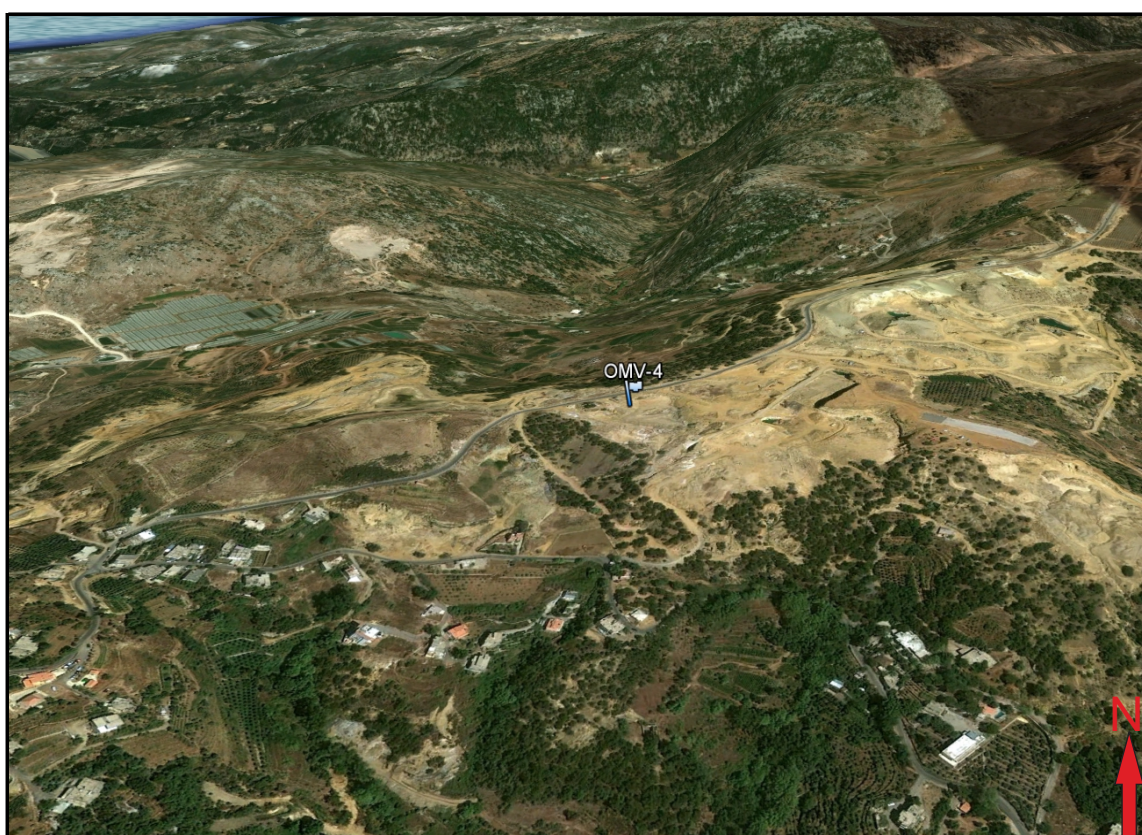


Photo Google Earth

Description

In this outcrop, the Lower Cretaceous Chouf sandstone shows white to reddish/brown sand layers with nicely developed foresets. A several dm-thick coal/clay layer serves as a marker horizon in this outcrop. Although numerous normal faults cut through the layers with offsets up to 1 m, the marker horizon records no significant downthrow along the exposed section. This observation suggests that most of the faults are high angle normal faults, which were rotating during extension in the same direction resulting in a domino or bookshelf type of deformation. Note that also the sections in this outcrop, which are not faulted, are cut by numerous compaction bands, which localized the meteoric fluids.

Structural Outcrop Analyses			Stop04
Outcrop No.			
Page			3
			UTM 36
Locality	Mairouba	E	755335
		N	3767938
Outcrop type	Sand pit	Elevation	1403 m

Location in the geological map

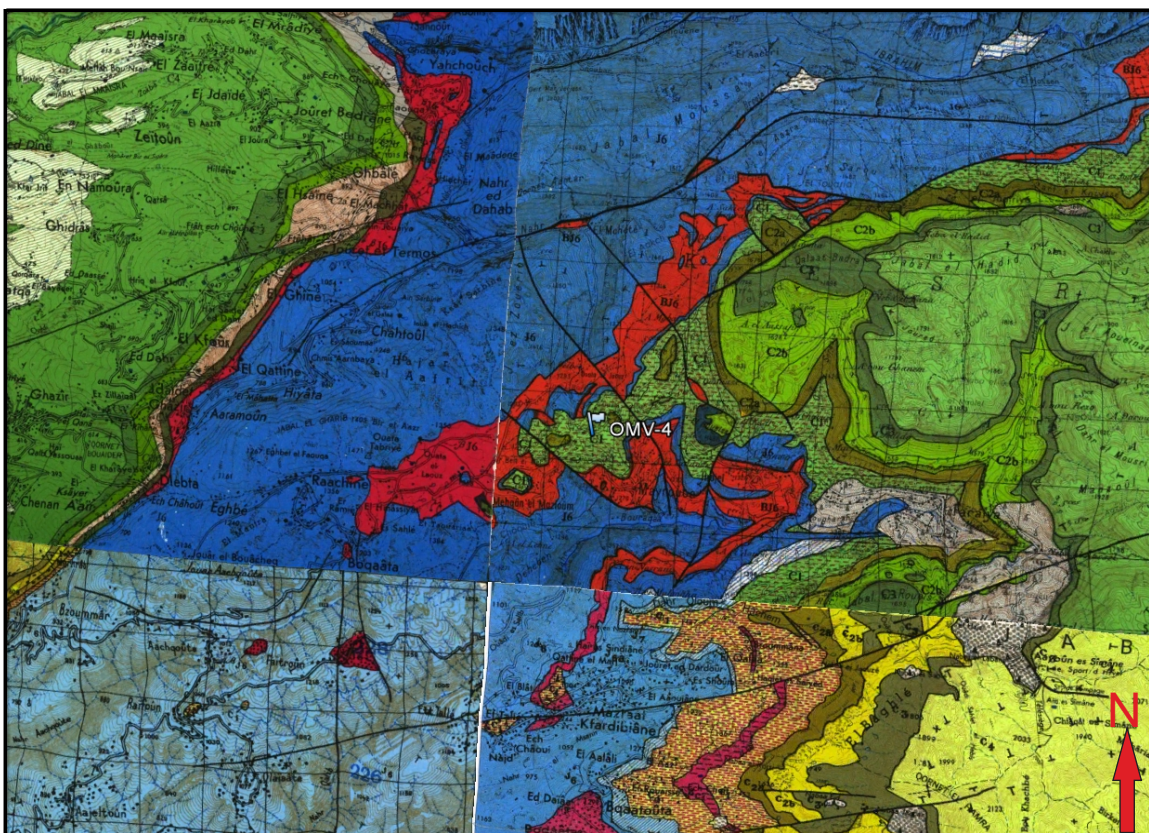


Photo Geological map of Lebanon, orig. 1:50 000 (Ministere des Travaux Publics. Beyrouth)

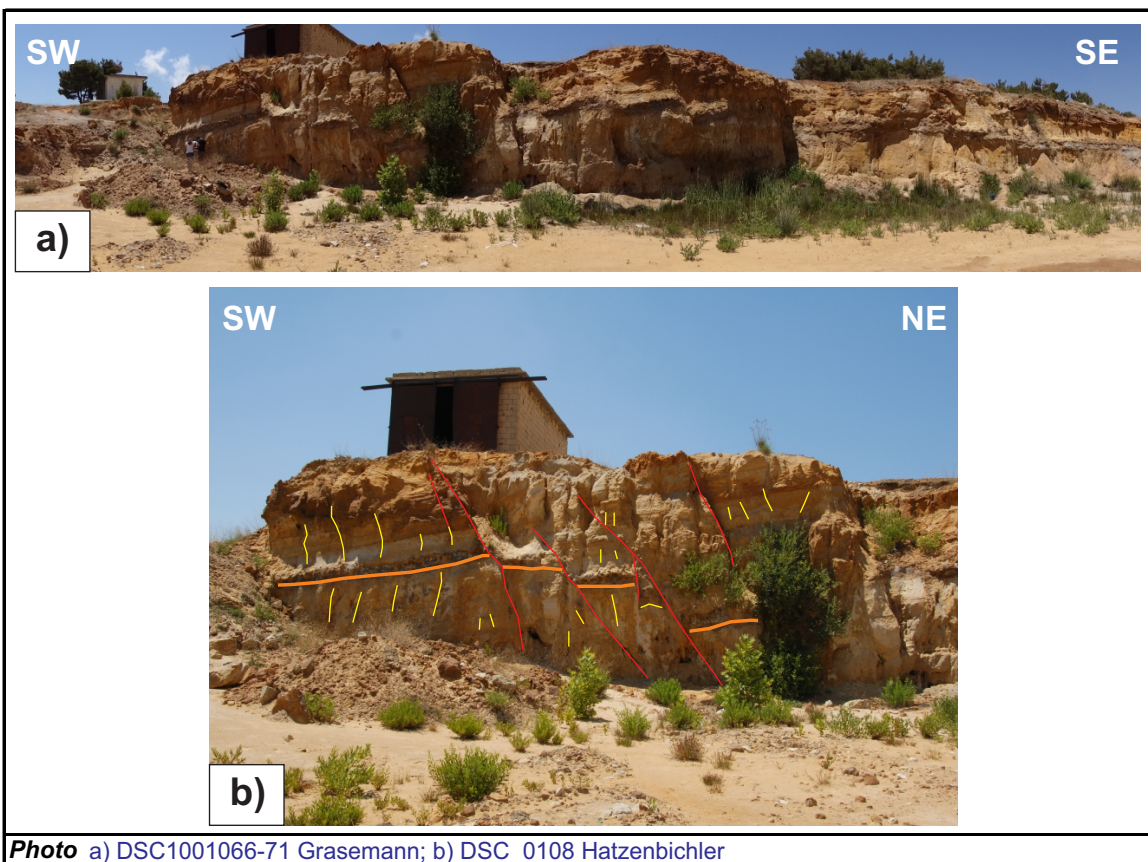
Structural Outcrop Analyses			Stop04
Outcrop No.			
Page			
			4
			UTM 36
Locality	Mairouba	E	755335
		N	3767938
Outcrop type	Sand pit	Elevation	1403 m

Location in the QuickBird image



Structural Outcrop Analyses			Stop04
Outcrop No.			
Page			5
			UTM 36
Locality	Mairouba	E	755335
		N	3767938
Outcrop type	Sand pit	Elevation	1403 m

Structural data interpretation

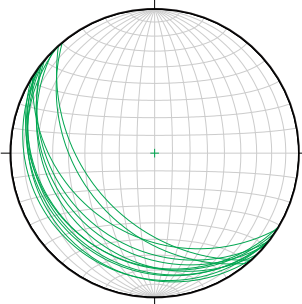


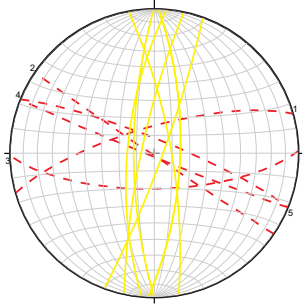
Description

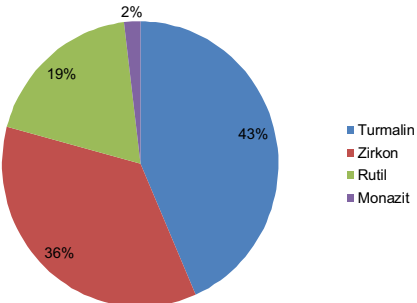
a) Stitched panorama of the investigated outcrop. Note the clay/coal marker horizon approximately in the middle of the exposed vertical section. Although several N-dipping faults with several dm-offset cut through the sequences, the marker horizon traces more or less horizontally through the outcrop. b) Mostly parallel and subordinated conjugate normal faults with an off-set of 30-50 cm. The general mean dip of the faults is 010/65. The conjugate set dip 180/80. Yellow line - deformation bands (compaction bands); red lines - fault trace; orange thick line - marker horizon.

Structural Outcrop Analyses		Stop04
Outcrop No.		
<i>Page</i>		6
UTM 36		
Locality	Mairouba	E 755335
		N 3767938
Outcrop type	Sand pit	Elevation 1403 m

Structural data interpretation

B Bedding	
<p>The bedding of the Chouf sandstone dips generally very shallow towards SW (220/15). Steeper dips and slight variations of the azimuth are the result of tilting of block by bookshelf-type of normal faulting.</p>	

F Fault set	
<p>Major faults, associated with an offset of several dm (green dashed great circles). The normal sense of shear indicates a roughly N-S oriented extension direction. Compactional deformation bands (yellow great circles) strike N-S and are older than the normal faults.</p>	

S Sample S4/02	
<p>The heavy mineral spectrum of the Chouf sandstone records a massif dominance of zircon and tourmaline but also rutile. The lack of other heavy minerals like apatite could be an indication of strong weathering of the detrital minerals.</p>	

Structural Outcrop Analyses		Stop05
Outcrop No.		
Page		1

		UTM 36	
Locality	Ain Ed Delbe	E	756226
		N	3768883
Outcrop type	Active sand pit	Elevation	1471 m

Interpreter	Bauer, Grasemann, Hatzenbichler
Date	6.7.2012

Tectonic unit	
Lithostratigraphic unit	Chouf Sandstone Fm.
Stratigraphic age	Lower Cretaceous
Lithology	Brown to white, coarse to fine sandstone with clays and lignites

References	Walley (1998): Tectonophysics 298, 37-62.
	Nader (2011): Journal of Petroleum Geology 34, 135-156.
	Homburg (2009): Journal of Geodynamics 47, 218-223.

Outcrop description



Photo	DSC05319 Bauer	Stop 05: Sandpit
-------	----------------	------------------

Structural Outcrop Analyses			Stop05
Outcrop No.			
Page			2
			UTM 36
Locality	Ain Ed Delbe	E	756226
		N	3768883
Outcrop type	Active sand pit	Elevation	1471 m

Location of the Outcrop

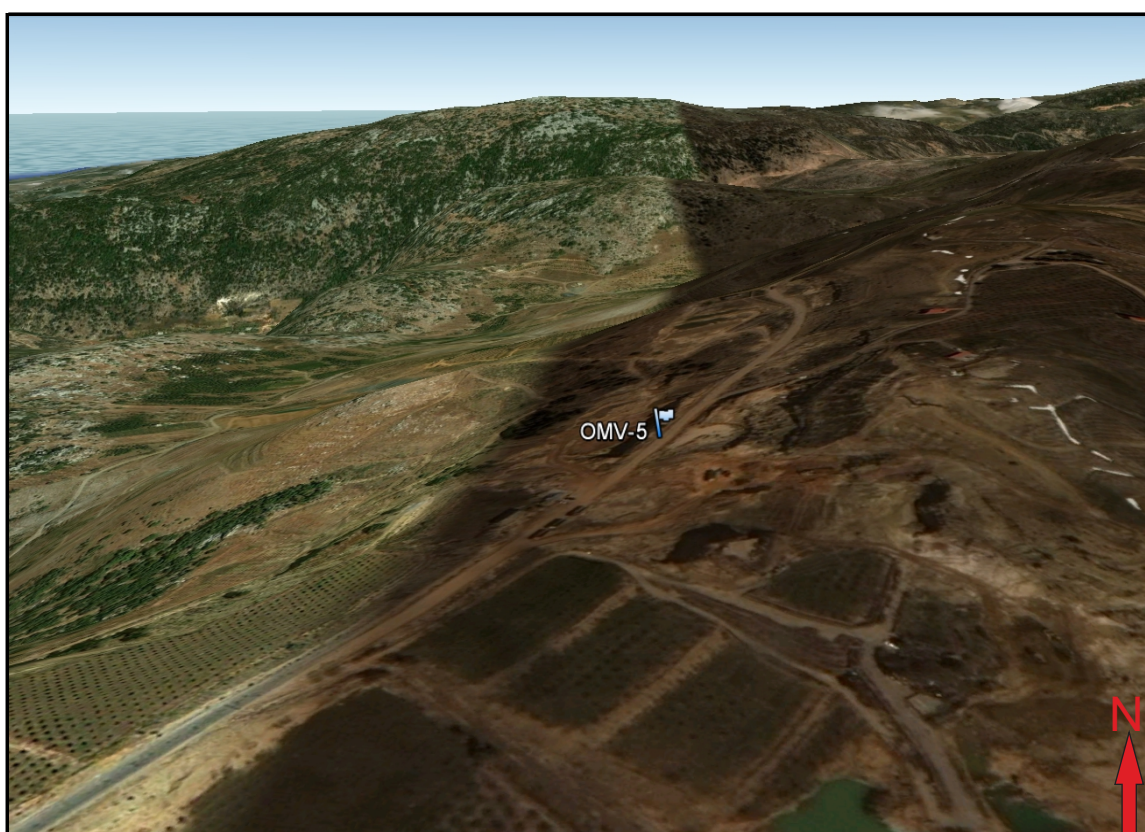


Photo Google Earth

Description

This spectacular outcrop in a sand pit shows a section through the Lower Cretaceous Chouf sandstone. Several systems eroding syn-sedimentary local channels could be observed. In this outcrop, the Chouf sandstone represents a fluvial to deltaic and/or littoral depo-system.

Structural Outcrop Analyses			Stop05
Outcrop No.			
Page			3
			UTM 36
Locality	Ain Ed Delbe	E	756226
		N	3768883
Outcrop type	Active sand pit	Elevation	1471 m

Location in the geological map

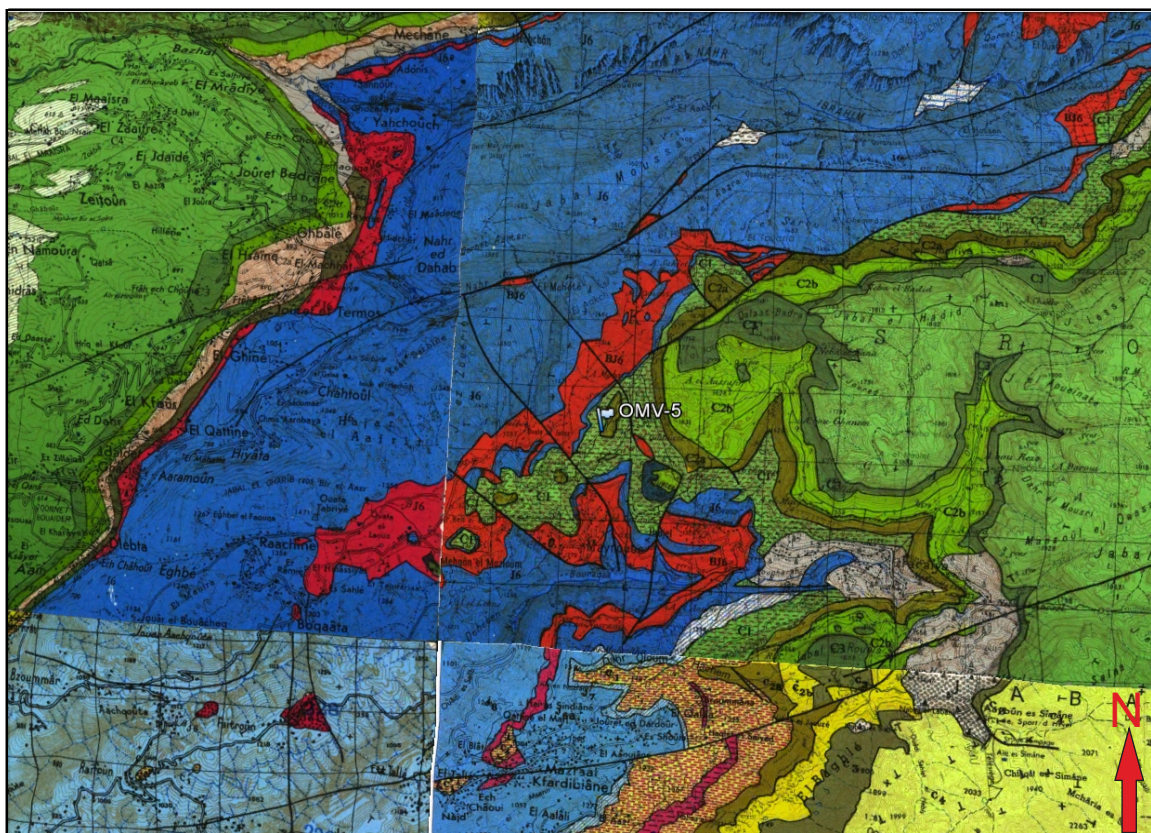


Photo Geological map of Lebanon, orig. 1:50 000 (Ministere des Travaux Publics. Beyrouth)

Structural Outcrop Analyses			Stop05
Outcrop No.			
Page			4
			UTM 36
Locality	Ain Ed Delbe	E	756226
		N	3768883
Outcrop type	Active sand pit	Elevation	1471 m

Location in the QuickBird image



Photo QuickBird image 1:5,000

Structural Outcrop Analyses			Stop05
Outcrop No.			
Page			5
			UTM 36
Locality	Ain Ed Delbe	E	756226
		N	3768883
Outcrop type	Active sand pit	Elevation	1471 m

Stratigraphic interpretation



Photo DSC05318 Bauer

Description

Erosive channel in the Chouf Sandstone cuts perpendicular to the channel axis (looking towards E).

The sedimentary bedding dips shallow towards E (109/15). Note the vertical joints and/or deformation bands (290/82), which could be related to a regional scale axial plane cleavage.

Structural Outcrop Analyses		Stop07
Outcrop No.		
	Page	1

			UTM 36
Locality	Bhassis	E	760428
		N	3772226
Outcrop type	Sandstone cliff	Elevation	1446 m

Interpreter	Bauer, Grasemann, Hatzenbichler
Date	6.7.2012

Tectonic unit	
Lithostratigraphic unit	Chouf Sandstone Fm.
Stratigraphic age	Lower Cretaceous
Lithology	Brown to white, coarse to fine sandstone with clays and lignites

References	Walley (1998): Tectonophysics 298, 37-62.
	Nader (2004) Journal of Petroleum Geology 27, 253-275.
	Walley (1983) Geologische Rundschau 72, 377-388.

Outcrop description



Photo	DSC_0120 Hatzenbichler	Stop 07: Sandstone cliff
-------	------------------------	--------------------------

Structural Outcrop Analyses			Stop07
Outcrop No.			
Page			2
			UTM 36
Locality	Bhassis	E	760428
		N	3772226
Outcrop type	Sandstone cliff	Elevation	1446 m

Location of the Outcrop

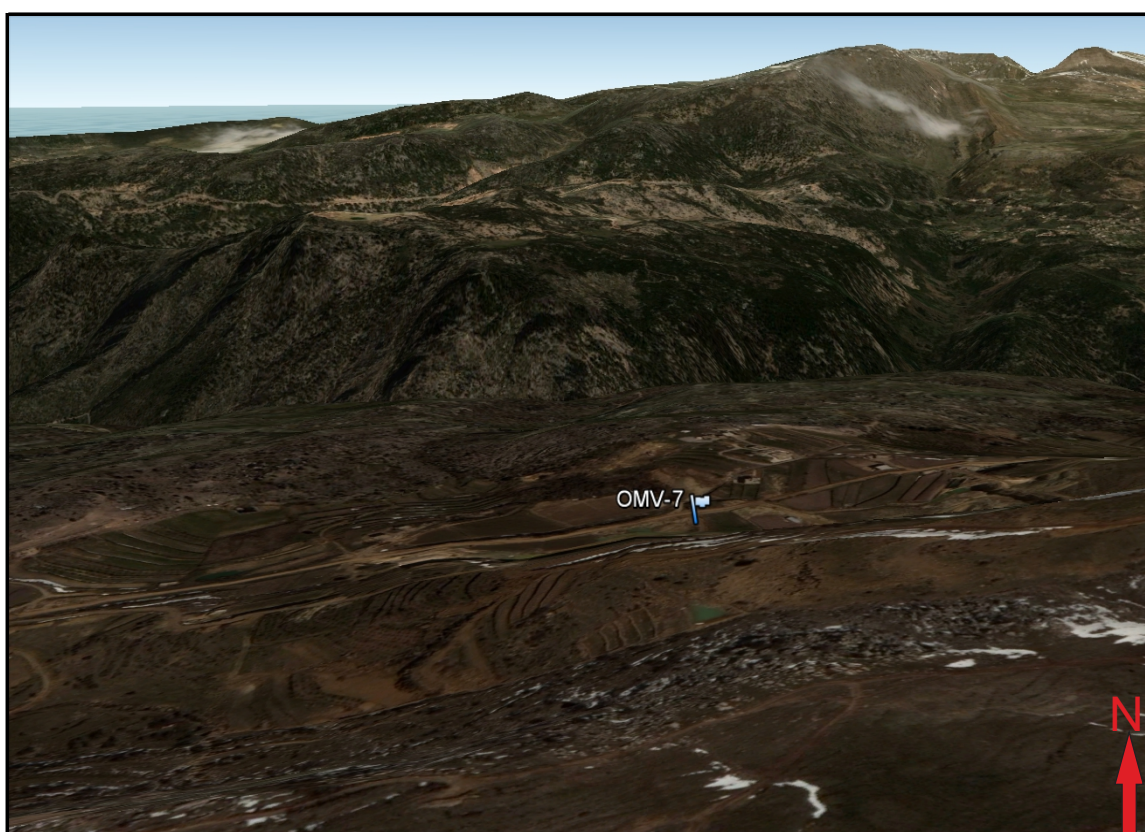


Photo Google Earth

Description

This outcrop shows a normal fault (sf 045/60), which offsets the marker layers in the Chouf sandstone for about 10 meters. The fault core, which is composed of dm thick clay smear acts as a significant barrier for the meteoric fluids. Sandstones in the hanging wall are differently coloured by iron oxide coating of the sand grains than the footwall which is almost unaffected by alterations. This outcrop was sampled for heavy mineral characterization and low temperature geochronology (fission track and/or (U/Th)-He).

Structural Outcrop Analyses			Stop07
Outcrop No.			
Page			3
			UTM 36
Locality	Bhassis	E	760428
		N	3772226
Outcrop type	Sandstone cliff	Elevation	1446 m

Location in the geological map

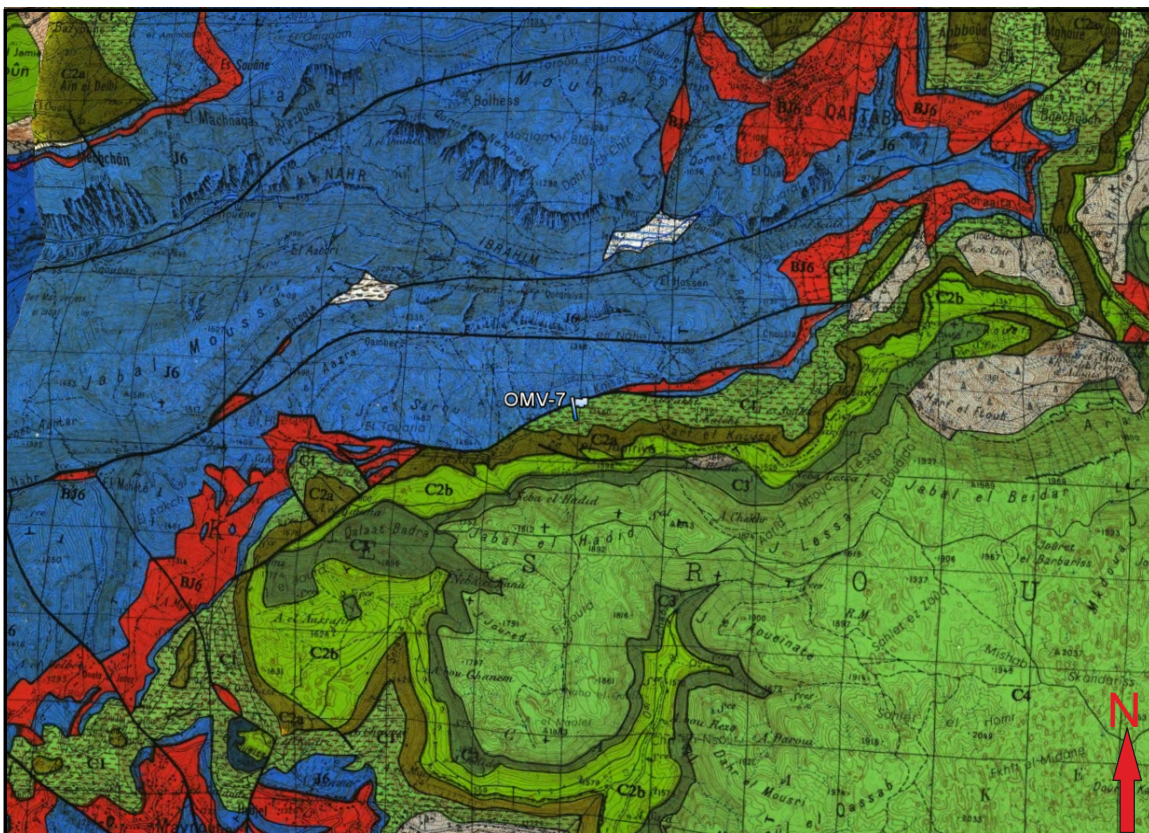


Photo Geological map of Lebanon, orig. 1:50 000 (Ministere des Travaux Publics, Beyrouth)

Structural Outcrop Analyses			Stop07
Outcrop No.			
			Page
			4
			UTM 36
Locality	Bhassis	E	760428
		N	3772226
Outcrop type	Sandstone cliff	Elevation	1446 m

Location in the QuickBird image



Structural Outcrop Analyses			Stop07
Outcrop No.			
Page			5
			UTM 36
Locality	Bhassis	E	760428
		N	3772226
Outcrop type	Sandstone cliff	Elevation	1446 m

Structural data interpretation



Photo DSC_0120 Hatzenbichler

Description

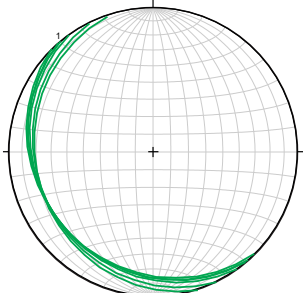
Chouf Sandstone with a layer of black clay (yellow line, 230/20) and an off-set of 10 meters along a normal fault (dashed red line 045/60). Note the abundant vertical deformation bands (i.e. disaggregation bands) which act as zones of weakness for the active erosion (orange lines 095/85).

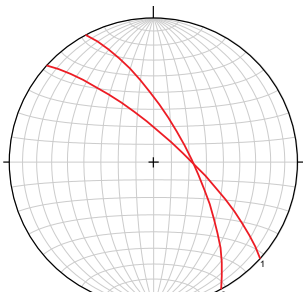
Structural Outcrop Analyses		Stop07
Outcrop No.		
	Page	6

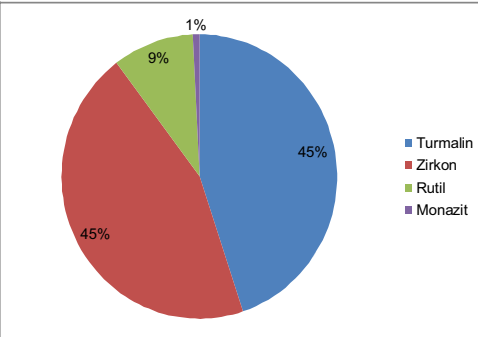
UTM 36

Locality	Bhassis	E	760428
		N	3772226
Outcrop type	Sandstone cliff	Elevation	1446 m

Structural data interpretation

B	Bedding	
	Bedding of the Chouf Sandstone dips gently towards SW (230/20).	

F	Fault set	
	NE-dipping normal faults (sf 042/75, 062/70) offsetting the bedding for about 10 meters.	

S	Sample S7/04	
	The heavy mineral spectrum of the Chouf Sandstone is characterized by a dominance of tourmaline and zircon. Besides rutile and very minor monazite other heavy minerals, especially apatite is generally missing.	

Structural Outcrop Analyses		Stop14
Outcrop No.		
Page		1

		UTM 36	
Locality	Hrazmin	E	757627
		N	3779901
Outcrop type	Road cut, abandoned quarry	Elevation	1260 m

Interpreter	Bauer, Grasemann, Hatzenbichler
Date	7.7.2012

Tectonic unit	
Lithostratigraphic unit	Chouf Sandstone Fm.
Stratigraphic age	Lower Cretaceous
Lithology	Brown to white, coarse to fine sandstone with clays and lignites

References	Walley (1998): Tectonophysics 298, 37-62.
	Fossen et al. (2007): J. of the Geological Society 164, 755-769.
	Schultz and Fossen (2008): AAPG Bulletin 92, 853-867.

Outcrop description



Photo	DSC_0177 Hatzenbichler	Stop 14 : Street outcrop
-------	------------------------	--------------------------

Structural Outcrop Analyses			Stop14
Outcrop No.			
Page			2
			UTM 36
Locality	Hrazmin	E	757627
		N	3779901
Outcrop type	Road cut, abandoned quarry	Elevation	1260 m

Location of the Outcrop

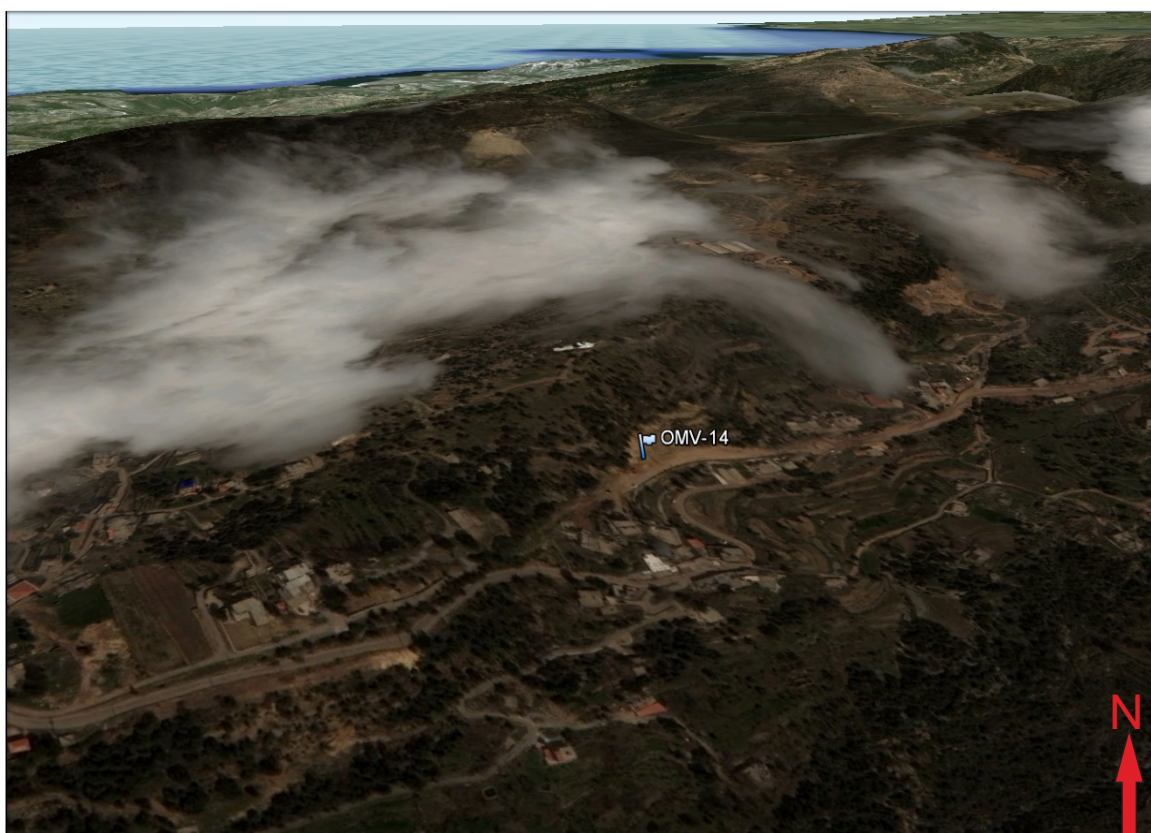


Photo Google Earth

Description

At this outcrop the Chouf Sandstone dips with about 20° towards SW. The layers have varying thickness and some prominent cross-bedding structures could be observed. Several compactional shear deformation bands of several centimeter thickness dip towards NE and SW. The deformation bands have almost no offset.

Structural Outcrop Analyses			Stop14
Outcrop No.			
Page			3
			UTM 36
Locality	Hrazmin	E	757627
		N	3779901
Outcrop type	Road cut, abandoned quarry	Elevation	1260 m

Location in the geological map

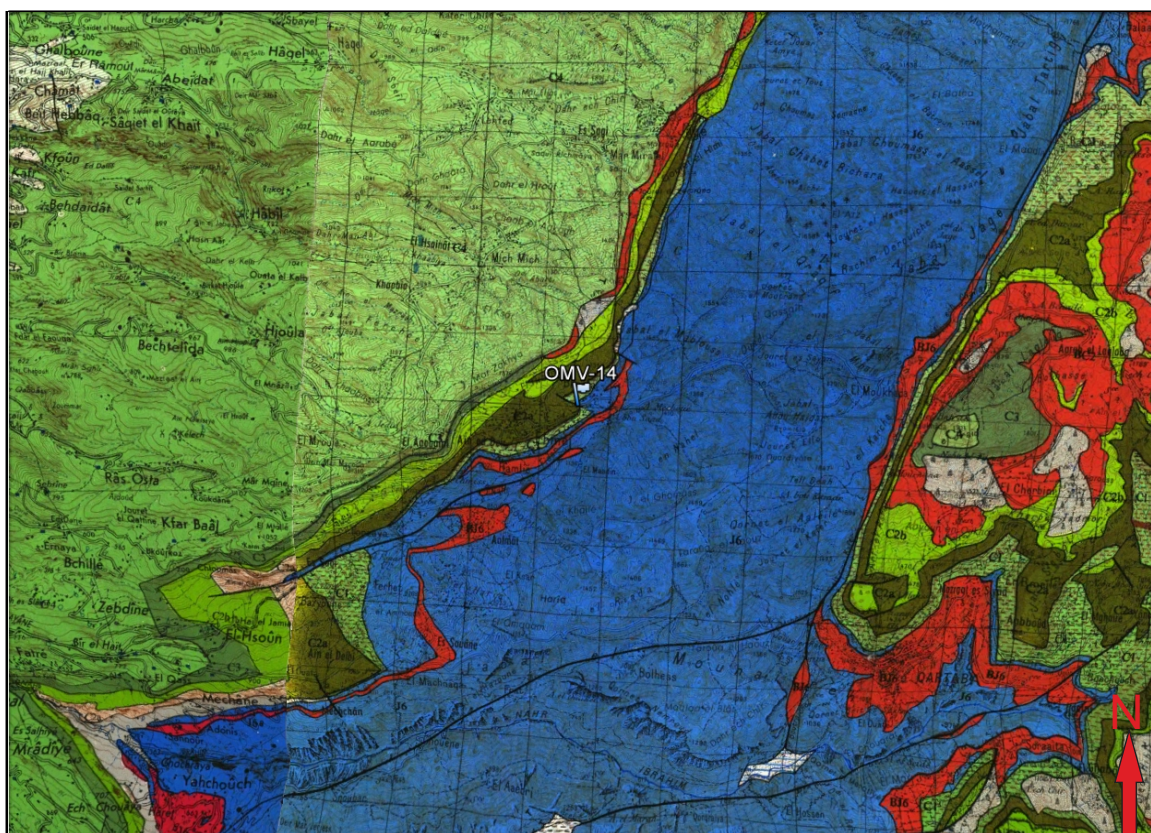


Photo Geological map of Lebanon, orig. 1:50 000 (Ministere des Travaux Publics, Beyrouth)

Structural Outcrop Analyses			Stop14
Outcrop No.			
Page			4
			UTM 36
Locality	Hrazmin	E	757627
		N	3779901
Outcrop type	Road cut, abandoned quarry	Elevation	1260 m

Location in the QuickBird image

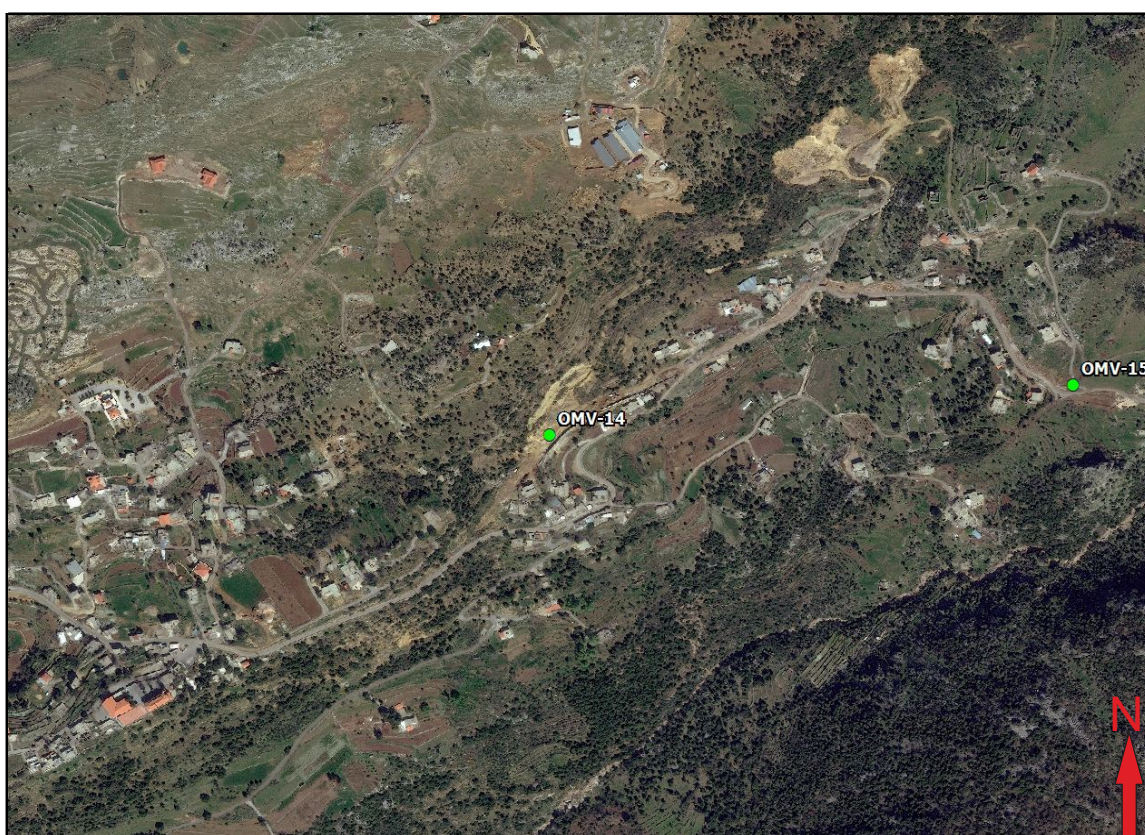
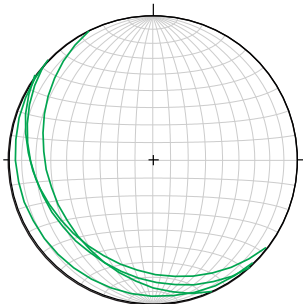
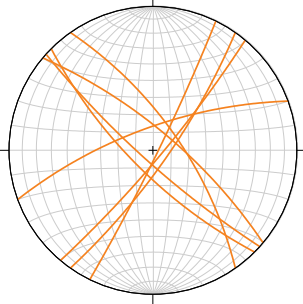


Photo QuickBird image 1:5,000

Structural Outcrop Analyses			Stop14
Outcrop No.			
Page			5
			UTM 36
Locality	Hrazmin	E	757627
		N	3779901
Outcrop type	Road cut, abandoned quarry	Elevation	1260 m

Structural data interpretation

<p>B Bedding</p> <p>The bedding of the Chouf sandstone dips generally very shallow towards SW (mean 225/15).</p>	
<p>DB Deformation Bands</p> <p>Conjugate set of contractional shear deformation bands. Both sets are very steep and strike roughly NE-SW and NW-SE, respectively. Because of the steep dip, the deformation bands cannot have formed during diagenesis but must have a tectonic origin. Note, however, that there is almost no offset along these structures.</p>	
<p>S Sample 14/1, 2, 5</p> <p>Due to strong coating of the grains no heavy mineral statistics could be obtained. Samples are currently chemically treated in the lab at the Department for Geodynamics and Sedimentology.</p>	

Structural Outcrop Analyses		Stop18
Outcrop No.		
Page		1

		UTM 36	
Locality	Moukhada	E	762510
		N	3779958
Outcrop type	Outcrop after a short walk	Elevation	1620 m

Interpreter	Bauer, Grasemann, Hatzenbichler
Date	7.7.2012

Tectonic unit	
Lithostratigraphic unit	Bikfaya Fm., Salima Fm., Chouf sandstone
Stratigraphic age	Upper Cretaceous
Lithology	Pale massive micritic Limestone

References	Walley (1998): Tectonophysics 298, 37-62.
------------	---

Outcrop description



Photo	DSC_0195 Hatzenbichler	Stop 18: Slightly dolomitized
-------	------------------------	-------------------------------

Structural Outcrop Analyses			Stop18
Outcrop No.			
Page			2
			UTM 36
Locality	Moukhada	E	762510
		N	3779958
Outcrop type	Outcrop after a short walk	Elevation	1620 m

Location of the Outcrop

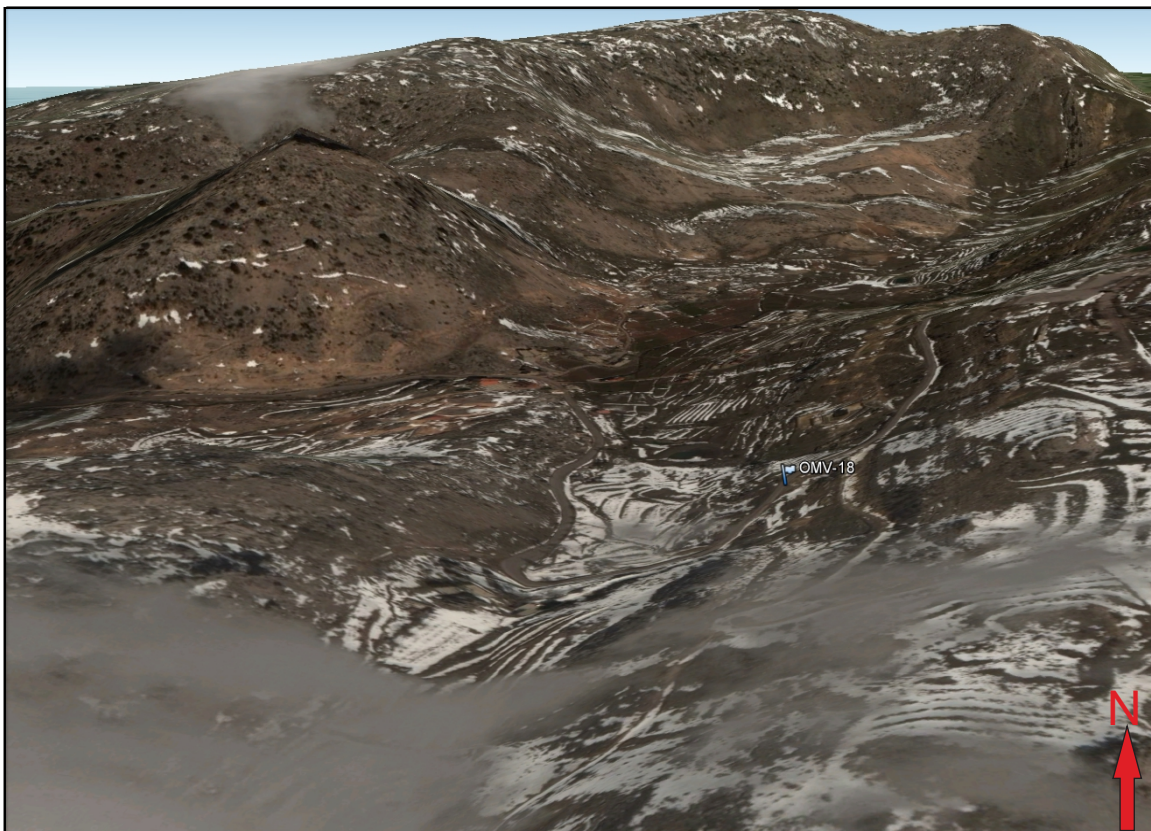


Photo Google Earth

Description

At this outcrop the border between the micritic limestones of the Bikfaya Formation and the brown-yellow oolitic grainstones/marls of the Salima Formation is exposed. Here the eastern limb of the Qartaba box fold is even slightly overturned and dips towards the west. At the same outcrop a strong penetrative axial plane cleavage is developed suggesting an inverted polarity of the limb.

Structural Outcrop Analyses			Stop18
Outcrop No.			
Page			3
			UTM 36
Locality	Moukhada	E	762510
		N	3779958
Outcrop type	Outcrop after a short walk	Elevation	1620 m

Location in the geological map

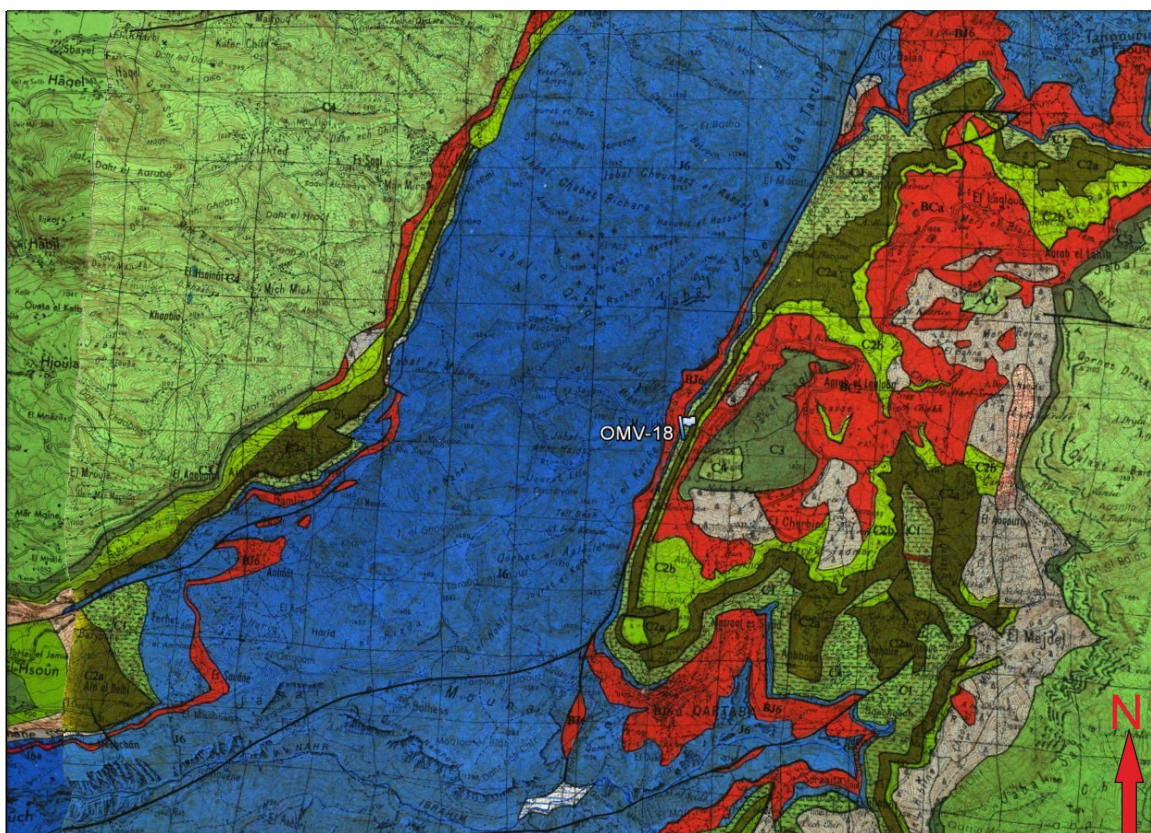


Photo Geological map of Lebanon, orig. 1:50 000 (Ministere des Travaux Publics, Beyrouth)

Structural Outcrop Analyses		Stop18
Outcrop No.		
Page		4

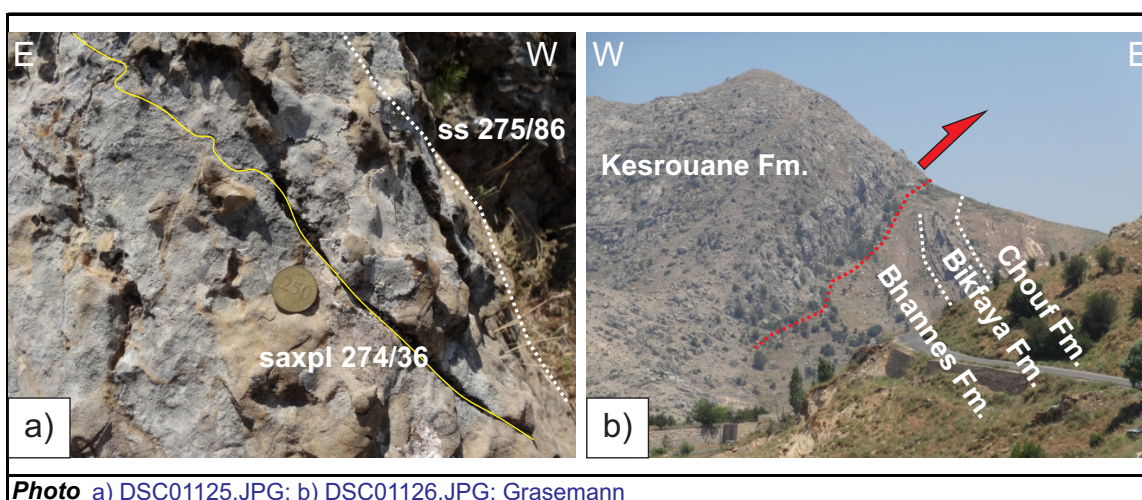
		UTM 36	
Locality	Moukhada	E	762510
		N	3779958
Outcrop type	Outcrop after a short walk	Elevation	1620 m

Location in the QuickBird image



Structural Outcrop Analyses			Stop18
Outcrop No.			
Page			5
			UTM 36
Locality	Moukhada	E	762510
		N	3779958
Outcrop type	Outcrop after a short walk	Elevation	1620 m

Outcrop observations



Description

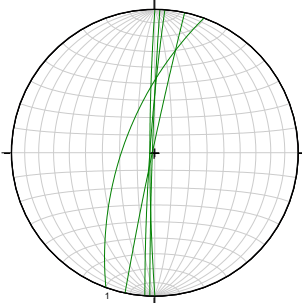
a) Detail of the overturned limb of Bikfaya Formation. The bedding, which is defined by syn-sedimentary pressure solution seams (stylolites, white dotted line) dips steeply towards W. The axial plane cleavage, which also dips towards the west, is defined by a pressure solution cleavage in form of wavy stylolites (yellow line). Note the cross cutting relationship between the syn-sedimentary stylolites, which are overprinted by the tectonic stylolites probably during the folding process. b) View towards the north on the eastern limb of the Qartaba structure. The Kesrouane Formation is locally thrust on the tilted Upper Jurassic and Lower Cretaceous sequence. The thrust might have formed due to limb-thrusting and reactivation of an axial plane cleavage of the monoclinial limb of the box fold.

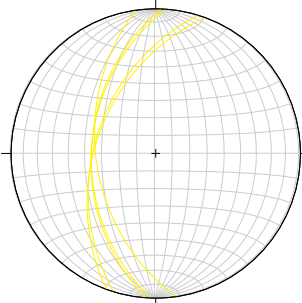
Structural Outcrop Analyses		Stop18
Outcrop No.		
	Page	6

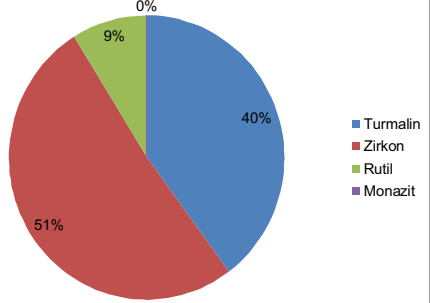
UTM 36

Locality	Moukhada	E	762510
		N	3779958
Outcrop type	Outcrop after a short walk	Elevation	1620 m

Structural data interpretation

B	Bedding	
	<p>The bedding in the overturned eastern limb in the Bikfaya Formation.</p>	

AP	Axial plane cleavage	
	<p>Axial plane cleavage in the Bikfaya Formation. Because the limb is overturned both the axial planes and the bedding dip to the west.</p>	

S	Sample S18/06	
	<p>The heavy mineral spectrum of the Chouf sandstone. Strong dominance of zircon and tourmaline.</p>	

Structural Outcrop Analyses		Stop23
Outcrop No.		
Page		1

		UTM 36	
Locality	Hourata	E	770316
		N	3787013
Outcrop type	Abandoned quarry on roadside	Elevation	1752 m

Interpreter	Bauer, Grasemann, Hatzenbichler
Date	7.7.2012

Tectonic unit	
Lithostratigraphic unit	Chouf Sandstone Fm.
Stratigraphic age	Lower Cretaceous
Lithology	Brown to white, coarse to fine sandstone with clays and lignites

References	Walley (1983): Geologische Rundschau 72, 377-388.
	Homberg (2009): Journal of Geodynamics 47, 218-223.
	Nader & Swennen (2004): Marine and Petrol. Geol. 21, 427-441.

Outcrop description



Photo	DSC_0212	Stop 23: abandoned quarry
-------	----------	---------------------------

Structural Outcrop Analyses			Stop23
Outcrop No.			
Page			2
			UTM 36
Locality	Hourata	E	770316
		N	3787013
Outcrop type	Abandoned quarry and roadside.	Elevation	1752 m

Location of the Outcrop

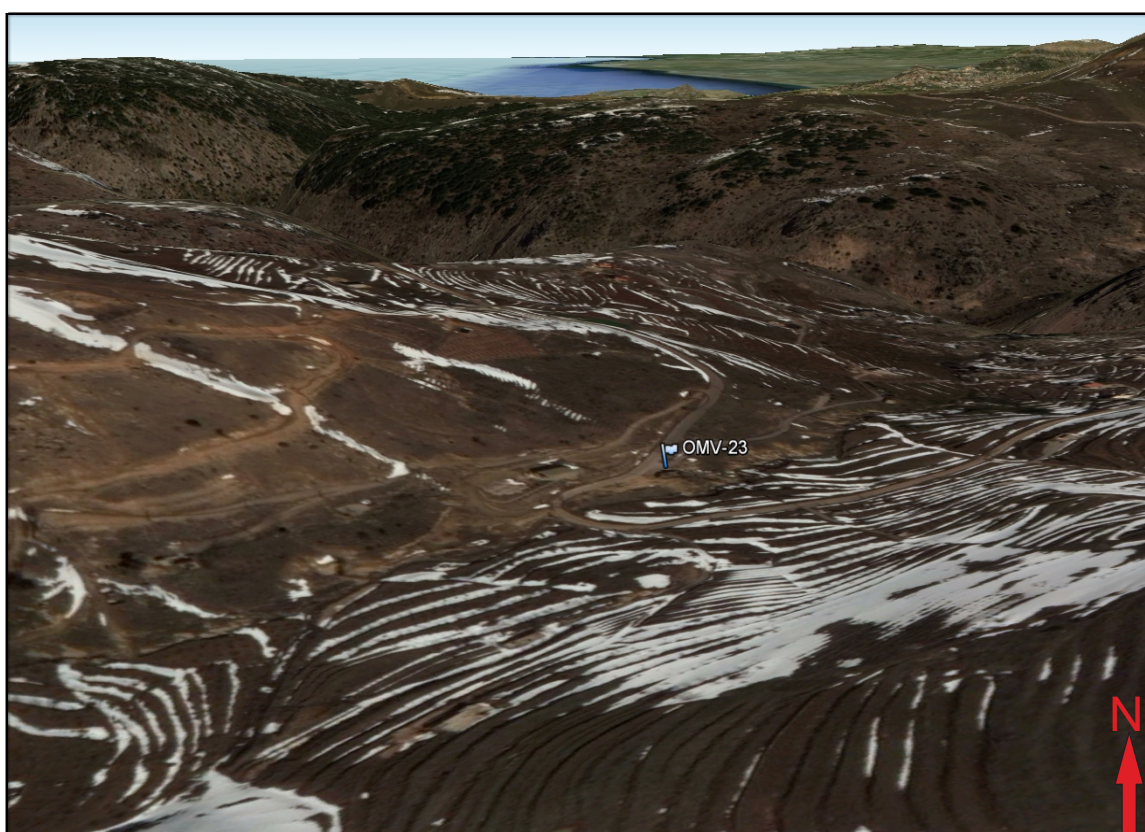


Photo Google Earth

Description

The sedimentary layering of the yellow to brownish sandstone dip at shallow angles towards the E (ss 090/22). Although deformation band structures are missing in this outcrop, a fault (sf 160/86) with unknown kinematics offsets the sandstones. A (Neptunian?) dyke with unclear three dimensional orientation has been observed.

Location in the geological map

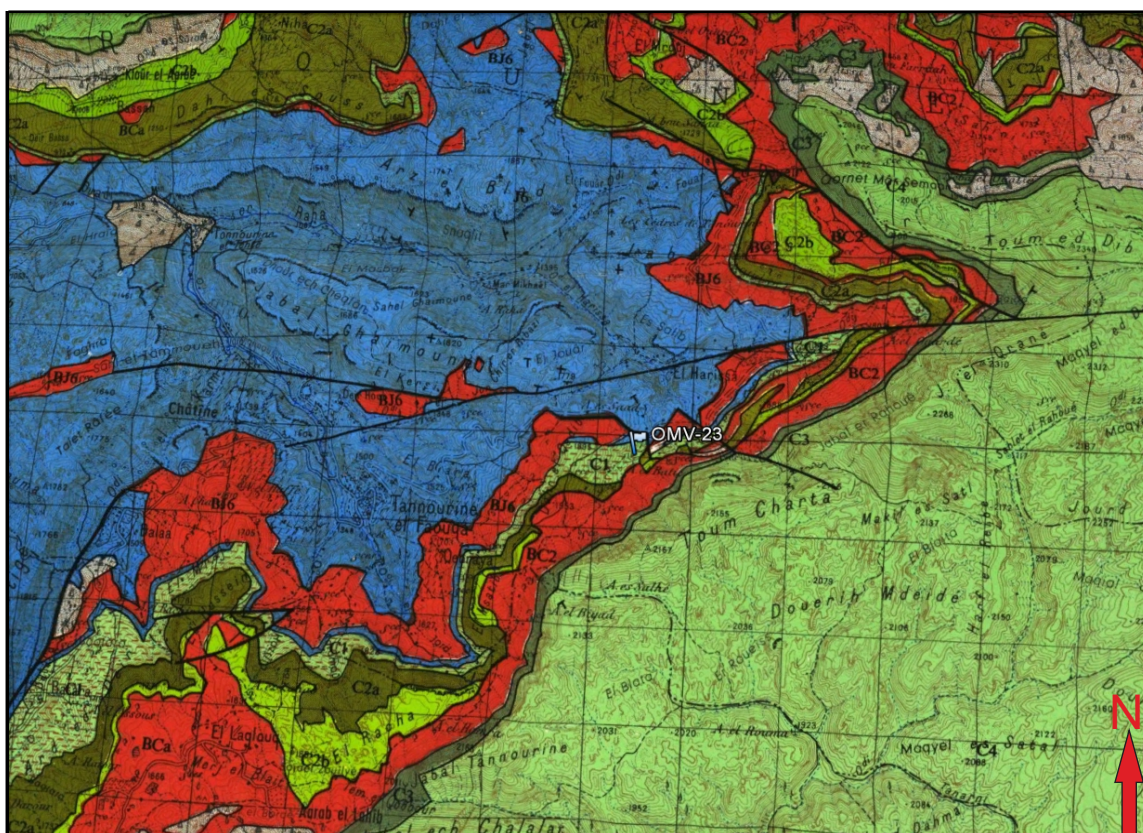


Photo Geological map of Lebanon, orig. 1:50 000 (Ministere des Travaux Publics. Beyrouth)

Structural Outcrop Analyses		Stop23
Outcrop No.		
Page		4

		UTM 36	
Locality	Hourata	E	770316
		N	3787013
Outcrop type	Abandoned quarry and roadside.	Elevation	1752 m

Location in the QuickBird image

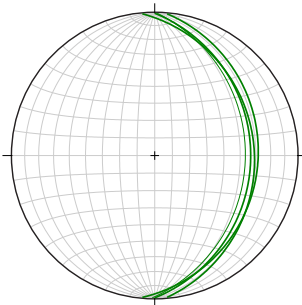


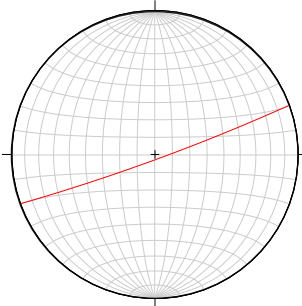
Structural Outcrop Analyses		Stop23
Outcrop No.		
	Page	5

UTM 36

Locality	Hourata	E	770316
		N	3787013
Outcrop type	Abandoned quarry and roadside.	Elevation	1752 m

Structural data interpretation

B	Bedding	
	<p>The bedding in the Chouf sandstone dips at shallow angle towards east.</p>	

F	Fault	
	<p>A vertical fault striking ENE-WSW with unknown kinematics.</p>	

S	Sample S23/07	
	<p>The sample was taken for provenance studies but heavy mineral spectrum could not be studied because of strong iron oxides staining. Low-temperature geochronology is in process.</p>	

 Qartaba Anticline	Final Report 2013-03-01	
--	--------------------------------	---

Structural Outcrop Analyses	Stop26
Outcrop No.	
Page	1

			UTM 36
Locality	Tannourine	E	770199
		N	3790607
Outcrop type	Outlook and Chouf sampling spot	Elevation	1720 m

Interpreter	Bauer, Grasemann, Hatzenbichler
Date	7.7.2012

Tectonic unit	
Lithostratigraphic unit	Kesrouane Fm., Bhannes Fm. and Chouf sandstone
Stratigraphic age	Upper Jurassic
Lithology	Limestones, basalts and sandstones

References	Walley (1998): Tectonophysics 298, 37-62.
-------------------	---

Outcrop description



Photo	DSC05452 Bauer	Stop 26: Kesrouane-Bhannes-Chouf (left-right)
--------------	----------------	---

 Qartaba Anticline	Final Report 2013-03-01	
--	--------------------------------	---

Structural Outcrop Analyses		Stop26	
Outcrop No.			
		<i>Page</i>	2
		UTM 36	
Locality	Tannourine	E	770199
		N	3790607
Outcrop type	Outlook and Chouf sampling spot	Elevation	1720 m

Location of the Outcrop

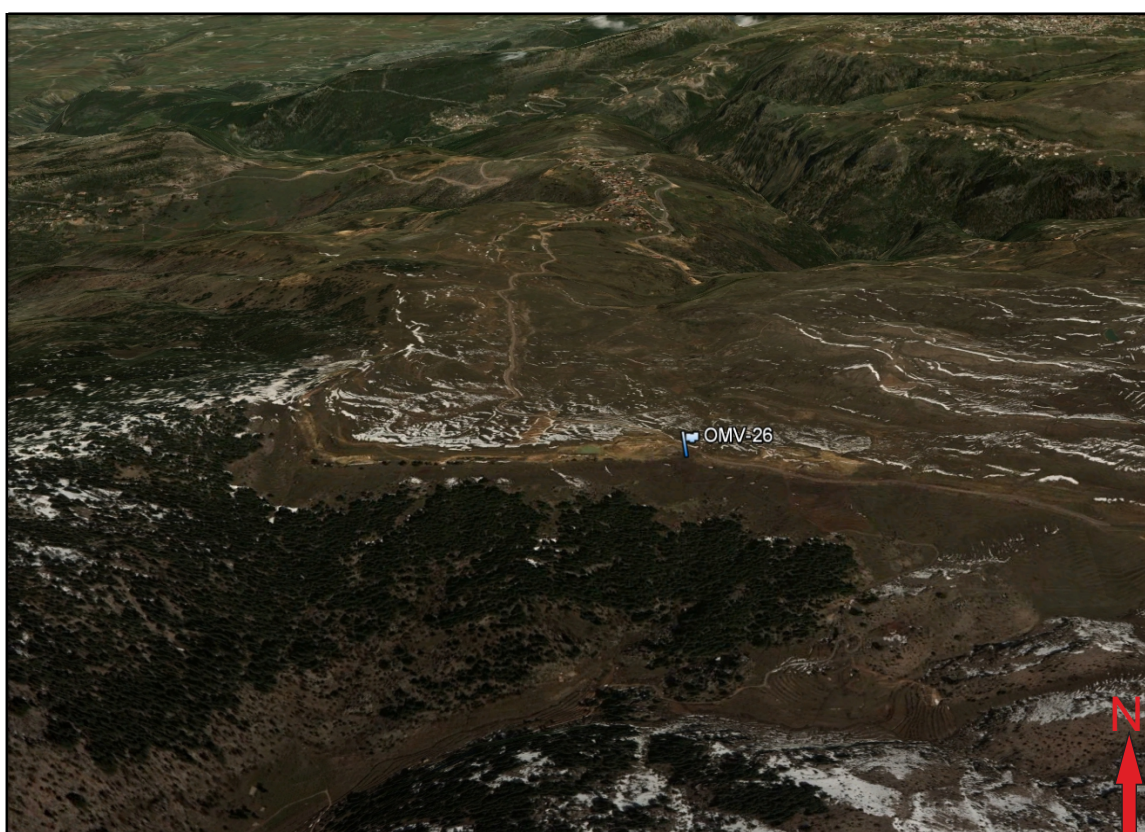


Photo Google Earth

Description <p>The top of the Kesrouane Formation has a irregular boundary with the Bhannes Formation, suggesting that the Kesrouane Formation formed a palaeo erosional surface, which was filled up by the basalts of the Bhannes Formation.</p>

 [Quartaba Anticline]	Qartaba Anticline	
Final Report 2013-03-01		

Structural Outcrop Analyses		Stop26	
Outcrop No.			
		Page	3
		UTM 36	
Locality	Tannourine	E	770199
		N	3790607
Outcrop type	Outlook and Chouf sampling spot	Elevation	1720 m

Location in the geological map

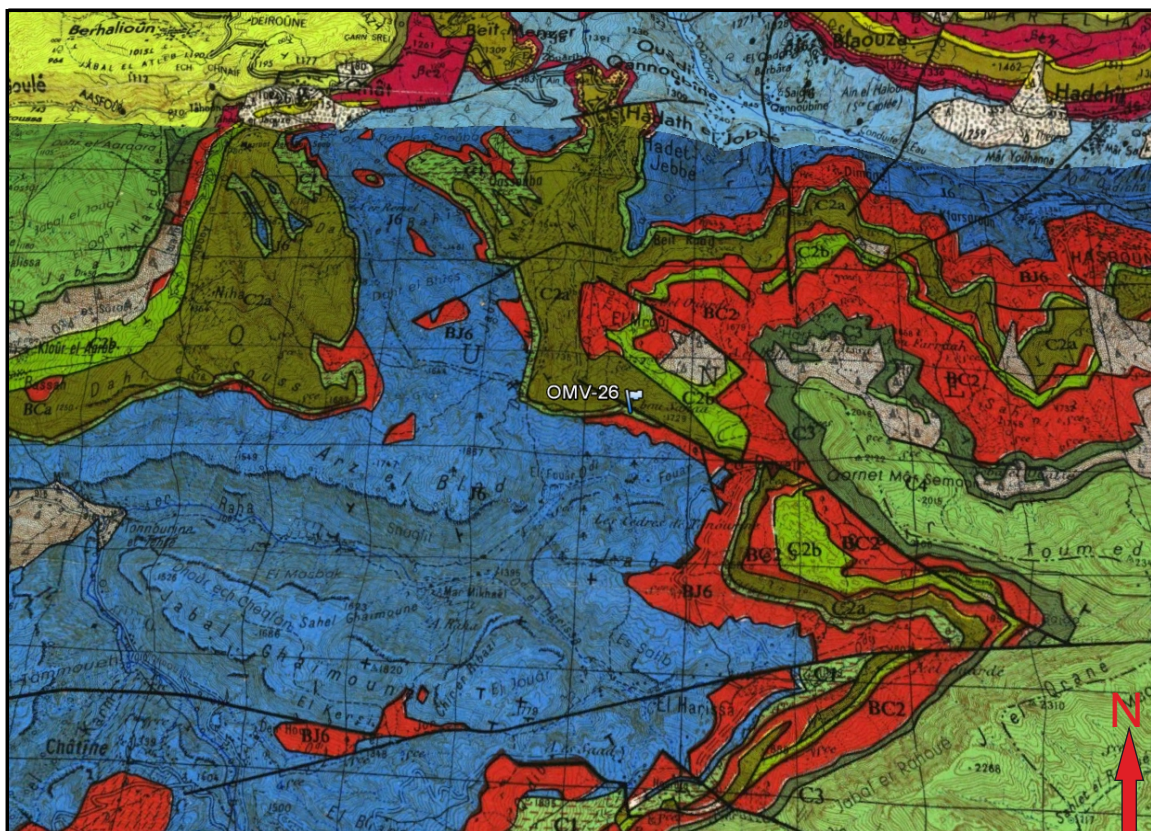


Photo Geological map of Lebanon, orig. 1:50 000 (Ministere des Travaux Publics. Beyrouth)

 Qartaba Anticline	Final Report 2013-03-01	
--	--------------------------------	---

Structural Outcrop Analyses	Stop26
Outcrop No.	
Page	4

			UTM 36
Locality	Tannourine	E	770199
		N	3790607
Outcrop type	Outlook and Chouf sampling spot	Elevation	1720 m

Location in the QuickBird image



Photo QuickBird image 1:5,000

 Qartaba Anticline	Final Report 2013-03-01	
--	--------------------------------	---

Structural Outcrop Analyses	Stop26
Outcrop No.	
Page	5

UTM 36

Locality	Tannourine	E	770199
		N	3790607
Outcrop type	Outlook and Chouf sampling spot	Elevation	1720 m

Structural data interpretation

S	Sample S26/08									
Similar to the other Chouf Sandstone samples, the heavy mineral spectrum is dominated by zircon, tourmaline and rutile.		<table><tr><td>Turmalin</td><td>49%</td></tr><tr><td>Zirkon</td><td>33%</td></tr><tr><td>Rutil</td><td>18%</td></tr><tr><td>Monazit</td><td>0%</td></tr></table>	Turmalin	49%	Zirkon	33%	Rutil	18%	Monazit	0%
Turmalin	49%									
Zirkon	33%									
Rutil	18%									
Monazit	0%									

 Qartaba Anticline	Final Report 2013-03-01	
--	--------------------------------	---

Structural Outcrop Analyses		Stop26	
Outcrop No.		6	
		<i>Page</i>	UTM 36
Locality	Tannourine	E	770199
		N	3790607
Outcrop type	Outlook and Chouf sampling spot	Elevation	1720 m

Panorama



Description

N-S panorama. From left to right: Chouf Fm. - Bhannes Fm. - Kesrouane Fm. In the center of the picture is the famous cedar forest of Tannourine with 60,000 trees, making it the 2nd largest cedar reserve in Lebanon.

III. Curriculum Vitae

PERSONAL DATA

Name: Harald Bauer
Nationality: Austrian

EDUCATION

03/2012 - MSc Earth Sciences at the University of Vienna
Topic: Tectonic evolution of the Northern Mount Lebanon region with particular reference to the Lower Cretaceous Chouf Formation (Lebanon)
Supervisor: Bernhard Grasemann
09/2011 - 01/2012 Erasmus student exchange program, University of Oviedo, Spain
10/2008 - 02/2012 BSc Earth Sciences at the University of Vienna
Topic: Strukturgeologie der Karstformen auf der Schneealpe (Stmk.)
Supervisor: Lukas Plan
09/2003 - 01/2001 Foreign studies in Győr, Hungary
09/1994 - 06/1998 Elementary School in Perchtoldsdorf, Austria

SCIENTIFIC ACTIVITIES / PUBLICATIONS

- Bauer, H., Exel, T. & Oberender, P. (2014): Expedition zur Gobholo-Höhle in Swasiland. - Höhlenkundliche Mitteilungen des Landesvereins für Höhlenkunde in Wien und Niederösterreich, 70 (5/6): 55-59.
- Oberender, P., Bauer, H., Exel, T., Lundberg, J.E.K., Scheuerer, M. & Sjöberg, R. (2014): Gobholo Cave - A granite cave in Swaziland. - Newsletter of the Pseudokarst Commission of the International Union of Speleology, 24: 29-34.
- Bauer, H., Hatzenbichler, G., Amon, P., Fallah, M., Tari, G. & Grasemann, B. (2013): Laser scan of the Grimming Mts. (Austria) with the latest LiDAR equipment: preliminary results. - Poster presentation at the European Geosciences Union General Assembly 2013, April 22-27, Vienna, Austria.
- Hatzenbichler, G., Bauer, H., Grasemann, B., Tari, G., Nader, F. H., Church, J., Schneider, D. & Zámolyi, A. (2013): The Lower Cretaceous Chouf Sandstone of Lebanon: Is it a synrift clastic sequence? - Poster presentation at the European Geosciences Union General Assembly 2013, April 22-27, Vienna, Austria.

- Bauer, H., Hatzenbichler, G., Plan, L. & Decker, K. (2012): Strukturgeologie der Karstformen auf der Schneealpe (Stmk.). - Die Höhle, 63: 18-31.

SKILLS

Languages:

- German: mother tongue
- English: fluent
- Hungarian: fluent
- Spanish: intermediate
- French: basics

Computer skills:

- advanced knowledge: Microsoft Office, Webdesign (HTML, Typo3), ArcGIS, CorelDraw, Geodin, Petrel
- elementary knowledge: Adobe Illustrator, AutoCAD, GoCAD, MatLAB

Absolvement of rock blasting training at the University of Natural Resources and Life Sciences, Vienna (BOKU) in 2010.

TUTORIALS

07/2013	Mapping course: Ötztal, Austria
02/2012	Mapping course: Bad Aussee, Austria

WORK EXPERIENCE

11/2013 - 02/2014	interpretation of a paleoseismologic trench at the University of Vienna in Vienna, Austria
01/2013 - 11/2013	geologic interpretation of caves at the Speleological Society of Vienna and Lower Austria in Vienna, Austria
03/2011 - 08/2011	geotechnical office assistant at Porr Umwelttechnik GmbH in Vienna, Austria
08/2010 - 09/2010	internship at Porr Umwelttechnik GmbH in Vienna, Austria
01/2008 - 07/2008	IT-Helpdesk agent at Siemens Business Services Ltd. in Cork, Ireland